1-1-2014

Development And Application Of Biomimetic Electrospun Nanofibers In Total Joint Replacement

Wei Song
Wayne State University,

DEVELOPMENT AND APPLICATION OF BIOMIMETIC ELECTROSPUN NANOFIBERS IN TOTAL JOINT REPLACEMENT

by

WEI SONG

DISSERTATION

Submitted to the Graduate School

of Wayne State University,

Detroit, Michigan

in partial fulfillment of the requirements

for the degree of

DOCTOR OF PHILOSOPHY

2014

MAJOR: Biomedical Engineering

Approved by:

Advisor	Date

ACKNOWLEDGEMENTS

I would never have been able to accomplish my Ph.D dissertation without the guidance of all my committee members, help from collaborators and friends, support from my family members and girlfriend.

I would like to express my deep gratitude to my academic advisor Dr. Weiping Ren. I wouldn't come here for the research without your recognition. Thanks for your excellent guidance, patience, great support and providing me the excellent research atmosphere for encouraging me to put innovation ideas into practices. I would also like to thank Dr. Guangzhao Mao, Dr. Howard Matthew, Dr. Karen Beningo, Dr. David Markel for guiding my research for the past few years and helping me to develop my knowledge in nano-science, chemistry, tissue engineering, cells biology, orthopaedic clinics, which crucially benefits my research work. Special thank goes to Dr. David Markel, who is the program director of the orthopedic surgery residency program at Providence hospital, Southfield, provides me great supports to use the laboratory facilities (Micro CT, Flow cytometer, RT-PCR,) and animal studies.

I would also like to thank Ms. Tong Shi as our lab manager for her magnificent helps in experiment during these years. Her expertise in biology gains me a lot of guidance in my research. And many thanks go to Nancy Jackson, Christopher Bergum, Dr. Jeff Flynn in orthopedic surgery residency program at Providence hospital and Liang Chen, Joseph Seta in Biomedical Engineering for their great helps in my research.

I would also like to thank my parents. They are always supporting me and

encouraging me with their best wishes.

Finally, I would like to thank my girlfriend, Tao Li. She was always there cheering me up and stood by me through both good and bad times.

PREFACE

All of the work presented henceforth was conducted in the Biomedical Engineering department at Wayne state university, Detroit, MI and Orthopaedic residency program research lab at Providence hospital, Southfield, MI. All projects involved animal tests were approved by University Institutional Animal Care and Use Committee.

A version of Chapter 3 has been published [W Song, DC Markel, T Shi, and Ren WP: Poly (vinyl alcohol)/collagen/hydroxyapatite hydrogel: Properties and in vitro cellular response. J Biomed Mater Res Part A: 100A: 3071–3079, 2012]. I was the lead investigator, responsible for all major areas of concept formation, data collection and analysis, as well as manuscript composition. Dr Weiping Ren was the supervisory author on this project and was involved throughout the project in concept formation and manuscript composition.

A version of Chapter 4 has been published [W Song, DC Markel, S Wang, R Blasier, T Shi, GZ Mao, and Ren WP: Electrospun polyvinyl alcohol-collagen- hydroxyapatite nanofibers: biomimetic extracellular matrix for osteoblastic cells. Nanotechnology, 23, 115101, 2012]. I was the lead investigator, responsible for all major areas of concept formation, data collection and analysis, as well as manuscript composition. Dr Weiping Ren was the supervisory author on this project and was involved throughout the project in concept formation and manuscript composition.

A version of Chapter 5 has been published [W Song, XW Yu, DC Markel, T Shi and WP Ren: Coaxial PCL/PVA electrospun nanofibers: osseointegration enhancer and controlled drug release device. Biofabrication, 5 (3), 035006, 2013]. I was the lead investigator, responsible for all major areas of concept formation, data collection and analysis, as well as manuscript composition. Dr. Weiping Ren was the supervisory author on this project and was involved throughout the project in concept formation and manuscript composition.

I was the lead investigator for the projects located in Chapters 6 and 7 where I was responsible for all major areas of concept formation, data collection and analysis, as well as the majority of manuscript composition. Nancy Jackson and Christopher Bergum were involved in Animal test. Ms. Tong Shi and Liang Chen contributed to materials preparation. Dr. Weiping Ren was the supervisory author on this project and was involved throughout the project in concept formation and manuscript edits.

TABLE OF CONTENTS

LIST OF TABLES

LIST OF FIGURES

CHAPTER 1 PROBLEM STATEMENT IN TOTAL JOINT REPLACEMENT

Total Joint Replacement

In recent years, total joint replacement (TJR) has been raise up critical debate due to increasing number of revision and replacement surgeries (Kurtz et al., 2007; Carr and Goswami, 2009). The major reason is the emerging problems from the materials used in Total joint arthroplasty (Kendal et al., 2013). Total joint arthroplasty is a highly reliable and successful surgery that has been performed for decades. TJR implant materials are mostly bio-inert and durable substance, such as alloy, bone cement, high density polymers, etc. (Bahraminasab et al., 2012). However, high risk of implant failure mostly occurred for earlier wear or infection (Bahraminasab et al., 2012). For performing over decades, the TJR operation includes replacing the arthritic joint surface with a hard metal head and soft polyethylene cup, and the stem of implant was inserted through the trebaculae to the bone marrow cavity, which are cemented or press-fit for secure fixation, as shown in Fig. 1.

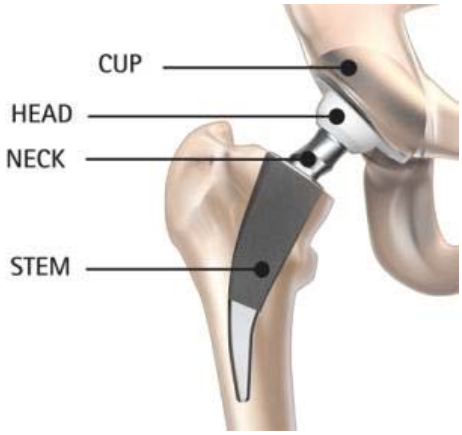

Fig.1 A typical total joint replacement prosthesis

The major used metal materials are Ti-based alloys, stainless steels and Co–Cr–Mo alloys, and polymers are ultra-high molecular weight polyethylene. Sometimes ceramics are substituted for metals, such as alumina, zirconia and their composite. There components are cemented by Polymethylmethacrylate (PMMA) or press fit to stabilize the implant. All of these materials are problematic to cause implant failure. There are numerous causes including excessive wear debris around interface between bone-implant, stress shielding in bone and generated soft tissue between prosthesis and bone due to micro motion, *Staphylococcus aureus* (SA) induced osteomyelitis, and so on. All of these causes can be categorized into septic and aseptic stimuli.

Aseptic loosening (AL)

Earlier reports about the extensive localized bone resorption resulting in loosening without infection was back to 1976 (Harris et al., 1976). Osteolysis was found directly associated around the area nearby implant surface and has been considered as the start of implant instability. The explanation in the earlier stage was that particles disease plays a dominant role in affecting surrounding tissue. This theory has pushing forward the research of cementless TJR, but the outcome wasn't turn better as expected in comparison with cemented implant. This result indicated the AL is a multifactorial issue.

Schmalzried et al. (Schmalzried et al., 1992) described that wear particles accessed to the joint fluid entering to the interface between bone and prosthesis.

Adequate relative movement generated wear particles including cement, UHMWPE, alloys and bone debris. Wear can occur through five major mechanisms: adhesion, abrasion, third body, fatigue, and corrosion. The detached particles accelerated metals or PE wear at the articulation. Followed by more particles fallen off, macrophages were activated for osteoclastogenesis or differentiated into osteoclast, which initiates bone resorption. The bone loss will enlarge the gap between implant and bone, which eases more wear particles into joint fluid and accelerates gradual loosening of the implant. Another theory from Van der V is that higher pressure of joint fluid moves the wear debris to effective joint space, which exposes the particles to macrophage cells resulting in pathogenesis of AL. In any case, wear debris from implant materials are involved in the initiation of AL.

Polymethylmethacrylate (PMMA) or bone cement are firstly used as fixation material in hip prosthesis in 1953 (Haboush, 1996). After decades of application, PMMA cement has become the golden standard approach to fix prosthesis components for joint replacement. However, long-term results indicate that cemented TJR in elderly patients are more satisfactory than younger patients (Sundfeldt et al., 2006). Debonding between cements and implant is considered as the main cause of reducing fixation duration. The stem part of prosthesis is in most frequency of cement debonding, where shear stress occurs all the time. It is notable that polished stem or uncoated stems are much easier to cause cement debonding (Sundfeldt et al., 2006). As cement aged, the brittleness of PMMA even elevates and

the wear debris generation becomes more severe (Howie et al., 1993). For younger patients with more daily activities, the chance of producing more cement debris in consequence of more micro-motion, which in turn cause more severe foreign body reactions, initiate osteolysis and loosening.

Ultra-high molecular weight polyethylene (UHMWPE) is the most commonly used polymer as bearing resistance or abrasion resistance materials on implant surface. The oxidation of PE will induce its degradation. The original smooth surface of PE that reduce friction and wear becomes rough and easy to wear down after oxidation degeneration (Sundfeldt et al., 2006). Super fine and irregular shape PE wear particles induced severe inflammatory response and subsequent osteolysis (Ren W.P et al., 2003; Ren et al., 2006).

Metals and their alloys, represents a large variety of engineering materials in application in medical device and implants (Bahraminasab et al., 2012). Stainless steel has been widely employed as orthopaedic implant for its easy availability, high strength, lower cost, easy fabrication, etc. (Sangeetha et al., 2010; Majid et al., 2011; Taira and Lautenschlager, 1992). However, the weakness of lower wear resistance limits its application. Moreover, the poor adherence to surrounding bone further increases the risk of inducing AL. The ion release from stainless steel in human body because of corrosion fatigue, cracking, pitting is another concern (Singh and Dahotre, 2007). Both Al and V released from implant are related to health problems, such as Alzheimer disease and neuropathy (Navarro et al., 2008; Okazaki and Gotoh, 2005). Ti

and its alloy have excellent properties including high strength, low density, resistance to corrosion, bioinert and son on. Ti related implants are advantageous since Ti is capable to integrate to surrounding bone, which is considerable for long-term fixation and avoid micro-motion. However, the shortcomings of Ti are still obvious. Though lower than stainless steel or CO-Cr alloys, the elastic modulus of Ti is still way out of the range of natural bone, which cannot reduce the stress shielding effect. Moreover, when Ti rubbed against itself or other materials, severe wear occurred (Nasser et al., 1990). The metallic wear particles cause adverse effect such as tissue blackening and metallosis (Dearnley, 1999). Therefore, the application of Ti and its alloy was restricted to area where wear resistance is not dominant. Cobalt-based alloys are superb in mechanical strength including high resistance to fatigue and corrosion induced cracking, which used mostly in stem of prosthesis for heavy load purpose. However, Co-Cr alloys with extreme high elastic modulus of about 240 GPa, causes stress-shielding effect and subsequent AL. Moreover, Co-Cr alloys has poor adherence to surrounding bone, and the released ions from Co-Cr are even more toxic than stainless steel.

In summary, the current used materials for joint replacement are vulnerable to fulfill some vital requirements, which mostly lead to long-term problems including AL. Researches has been carried on to explore alternative or new approach to replace or improve existing materials.

Septic loosening (SL)

Bone and joint infection or osteomyelitis is painful complication that it is extremely hard to treat. The successful rate of antimicrobial therapies in other infectious disease was not well applied in bone and joint infections (Lew and Waldvogel, 2004). Effective treatment usually involves a combination of implant removal, extensive debridement, and two-stage re-implantation, often with use of antibiotic spacers and cements. There is a clinical challenge for local antibiotic delivery including insufficient antibiotic content and burst drug release. Osteomyelitis is a microorganism induced inflammatory process accompanied with osteolysis and bone degeneration (Waldvogel et al., 1970). Osteomyelitis most commonly followed a continuous spread of contamination from trauma, bone surgery and joint replacement. The mechanism of the osteomyelitis is demonstrated to be associated with inflammatory response to invaded microorganism or bacteria.

Numerous inflammatory factors were induced by leucocyte, which were involved in necrosis of tissue and dissolving bone tissue. Bone debris channeled by blood supply formed sequestra and continue to provide colony space for bacteria growth, as shown in Fig.2. It is hard for antibiotics to reach to the infected site. Once infection becomes severe, osteoclasts were always associated to digest bone tissue and increase osteoporosis.

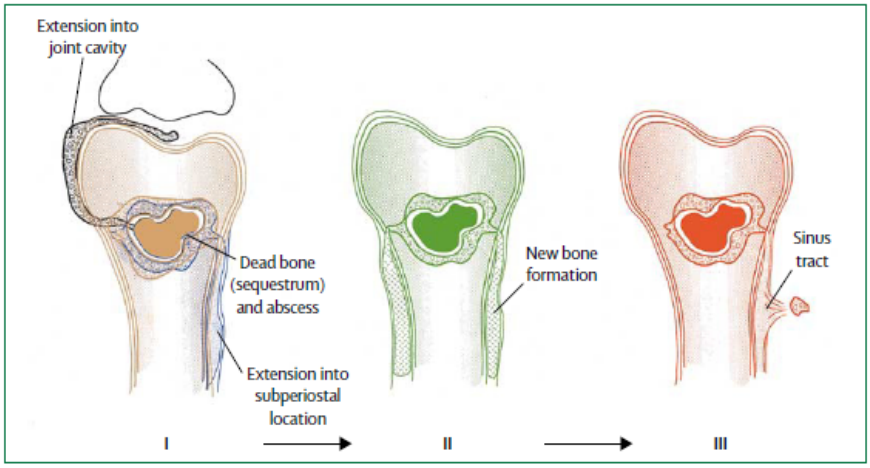

Fig.2 Illustration of osteomyelitis

The cause of osteomyelitis is associated with various microbial and host factors. *Staphylococcus aureus* (SA) is by far known as the most common microbial involved in osteomyelitis. The adhesion of SA to prosthesis surface is considered as the most crucial step for bacterial colonization and infection in early stage. SA has specific adhesins on its surface that enable to interact with host proteins, such as fibrinogen, fibronectin, collagen, vitronectin, laminin, thrombospondin, bone sialoprotein, elastin, etc. SA can also form biofilm, which is hard to treat by antibiotics. Due to the difficulty to distinguish mechanical loosening and infectious loosening in the earlier period of joint replacement, the current technology to diagnosis osteomyelitis is still need to be improved.

The medical management of osteomyelitis is well developed. Antibiotic prophylaxis has been used successfully to prevent wound infections after surgery (Boxma et al., 1996). Standard preoperative preparations (including antimicrobial shower, shaving, and soap-disinfectants) are also considered as effective to reduce

the risk of surgery infection (Lucet et al., 1990). Antimicrobial therapy is strictly administered via antistaphylococcal penicillins or first-generation (cefazolin), or second-generation (cefamandole and cefuroxime) cephalosporins decrease the rates of postoperative infection (Classen et al., 1992). However, this treatment carries risks of complications associated with a long stay in hospital and adverse events due to the use of intravenous catheters, as well as associated personal and economic costs from the extended hospital stay. The current approach to treat infected prosthesis is complete removal of the implant and replace with new one, which is high cost and suffering to patients. Therefore, a sustainable local delivery of antibiotics from prosthesis that can effectively inhibit bacteria growth is highly demanded.

CHAPTER 2 CURRENT APPROACHES

Background

Each year, over 700,000 total joint replacement (TJR) operations (hip and knee)

are performed in the US (Berry et al., 2002), and the number continues to increase with an aging population. Aseptic loosening (AL) is the most common cause of TJR failure and its incidence continues to increase(Kroell et al., 2009). Implant stability and a long-term survival of TJR require early osseointegration (the direct anchorage of an implant by bone formation at the bone-implant surface). An early and rapid osseointegration requires the recruitment of bone marrow stromal cells (BMSCs) to the periprosthetic site(Lee and Goodman, 2008). After surgery, the gap between the implant surface and surrounding bone needs to be completely bridged by newly formed bone. There is compelling evidence that a defective implant osseointegration (the formation of a piece of fibrous membrane between the implant surface and surrounding bone) leads to implant instability, micromotion, osteolysis and loosening (White et al., 2012b; Boos et al., 2008). Kärrholm et al.(Karrholm et al., 1994) reported that the subsidence of the implant is associated with an increased risk of AL. Ryd et al.(Ryd, 1992) proposed that the occurrence of implant instability and micromotion represent two of the risk factors of early implant loosening in both knees and hips. The rate, quantity and quality of osseointegration are closely related to the physiochemical and biological properties of the implant surface (de Jonge et al., 2008). More efforts are required to develop a “bone like” implant surface that shows potential for implant osseointegration.

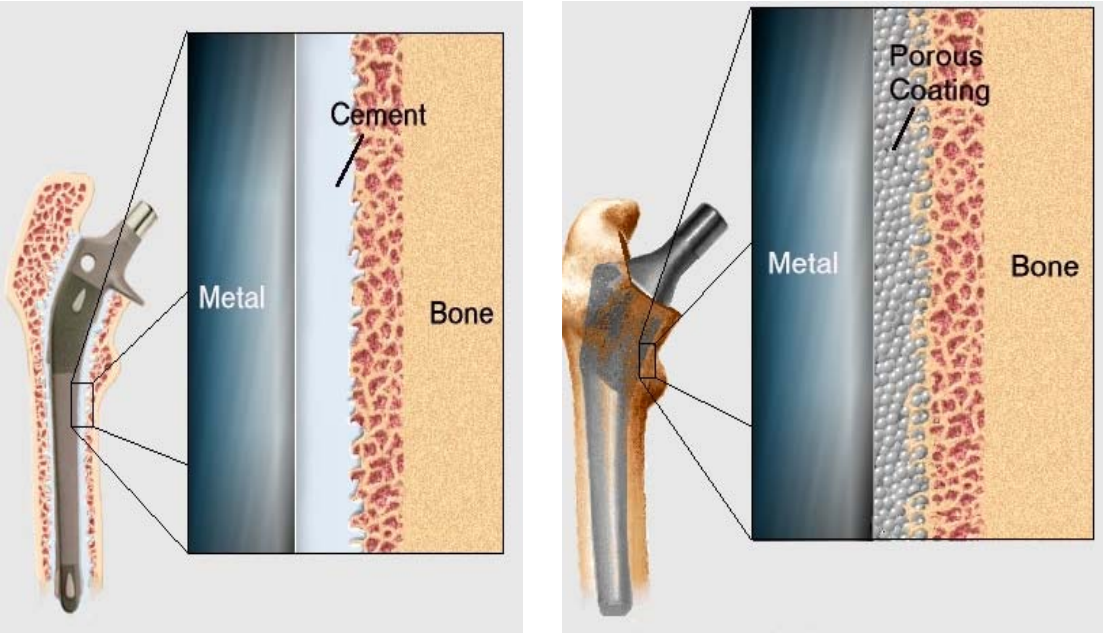

Fig. 3 Current approaches of prosthesis fixation: (left) cemented and (right) biological coating

Wear debris induced aseptic loosening (AL), which is associated with the presence of a macrophage response to wear debris particles accumulated at the interface between the implant component and the surrounding bone, is considered as a major cause for orthopaedic prosthesis failure (Bullough et al., 1988). The greatest numbers of macrophages were present in membranes from patients in all cases were associated with the presence of wear debris (stainless steel, chrome cobalt particles, PMMA, etc.) (Lennox et al., 1987). Biological coatings, or so called cementless porous coatings was deposited biomimetic Ca-P ceramics on implant surface to attempt to overcome the limitations of cement fixation. Cementless porous coating that avoids screw fixation may prevent potential egress of polyethylene particles through the shell decreases the amount of polyethylene wear debris introduced to the pelvis. However, the limitations of cementless coatings are still obvious for the brittleness, poor adhesion strength, etc

(Xu et al., 2006). Therefore, development of a “bone-like” interface between implant and surrounding bone tissue that provides reliable mechanical support would significantly reduce the risk of AL.

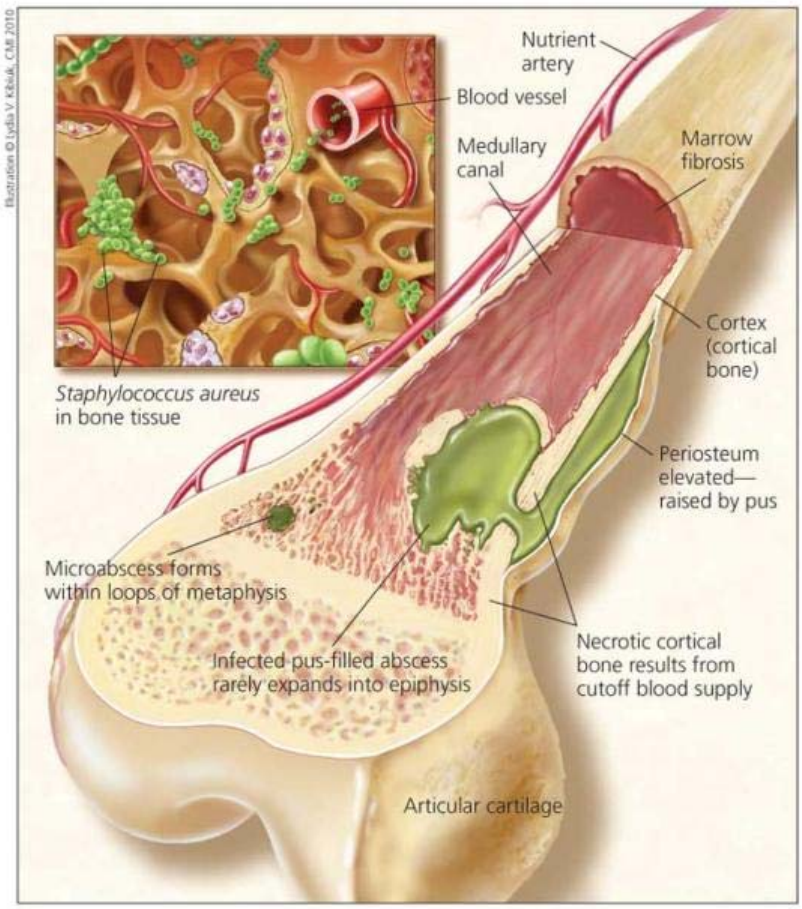

Fig.4 Illustration of S. aureus induced osteomyelitis

From another aspect, implant infections represent the most feared complications in orthopedic surgery(Perka and Haas, 2011) that eventually cause the implant failure. The incidence of periprosthetic infection after TJR (hip and knee) is > 2% among the Medicare population (Kurtz et al., 2010; Ong et al., 2009). This is a large number considering approximately 581,000 total knee and more than 193,000 total hip replacements are performed each year in the US alone. The incidence of periprosthetic

infection is higher after revision surgery than after primary surgery. Furthermore, 15% of hip revisions and 25% of knee revisions are due to implant infection (Bozic et al., 2009). Implant infection causes loss of supporting bone, as shown in Fig.4. Bacteria including Methicillin-resistant *Staphylococcus aureus* (MRSA) have a high affinity to bone, leading to osteonecrosis and osteolysis. Treatment usually requires that the implant be entirely removed, the surrounding tissue cleared of infection, and then a second prosthetic device is implanted. This can take months and an average of $50,000 per case. MRSA is one of the leading pathogens involved in periprosthetic infection (Pulido et al., 2008). The percentage of prosthetic infection with MRSA is increasing and the death rate from MRSA is 2.5 times greater than from non-resistant S. aureus infection (Fry and Barie, 2011). MRSA adhere to the implant surface, replicate and become embedded within a self-produced matrix of extracellular polymeric substance (biofilm) (Xu and Siedlecki, 2012). Numerous strategies have been attempted to prevent bacterial adhesion and biofilm formation by either implant surface fabrication or incorporation of antibiotics into the implant devices for local administration (Kankilic et al., 2011; Simchi et al., 2011a). Thus, to develop a bactericidal implant surface that provides a local sustained delivery of antibiotics to the bone/implant interface are highly demanded.

To summarize, our study is targeting on developing a bioactive and biocompatible substrate covering the orthopaedic implant surface to promote osseointegration, prevent wear-debris induced AL and inhibit osteomyelitis.

Current approaches

Hip implants may be cemented, cementless (press-fit) or a combination of both, depending on the method used to hold the implant in place. A cemented hip implant is designed to be used with bone cement, which was first used in hip replacement in 1961. First, the femoral canal is prepared and then bone cement is introduced into the femur. The surgeon then positions the implant within the femoral canal and the bone cement helps to hold it in the desired position, providing initial fixation. Cemented implants are more commonly used in older patients, patients with rheumatoid arthritis or younger patients with poor bone quality.

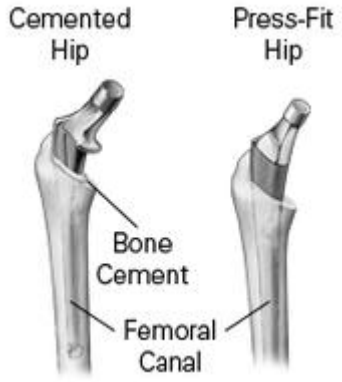

Fig.5 Cemented and Press-Fit Hip prosthesis

A press-fit hip implant is designed to be inserted into the prepared femoral canal without the use of bone cement, as shown in Fig.5. Press-fit fixation has been utilized in total hip replacement since as early as 1943. Initially, the femoral canal is prepared in much of the same way as a cemented hip implant; however, a press-fit implant is designed so that the implant fits tightly into the canal at the time of surgery. The rough

surfaces on the press-fit hip implant are designed to engage the bone within the canal, permitting bone to grow onto the roughened surface of the implant. Press-fit implants are more commonly used for younger, more active patients and patients with good bone quality.

In conclusion, new materials and technologies are therefore developed to fulfill the requirements from total joint replacement. Despite the advance in coating or spraying technologies was rapid, a completed solution to overcome the shortcomings of AL / SL induced TJR failure is still absent. Thus, there is an urgent need for a multi-functional biomaterial as a “bone-like” interface that can be developed to match biological, physiochemical and clinical requirements to integrate the bone tissue and implant components.

CHAPTER 3 PVA-HA-COLLAGEN HYDROGEL BIOLOGICAL COATING

Introduction

Implant fixation and the long-term survival of a TJR require a functional and "bone-like" implant surface matrix that will support the initiation of periprosthetic osseointegration. Basic science research and clinical trials have indicated that hydroxyapatite (HA) coating on the implant surface can enhance both the bone ingrowth and bony apposition (Geesink et al., 1987; Kim et al., 2003; Landor et al., 2009; Massaro et al., 2001; Race et al., 2010; Shepperd and Apthorp, 2005; Yoon et al., 2007; Mai et al., 2010; Gracia et al., 2010; Springer et al., 2009). However, the non-physiological surface of HA coating leads to diminished initial osseointegration of implanted prostheses (Goosen et al., 2009; Chung et al., 2008). An additional limitation of HA coating includes its brittle nature (Song et al., 2010a; Leeuwenburgh et al., 2006; Ning and Dai, 2003).

Natural bone is composed of nanohybrid organic–inorganic components shown in Fig.6. The organic matrix is mainly type I collagen (Col) which provides bone its flexibility and resilience, and the inorganic phase is composed of the mineral hydroxyapatite (HA) which is responsible for the stiffness and strength of bone. The organic–inorganic constituents combine together to provide a mechanical and supportive role in the body (de Jonge et al., 2008). It has been a long-term goal for biomaterial scientists to fabricate a "bone-like" HA coating surface that mimics the biological, structural and mechanical behavior of natural bone (de Jonge et al., 2008).

Col and HA have potential in mimicking natural bone matrix. It has become a rapidly expanding research area since a synthesized HA and Col composite could be applied for better bioactive bone graft for bone repair (Dawson et al., 2008; Wahl et al., 2007). The combination of both a ceramic and a protein polymer within one material is expected to enhance the adhesion, proliferation and differentiation of osteogenic cells (osteoblast and osteoblast precursor cells), thereby offering a benefit over current non-physiological HA coating.

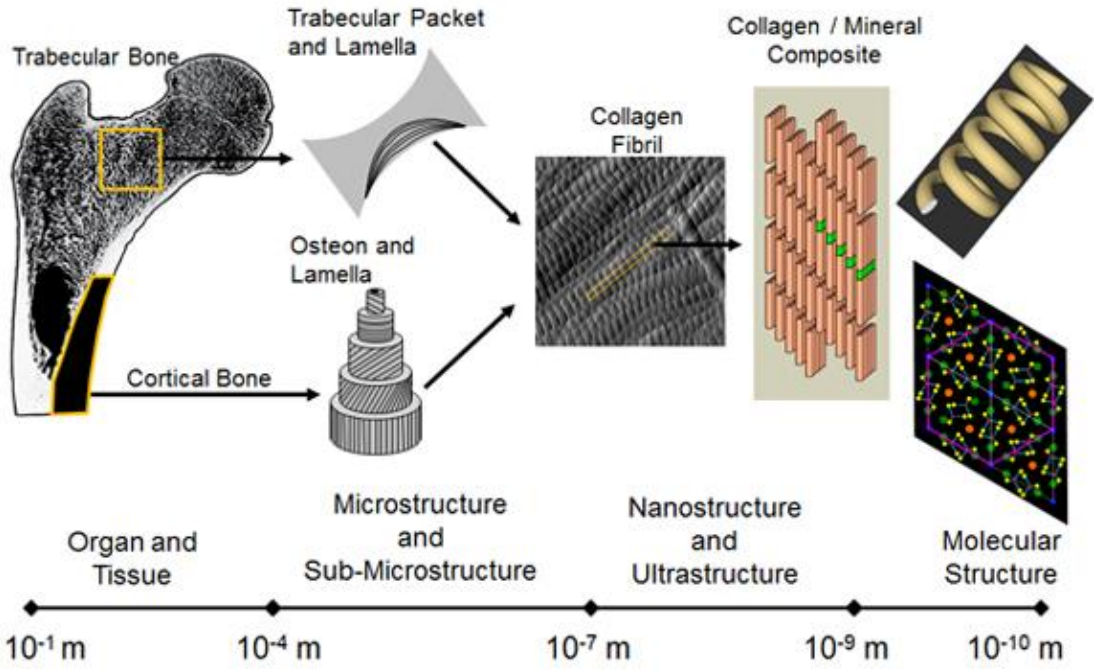

Fig.6 Bone tissue from microstructure to molecular structure

Polyvinyl alcohol (PVA), a water-soluble polymer, has been used extensively as a scaffold supporting material for tissue engineering applications. It endows mechanical strength and safety (Ngawhirunpat et al., 2009; Sailaja et al., 2009). We propose that PVA represents a promising scaffold coating material because of its biocompatibility, proven mechanical strength and anabolic effect on bone formation

(So et al., 2007; Matsumura et al., 2009; Ngawhirunpat et al., 2009; Sailaja et al., 2009). In addition, PVA hydrogels have been used in a number of biomedical applications including soft contact lenses, cartilage implants, drug-delivery matrices, temporary skin covers or burn dressings and artificial organs. This is because of their inherent non-toxicity, non- carcinogenicity, good biocompatibility, and desirable physical properties such as rubbery or elastic nature and high degree of swelling in aqueous solutions. Since pure PVA is bioinert and has limited capability to interact with the bone microenvironment, we propose to develop a "bone-like" PVA coating by incorporation of both Col and HA.

The objective of our study was to develop biodegradable PVA/Col/HA composite hydrogels to mimic the topological structure of human bone tissue. The physiochemical properties of the hydrogels (viscoelasticity, swelling, stability, mechanical strength, and embedded erythromycin release dynamics) were described. In addition, the in vitro cellular behaviors of both osteoblastic MC3T3 cells and RAW 264.7 monocytes grown on the PVA/Col/HA hydrogel composites were examined.

Materials

PVA (Mw~205,000), HA (<200 nm particle size), Col type I (from rat tail) and erythromycin were purchased from Sigma-Aldrich (St. Louis, MO). Murine MC3T3-E1 preosteoblast cell line and murine RAW 264.7 macrophage cell line were obtained from ATCC (Manassas, VA). Alpha-modified minimum essential medium (α-MEM) was

purchased from Invitrogen (Carlsbad, CA). Alkaline phosphatase (ALP) assay kit was from BioVision (San Francisco, CA). 3-(4,5-Dimethylthiazol-2-yl)-2,5-diphenyltetrazolium bromide (MTT) assay kit was from ATCC (Manassas, VA). Bovine albumin conjugated to fluorescein isothiocyanate conjugate (Albumin FITC) was purchased from Sigma-Aldrich (>7% mol FITC albumin). Ultrapure water (DNAse, RNAse Free, 0.1 micron filtered) was purchased from Invitrogen Corp.

Preparation of PVA/HA/Col hydrogel

Aqueous solutions of 13 wt.% PVA was prepared by dissolving pre-weighed quantities of PVA in distilled water and heating for 6 h at 90°C. Pre-weighed HA nanoparticles were then added to the PVA solution and thoroughly homogenized by stirring at 60°C for 4 hours at various HA/PVA ratios (w/v) (4%, 7%, 10% and 15%). The PVA solution was cooled slowly to room temperature. Then Col was mixed with the HA/PVA emulsion by stirring at room temperature to form a PVA/HA/Col solution with a final Col percentage of 13% (v/v). Secondly, 150 µL of PVA/HA/Col solution was cast into each well of a 24- or 96-well cell culture plate (Corning, Lowell, MA) until it was spread smoothly to form a coating. A freeze-thaw (F-T) treatment was used to physically crosslink the coated hydrogel. Briefly, coated plates were frozen at -20°C overnight and slowly thawed in a sterile hood (Labconco, Kansas City, Missouri) with the UV light on. The number of F-T cycles ranged from 1 to 3 (C1, C2 and C3, respectively) to prepare hydrogels with different degrees of crosslinkage. In this study, two types of coated hydrogel samples with different dimensions were separately

prepared for different assays. The thinner one (1.9 cm^2 × 0.1 cm) was prepared from a 24-well plate, while the thicker one (0.3 cm^2 × 0.5 cm) was prepared from a 96-well plate. Both types of hydrogels were air-dried in a sterile hood until weights were comparable.

Rheology of PVA/HA/Col hydrogel

An AR2000 rheometer (TA Instruments Inc., New Castle, DE) with a standard steel-parallel-plate geometry of 20 mm diameter was used for the rheological characterization of PVA/HA/Col hydrogels with (C3) or without F-T treatment before air-drying. Test methods of oscillatory stress sweep and frequency sweep were employed. The stress sweep was performed at a constant temperature (25°C) and frequency constant (2π rad/s) while increasing the stress level from 0.01 to 100 Pa. The linear viscoelastic region (LVR), from 0.01 to 100 Pa, was determined as safe region without structural breakage from oscillatory stress. Samples were subjected to a steady stress ramp and the corresponding storage modulus (*G'*) and loss modulus (*G"*) were measured. The frequency sweep was performed at a fixed stress corresponding to the point in the middle of the LVR profile. The oscillatory frequency was increased from 0.1 to 100 rad/s, and the plots of *G'* and *G"* toward frequency were obtained from manufacturer-provided software. Complex viscosities (η^*) were obtained from a flow test to plot against frequency as well.

Mechanical testing

The aforementioned thicker hydrogel samples for mechanical testing were

prepared with (C3) or without F-T treatment. These samples were tested in unconfined uniaxial compression using a universal servohydraulic test machine (Instron 4302, Norwood, MA) at a speed of 0.01 mm/sec. The maximum strain level was set to be 0.5, where the failure of the specimens was well observed. The engineering compressive stress (σ) - strain (ε) curve relationship was calculated from the Instron linear variable differential transformer (LVDT) and load cell measurements. Each group was measured in triplicate.

Swelling of hydrogels

Gels were allowed to dry in a sterilized hood until drying was complete (as verified by no change in gel weight) before swelling. For all swelling experiments, each initial hydrogel coating film was gently torn off and allowed to swell in 3 mL of sterile water at 37°C overnight. After the supernatant was discarded, samples were weighed as *W*(wet). Samples were then dried again and weighed as *W*(dry). Thus, the amount of water uptake (*WU*) was measured to evaluate the swellings by *WU* (%) *= 100 x* (*W*(wet)-*W*(dry))/*W*(dry). The initial weight of gels before swelling was also measured as reference. To further study the biomolecule-loading capability of PVA hydrogels, the incorporated Albumin FITC released from hydrogels into aqueous solution was quantified. Albumin FITC was encapsulated into PVA/HA/Col hydrogels by thorough homogenization during preparation. The PVA/HA/Col/Albumin FITC hydrogel was soaked in PBS at 37 ºC. The fluorescence intensity of supernatant was measured at each time interval of 0, 2, 4, 6, and 24 h via a UV/VIS Spectrophotometer at 485/528

(excitation/emission) nm (BioTek Synergy HT).

Bactericidal activity assay

In order to evaluate the drug delivery capability of PVA/HA/Col hydrogels, a 14-member lactone ring macrolide antibiotic, erythromycin (EM), was incorporated during hydrogel preparation. Briefly, a EM-ethanol solution was gently added to PVA and homogenized thoroughly with an ultimate concentration of 50 μg/mL (final ethanol concentration was < 1%). The hydrogel was used to coat a petri-dish (*d*=35 mm) instead of wells in a 24- or 96-well plate for this assay and F-T for 1, 2, and 3 cycles. A modified minimum inhibitory concentration (MIC) assay was developed to measure the bactericidal activity of released EM from the hydrogel. First, a Mueller–Hinton broth inoculated with *Staphylococcus aureus* (*S. aureus*) at the concentration of 1–2 $\times 10^8$ colony forming units/ml (CFU/ml) (OD reading at 625 nm was around 0.08-0.1) was prepared. Second, 2 mL of sterile PBS was added to the coated petri-dish and incubated at 37°C. Supernatant was withdrawn at 5, 24, 29, 49, 121 and 194 h and immediately added to 1 mL bacteria-suspended broth (OD=0.1). The bacterial suspensions were further incubated at 37°C overnight and then measured. The bactericidal activity was evaluated by dynamic measurement of OD reading at 625 nm (Song et al., 2011b). Bacterial culture suspension in the absence of EM was included as a positive control.

Culture of MC3T3 and RAW 264.7 cell lines

MC3T3 cells were seeded at a density of 5×10^4 cells/well (24-well plate) onto the

surfaces of coated PVA/HA/Col hydrogels. MC3T3 cells were then cultured for 11 days in α-modified minimum essential medium (α-MEM, Invitrogen) supplemented with 10% fetal bovine serum (FBS, Invitrogen), 10 mM β-Glycerophosphate (Sigma Aldrich), and 1% (v/v) mixture of penicillin and streptomycin (Invitrogen) at 37ºC in a humidified incubator with 5% CO_2. In separate experiments, RAW 264.7 cells were seeded on the coated hydrogels at a density of 5×10^4 cells/well (24-well plate) onto the surfaces of coated PVA/HA/Col hydrogels. RAW 264.7 cells were then cultured in Dulbecco's modified Eagle's medium (DMEM, Invitrogen) supplemented with 10% FBS (Invitrogen) and antibiotics (1% (v/v) mixture of penicillin and streptomycin) for 72 hours. Cells cultured in the absence of PVA/HA/Col hydrogels were included as controls.

MC3T3 cellular response

Cytotoxicity was determined by measuring the release of lactate dehydrogenase (LDH) from dead or dying cells into the culture medium by colorimetric method following the manufacturer's instruction (Roche Diagnostics BmbH). Blank culture medium was used as a blank control and the total cell lysate was used as a positive control. LDH activity was expressed as mean optical density (OD). Attachment and proliferation of the murine osteoblastic MC3T3 cell line on PVA/HA gel matrices were investigated by measuring the content of MTT (3-(4,5-Dimethylthiazol-2-yl) -2,5-diphenyltetrazolium bromide) in cell lysates from the gel. The influence of HA incorporation, HA ratio and F-T cycles on cell viability was investigated via LDH and MTT assays.

After seven days in culture, the cells were stained using a live/dead cell viability kit (Invitrogen). The effects of HA and EM incorporation, HA ratio, collagen content, etc. on MC3T3 cells' viability were investigated. To induce MC3T3-E1 cell differentiation, the basic medium was supplemented with 0.2 mM ascorbic acid and changed every 3 days. After culturing 11 days, the cells (ALP assay buffer 250 µl/well) were harvested to collect lysate for the ALP assay according to manufacturer's protocol.

RAW 264.7 cellular response

The nitrite (NO_2^-) concentration released from RAW 264.7 cells was measured to investigate the macrophage activation (Bosnjakovic et al., 2011). Instead of using lipopolysaccharide stimulation, PVA/HA/Col hydrogel was mixed with seeded RAW cells as inducers for macrophage activation. After culturing for 72 h, cell culture supernatants were analyzed for nitrite (NO_2^-) by the Griess reaction (Green et al., 1982). Briefly, 80 µL of collected medium were mixed with 40 µL of Griess Reagent 1 (1% solution of sulfanilamide in 5% phosphoric acid) and 40 µL of Griess Reagent 2 (0.1% solution of N-(1-napthyl)ethylene-diamine in H_2O) at 25ºC and kept in the dark for 15 min before the OD was determined. Fresh culture medium was used as the blank in all experiments. The amount of nitrite was calculated from a sodium nitrite standard curve.

Statistical analysis

Data were analyzed with SPSS Version 12.0 (SPSS Inc., Chicago, IL, USA). All values

are expressed as mean ± standard deviation. Analysis of Variance (ANOVA) was used to analyze the experimental data from all the experiments. Statistical significance was set to p <0.05.

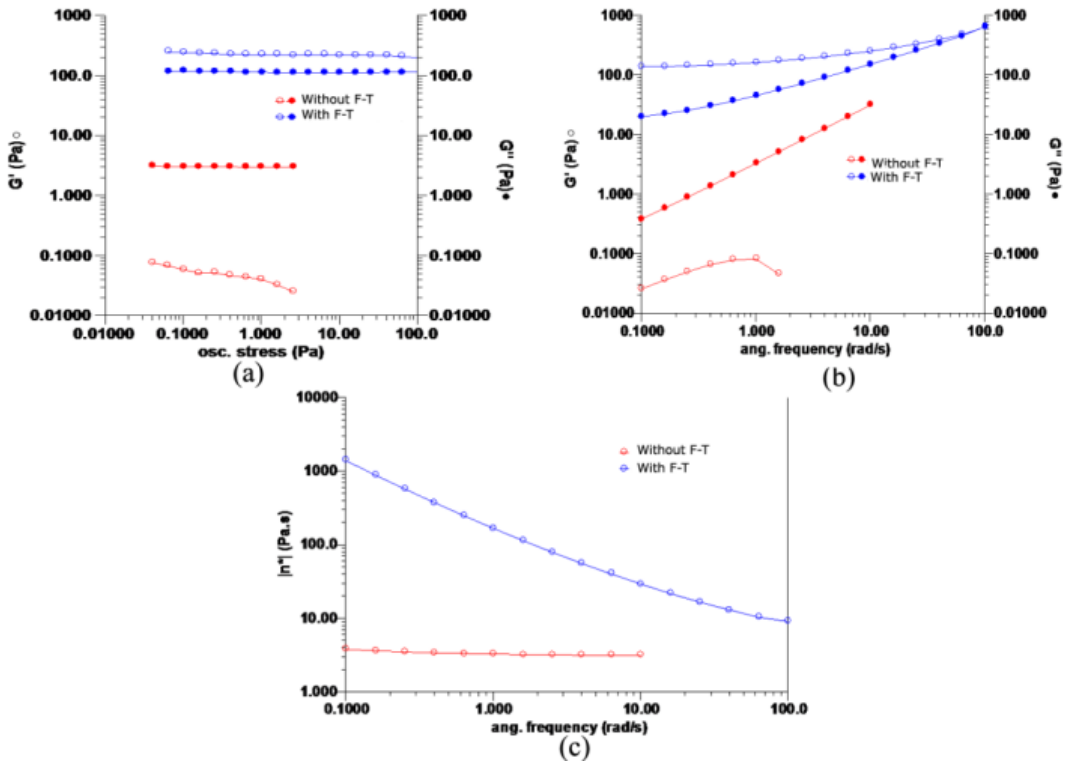

Fig. 7 Rheological properties of PVA/Col/HA gels before and after F-T treatment (C3); HA content = 10%. Storage modulus (*G'*) and loss modulus (*G''*) profiles across: (a) a oscillatory range of 0.01–100 Pa at 25°C; (b) a frequency sweep of 0.1–100 rad/s at 25°C, and (c) complex viscosity across a frequency sweep of 0.1–100 rad/s at 25°C.

Results

Rheological properties of hydrogel

Fig. 7(a) shows the storage modulus (*G'*) and loss modulus (*G"*) independence of oscillation stress sweep for the applied non-destructive stress on F-T (C3) and non-F-T

PVA/Col/HA hydrogel before air-drying. In the stress range from 0.01 to 100 Pa, the non-F-T gel showed higher *G″* than *G′*, indicating the prevalence of viscous fluid behaviors, while the F-T gel showed higher *G′* than *G″*, indicating the dominant elasticity. The conversion of *G′* over *G″* of the hydrogel after F-T suggested the formation of an intermolecular network structure. Fig. 1 (b) shows the *G′*/*G″* dependence of the frequency sweep with fixed stress load on F-T (C3) and non-F-T hydrogels. The viscoelastic behaviors of both samples were in agreement, as both showed stress sweep. An increase in both *G′* and *G′′* as the frequency increased was revealed and the decrease of *G′* slope along with the frequency decrease suggested the weakly structured system in the F-T hydrogel. The merging of *G′*-*G″* plot at higher frequencies (>10 rad/s) indicated the breakage of network structure for the F-T hydrogel. As shown in Fig. 1 (c), the complex viscosities (η^*) of the F-T hydrogel were decreasing across the frequency range (indicating pseudoplastic behavior), while the η^* of the non-F-T hydrogel showed independence from frequency change (indicating a non-cross-linking structure). The dismantling of structural linkage caused by higher frequencies of shear stress was more significantly revealed as the η^* decrease of F-T hydrogel. Taken together, the F-T process was capable of forming a cross-linked structure in the PVA/Col/HA hydrogel, which modified its viscoelasticity.

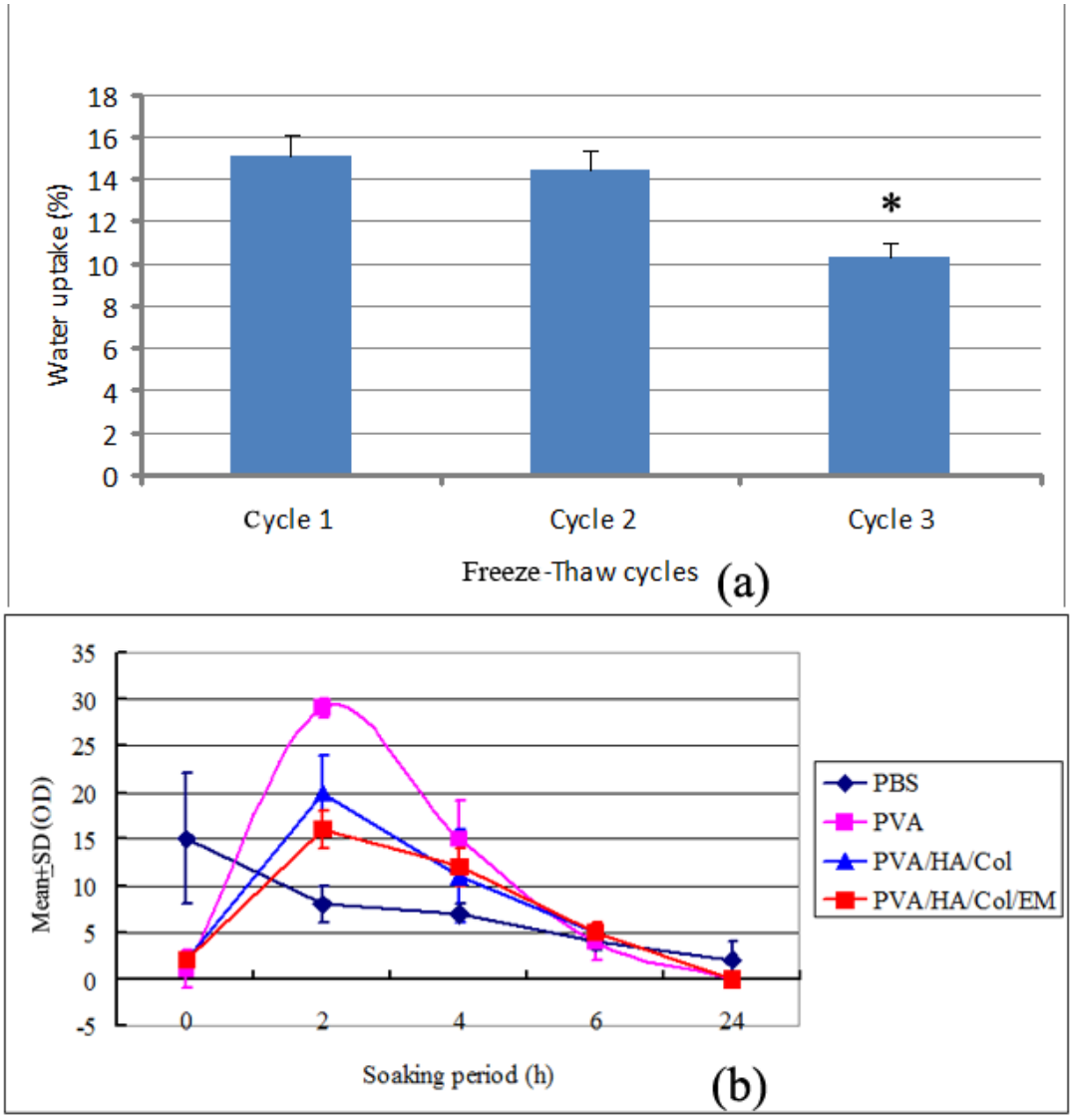

Fig. 8 (a) Swelling properties of PVA/Col/HA gels after 1, 2 and 3 cycles of F-T treatment and (b) quantification on fluorescence intensity of released albumin FITC from PVA, PVA/Col/HA and PVA/Col/HA/EM gels; HA content = 10%. *n*=3, **p*<0.05 for C3 versus C1 and C2.

Swelling property and FITC release from hydrogels

All PVA/Col/HA hydrogels prepared by F-T (C1, C2 and C3) treatments were swelled in water to evaluate the swelling and dissolution behaviors. The percentage of water uptake can be considered as proportional to the swelling ratio of hydrogel, as shown in Fig. 8 (a). It can be seen that the swelling ratio of hydrogel was decreased

with the increase of F-T cycles. Hydrogel treated for 3 cycles of F-T (C3) showed the minimum water uptake amount, which suggested the least swollen structure. The increased F-T cycles lead to increased physical cross-linking and therefore higher degrees of crystallinity (Hassan and Peppas, 2000b). Thus, the immobility of molecules in hydrogel with higher cross-link density and crystallinity limited the swelling ratio of hydrogel treated by more F-T cycles.

The measurement of incorporated Albumin-FITC releasing into the culture medium demonstrated the extended release of entrapped components, as shown in Fig. 8 (b). The FITC fluorescence signal in PBS constantly decreased during the 24-hour incubation, while FITC released from the PVA gel peaked at 2 h before decaying gradually. FITC entrapped in PVA, PVA/Col/HA and PVA/Col/HA/EM all released in the same pattern.

Mechanical property of hydrogels

Fig. 9 (a) shows the measured stress-strain for compressing the PVA/Col/HA hydrogel with (F-T) or without F-T (non-F-T) treatment. It showed that the stress vs. strain curve of F-T hydrogel went over a linear elastic region of <10% strain, and a logarithmic plastic or densification region after stress yielding point under further loading. In comparison, the slope of non-F-T hydrogel in elastic region was smaller, and stress level was lower, which indicated the softer nature in content. After the yield point, both F-T and non-F-T hydrogels continued deformation on account of strain hardening in a similar pattern and slope. The integral of the stress–strain curve

represents a specific energy (energy per unit volume) that the hydrogel structure could absorb. F-T hydrogel showed higher energy absorption capability during loading stage. Fig. 9 (b) showed the F-T hydrogel maintained a higher Young's modulus as well, as calculated from the linear curve in elastic region.

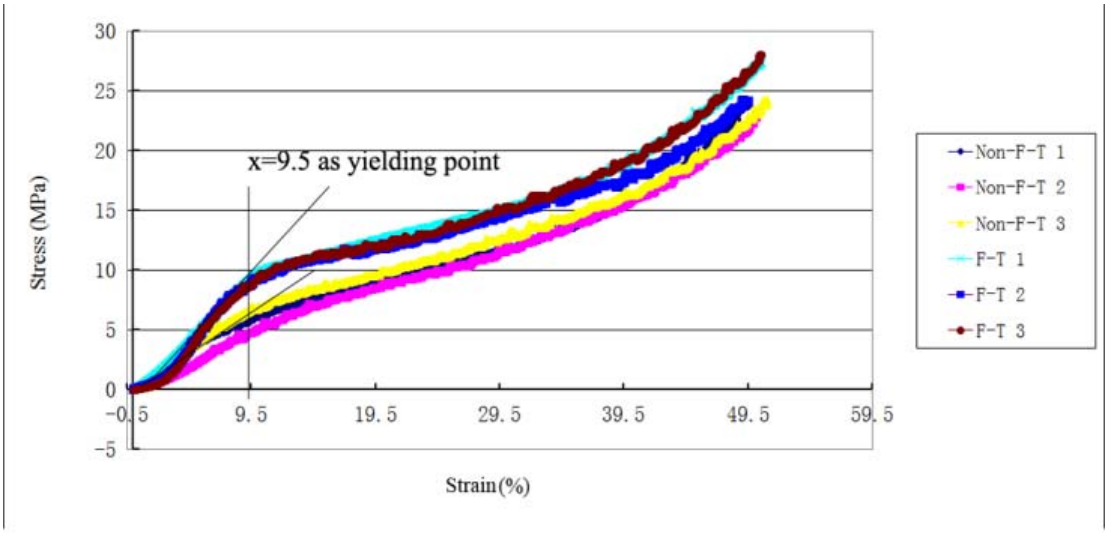

(a)

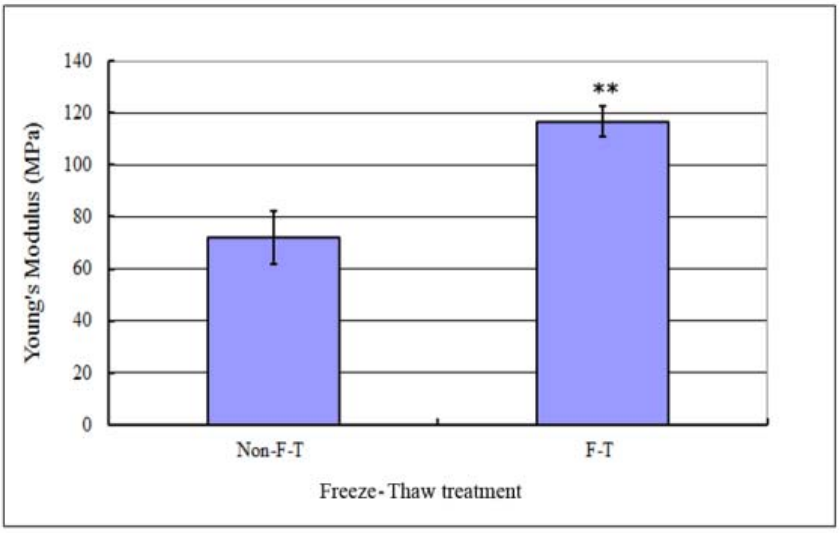

(b)

Fig. 9 (a) The compressive stress (σ) - strain (ε) curves and (b) calculated Young's

modulus of PVA/Col/HA gels without and with F-T treatment (C3). n=3, **p<0.005 related to F-T against Non-F-T.

Bactericidal activity

EM, one of the macrolide antibiotics, has been used for infectious diseases for more than 50 years. EM is susceptible to loss of its bactericidal activity in the acidic environment. We incorporated EM into the PVA/Col/HA hydrogel using 1, 2 and 3 cycles of F-T treatments to study its bactericidal activity after release. In Fig. 10, the results of a semi-quantitative bactericidal activity assay shows the bacterial growth was inhibited by EM released during culturing, which suggested hydrogels treated by different F-T cycles were capable of retaining the drug stability before release. Moreover, medium from hydrogel treated with 3 F-T cycles showed significantly higher inhibitory effect (p<0.05) within 29 h on bacterial proliferation, which indicated the longer sustained release. Bacterial growth was suppressed for over 49 h of culture, suggesting the EM stability released from hydrogels. These data indicated that EM retained longer durability and bactericidal activity in PVA/Col/HA hydrogel.

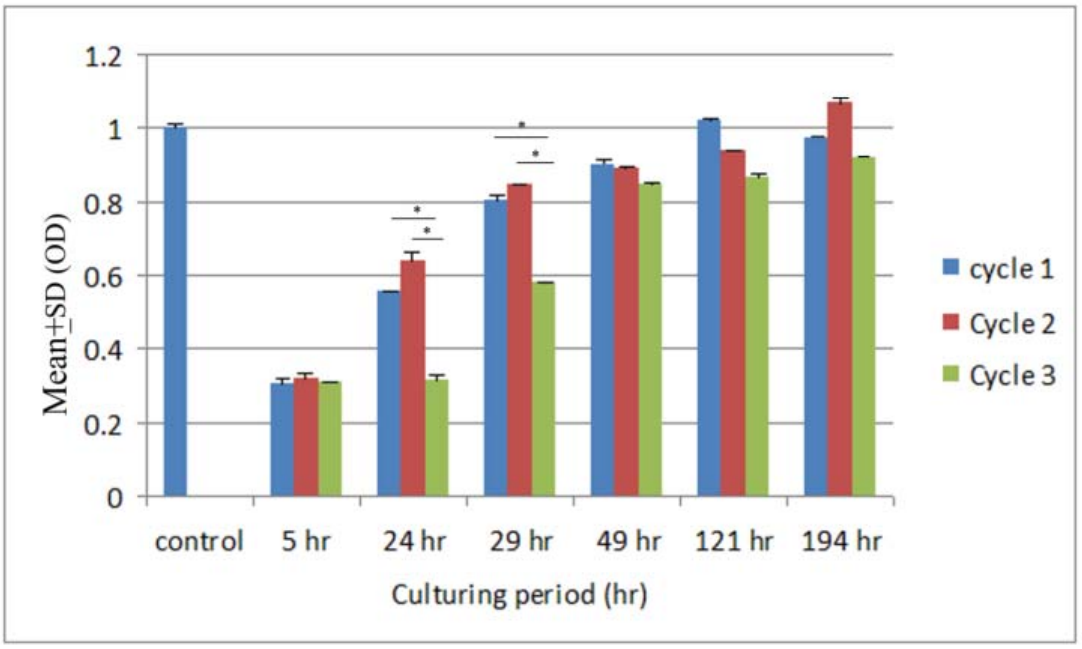

Fig. 10 Bactericidal activity of released EM from PVA/Col/HA gels treated by 1, 2 and 3 F-T cycles. A semiquantitative bacterial growth inhibition assay in broth treated with medium containing released EM at predetermined time points. Control—the initial OD of bacterial solution. *n*=3.

Viability and growth of MC3T3-E1 cells

Live-dead cell staining was utilized to study the cell viability of MC3T3 cells with PVA/Col/HA gel after 7 days in culture, as shown in Fig. 11. The attachment and proliferation of live MC3T3 cells (green) seeding on gel matrix can be visualized, showing well the compatibility of the cell with the gel. However, the morphology of cells growing on gels with different components and percentages of HA differed, and cell density varied as well. Cells seeded on PVA gel showed less proliferation in comparison with control cells. The addition of collagen and EM further reduced the live cell amount. However, cells on PVA gel incorporating HA showed higher density and well-spreading morphology. In comparison, PVA gels with 7% and 10% of HA had higher cell density and evenly-spreading morphology than 4% and 15%. The addition

of collagen and EM enhanced the cell attachment and proliferation as well. There were only a few dead cells (red) observed, which indicated the cytocompatibility of prepared gel matrices.

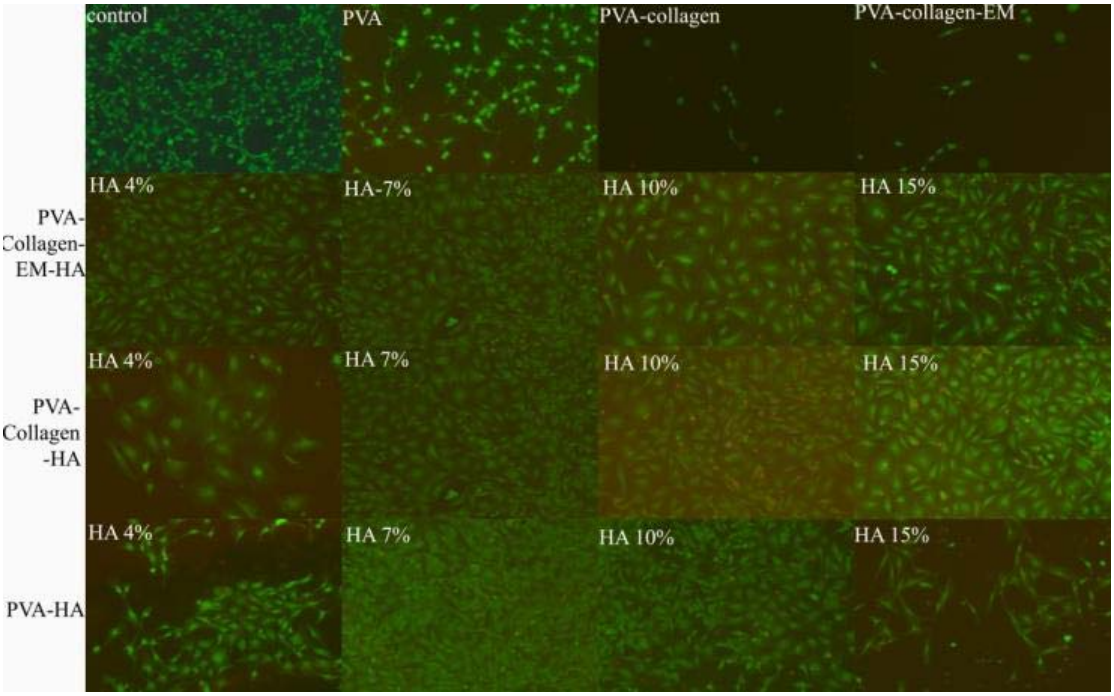

Fig. 11 The live (green) -dead (red) staining of MC3T3 cells cultured on PVA, PVA/Col, PVA/Col/EM, PVA/Col/HA, PVA/Col/HA/EM, and PVA/HA with HA percentages of 4%, 7%, 10% or 15% for 7 days. Magnification: 100×.

To determine whether PVA/Col/HA hydrogel was cytotoxic, the LDH activity released into the culture medium was measured. As shown in Fig. 12 (a, b), the LDH activity in culture medium from F-T hydrogel (C1, C3) treated cells is lower than that in untreated cells (no gel coating), suggesting that PVA/Col/HA hydrogel provided a “bone-like” matrix for cell growth and reduced the number of apoptotic or dead cells during cell culture. Since the intracellular LDH corresponded to the number of cells in the culture, quantification of LDH activity in cell lysates can be used to measure cell growth. As shown in Fig. 12 (c), an enhanced cell growth was found in hydrogel-treated

cells as compared to untreated cells. In addition, the incorporation of different amounts of HA (4%, 7%, 10% and 15%) into PVA gels greatly enhanced the cell growth, especially in the hydrogel with 10% HA incorporation. The incorporation of Col and EM showed little effect on cell growth. The enhanced cell growth on the PVA/Col/HA hydrogel was further confirmed by the counts of total cell numbers 3 days after culture (Fig. 12 (d)) and the MTT assay (Fig. 12 (e, f)).

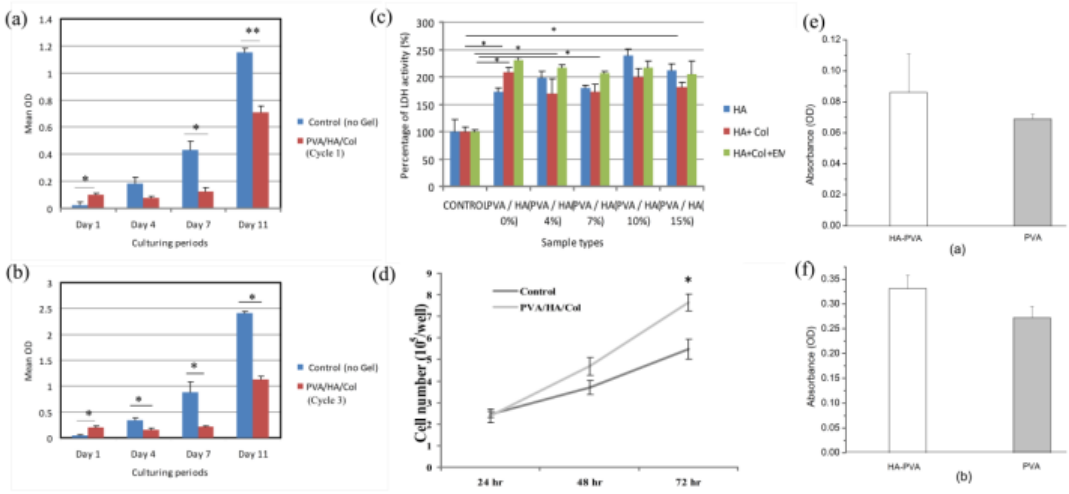

Fig. 12 MC3T3 cell activity assay. LDH levels in culture medium from MC3T3 cells on PVA/Col/HA gels after (a) 1 and (b) 3 cycles of F-T treatment in 11 days, HA content= 10%. (c) LDH levels in cell lysate from MC3T3 cells on PVA/Col/HA gels with 4%, 7%, 10% and 15% of incorporated HA after culturing for 7 days. (d) Cell numbers quantified from cells growing on PVA/Col/HA gels and well plate (control) during 72 hours of culturing, HA content= 10%. MTT assay results of MC3T3 cells on gels with and without HA incorporation after (e) 3 days and (f) 7 days of culture, HA content= 10%. n=3, *p<0.05, **p<0.005.

ALP activity of MC3T3 cells

To determine the effects of PVA/Col/HA hydrogel on osteoblast differentiation, intracellular ALP activity was measured. As shown in Fig. 13, a higher ALP activity was found in cells cultured on hydrogels with F-T treatment (C1 and C3) compared to untreated cells.

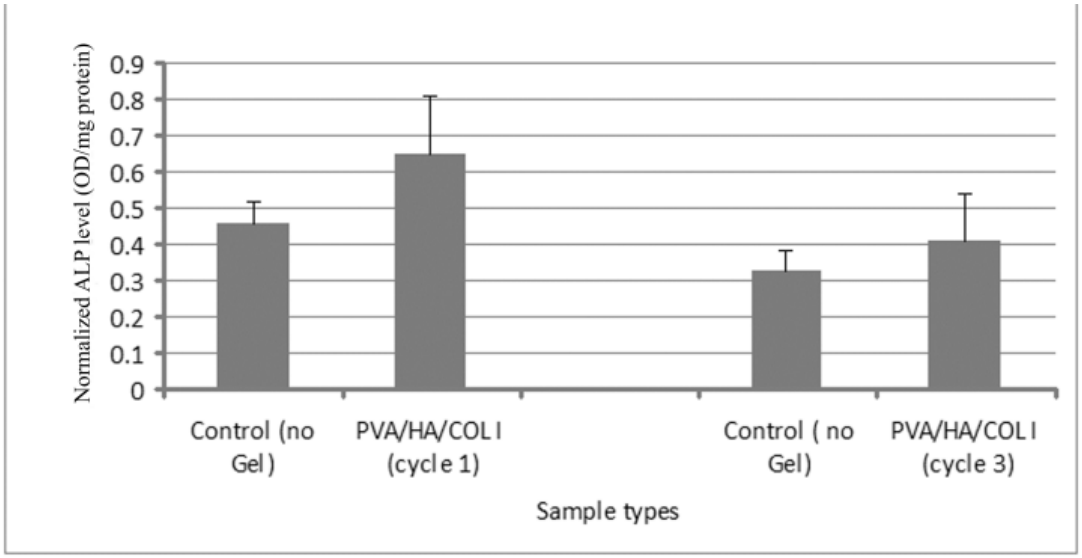

Fig. 13 Normalized ALP activities of MC3T3 cells cultured on PVA/Col/HA gels with 1 and 3 cycles of F-T treatments. Control—cells cultured on well plate. *n*=3.

Viability and nitric oxide (NO) production of RAW 264.7 cells

As shown in Fig. 14 (a), there was no significant difference in the released LDH activity in hydrogel-treated cells as compared to untreated cells. The incorporation of HA (0-15%) in the PVA/Col gels had little effect on the released LDH activity. Interestingly, the incorporation of EM resulted in a significant reduction (*p<0.05) of released LDH activity in PVA/Col gels with both 10% and 15% of HA incorporation.

NO synthesis is increased in a various types of diseases and represents one of the inflammation markers. An increase of NO production can be induced by lipopolysaccharide (LPS) stimulated treatment of RAW 264.7 macrophages (Lee et al., 2010). As compared to cells growing on HA incorporated gels, RAW cells cultured on non-HA incorporated gels had significantly higher NO production (Fig. 14 (b)). The incorporation of HA showed a dose-dependent reduction of NO production, and the

incorporation of Col in the gels had a slight additional effect in reducing the NO production. The addition of EM had no effect on NO production.

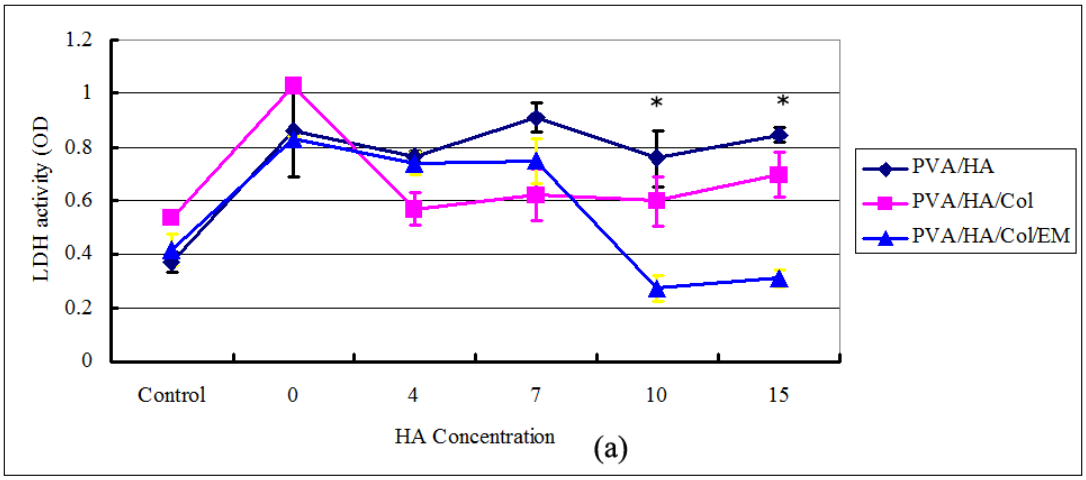

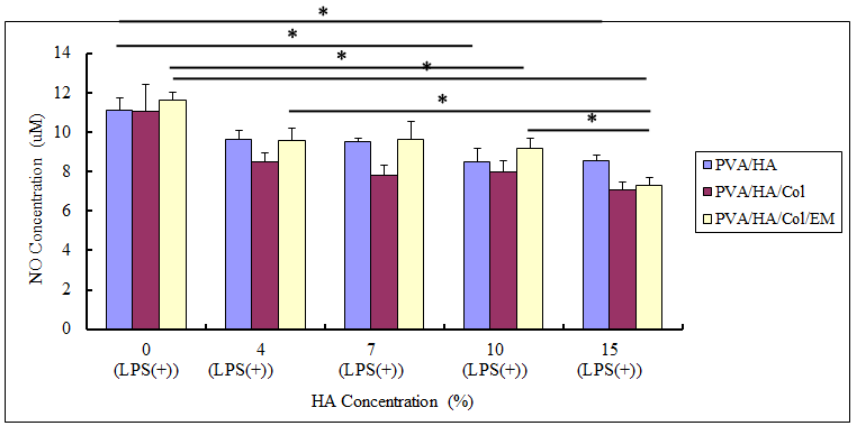

(b)

Fig. 14 LDH and NO assays for RAW 264.7 macrophage cells cultured with gels. (a) LDH levels in cell lysate from RAW cells on PVA/HA, PVA/Col/HA and PVA/Col/HA/EM gels with HA percentage of 4%, 7%, 10% and 15% for 14 days of culture. (b) NO produced from activated RAW cells growing on PVA/HA, PVA/Col/HA and PVA/Col/HA/EM gels with HA percentage of 4%, 7%, 10% and 15% for 14 days of culture. n=3, *p<0.05.

Discussion

Failure of osseointegration (direct anchorage of an implant by bone formation at the bone-implant surface) represents one of the main causes leading to implant failure

and loosening (Ramaswamy et al., 2009). Development of “bone-like” implant surface substitutes that are ‘‘intelligent” to enhance osseointegration is a clinical challenge. We reported here a “bone-like” PVA/Col/HA hydrogel composite that mimics the biological, structural and mechanical behavior of natural bone. We found that PVA/Col/HA gel provides a 3D scaffold matrix to increase preosteoblast cell adhesion, proliferation, and differentiation. The PVA/Col/HA hydrogel composite also can be used as a drug delivery device for a sustained and controllable release of antibiotics (e.g., EM) and other drugs.

A bioactive implant surface can be created by the immobilization of biomolecules into the implant surface coating matrix (de Jonge et al., 2008). Two approaches have been reported to immobilize biomolecules onto coating matrix: (1) covalent attachment to active surface groups, and (2) non-covalent interactions by physical adsorption (van der Waals, ionic bonds, hydrogen bonds, or hydrophobic interactions). Physical adsorption, such as dip-soaking method, is simple and can be performed under mild conditions. The limitations of dip-soaking method include low coating efficiency, burst release of embedded biomolecules and the impact of the solution’s nature (pH, temperature and ion strength, etc.). Wahl et al. (Wahl and Czernuszka, 2006a) reviewed the most common routes for fabricating Col/HA composites and found that the mechanical and biological properties of these Col/HA composites can be improved by the modification of the collagen type, the cross-linking methods, etc.

PVA, a highly water soluble polymer, was used to embed HA/Col/EM in the

current study. It has been demonstrated that the encapsulated nano-HA and collagen can form hydrogen bonds with PVA molecules (Asran et al., 2010a). Matsumura et al. (Matsumura et al., 2009) demonstrated that the incorporation of HA in the PVA gel significantly enhanced the cell adhesion, differentiation and growth in a murine pre-osteoblast MC3T3-E1 cell line. FTIR analysis showed that the inclusion of HA in the PVA gel remarkably enhanced the material strength, lowered the swelling and resulted in a longer drug release (Tang et al., 2009). A hydrogen bond interaction between PVA and HA through their -OH groups leads to the development of mineralized structure with functionalized surfaces and improved thermal properties. The unique physiochemical features of the PVA/HA composite represent a promising formulation for a wide variety of future applications in the field of bone regeneration. Our data indicated that the PVA/Col/HA gels are not only “biomimetic” (structural, mechanical, cellular and molecular), but also provides a sustained and controlled local EM release, as these events are most significant to the orthopedic infection and bone defect. The composite of Col and HA in the implant surface (Fan et al., 2005; Schliephake et al., 2003) improves early bone ingrowth and behaved mechanically in a superior way than the individual components. The ductile properties of Col increased the poor fracture toughness of HA. The addition of Col to the HA structure provides additional advantages, such as shape control, spatial adaptation, increased particle and defect adhesion, and the capability to favor clot formation and stabilization (Wahl and Czernuszka, 2006b).

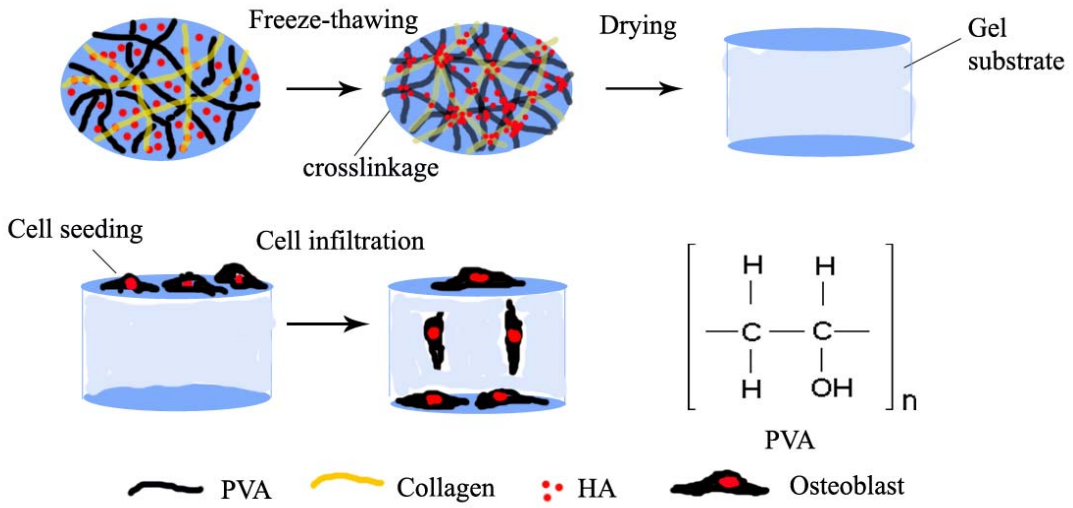

Fig.15 Illustration of gelation process of PVA-HA-Collagen hydrogel and cell infiltration in gel matrix

A repeated freeze-thawing (F-T) treatment provided physical cross-linking of the PVA hydrogel by the intermolecular hydrogen bond formation (Hassan and Peppas, 2000b). Our results indicated the stiffness of gel increased as F-T cycles increased. Interpenetrating network structure of the denser PVA hydrogel provides an extracellular matrix (ECM) like structure that promotes the cell adhesion, proliferation and differentiation. In physiological conditions, ECM provides cells with topographical features that trigger intracellular signaling cascades by interacting with the cells through their transmembrane integrin receptors. The encapsulation of nano-HA and Col in the PVA gel provided numerous anchorage sites and appropriate mechanical reinforcement for the cell adhesion and growth, as we observed (Figs. 5-8). In addition, PVA hydrogel is hydrophilic and biodegradable and has been used as one of the drug delivery devices (Jensen et al., 2011). In this study, we embedded the EM into the PVA/Col/HA gels and found that the physically cross-linked PVA/Col/HA gels

significantly extended the EM release and retained longer bactericidal activity.

This study has some limitations. First, PVA gel has a relatively weak adhesion strength as compared to HA coating, and a paste of PVA gel coating might reduce the porosity and interconnectivity beneath the implant's HA coating. Although the PVA coating is degradable after being put into a physiological environment, the potential impacts of PVA coating-induced reduction of pore porosity and pore interconnectivity on cellular behaviors and bone ingrowths warrants further investigation. Second, we need to determine whether the HA and Col has been dispersed evenly in the capsulation of hydrophilic PVA gels, which might interfere with the biomimetic nature of the PVA gel matrix and the cell behavior. Finally, the physiochemical properties and optimal formulations of PVA/Col/HA gels need to be characterized in order to reach the desired drug release profiles.

Conclusion

An implant surface PVA/Col/HA gel coating matrix was developed and characterized. We found that the PVA/Col/HA gel provides a "bone-like" extracelluar matrix and its mechanical strength can be enhanced by repeated freeze-thawing cycles. PVA/Col/HA gel matrix is biocompatible and enhances the adhesion, growth and differentiation of bone cells in vitro. In addition, PVA/Col/HA gel can serve as a sustained drug release carrier to enhance osseointegration and prevent prosthesis infection.

CHAPTER 4 MONOLITHIC ELECTROSPUN NANOFIBERS

Introduction

Natural bone is composed of a complex hierarchical structure with mineralized collagen fibrils and HA nanocrystals (Stanishevsky et al., 2008). The organic matrix is mainly Type I Collagen (Col) which provides bone its flexibility and resilience, and is important for cell adhesion and migration (Stanishevsky et al., 2008). The inorganic phase is composed of mineral hydroxyapatite (HA) which is responsible for the stiffness and strength of bone. Nano scale-HA crystals are crucial for osteoinduction, biomineralization and osteointegration (Wei and Ma, 2004). The organic–inorganic constituents combine together to provide a mechanical and supportive role in the body (Pramanik et al., 2009). Osseointegration is defined as the direct anchorage of an implant by bone formation at the bone-implant surface. Many research efforts have been directed towards improving the bone/implant interface, with the aim of accelerating bone healing and improving bone anchorage to the implant (Park, 2011; Gittens et al., 2011; Hermida et al., 2010; Junker et al., 2009; de Jonge et al., 2008; Borsari et al., 2007; Perla and Webster, 2005). One of many research strategies is to develop a biopolymer-based implant surface with “bone-like” nature (structural, mechanical, and biological behavior) (Omar et al., 2010; Zhang et al., 2010; Tan et al., 2006; De et al., 2004). HA composites with biodegradable polymers, such as poly lactide (PLA) or poly (lactide-co-glycolide) (PLGA) (Kim et al., 2006b), were fabricated

to reduce the implant surface fragility. However, unfavorable effects of acidic degradation products (lactic and glycolic acid) from these polymers on the cells surrounding the implants have become a concern (Estey et al., 2006; Fu et al., 2000). Polyvinyl alcohol (PVA), a water-soluble and biodegradable polymer, has been used extensively in the pharmaceutical industry because of its biocompatibility, proven mechanical strength and anabolic effect on bone formation (So et al., 2007; Matsumura et al., 2009; Ngawhirunpat et al., 2009; Sailaja et al., 2009). In addition, PVA has self-crosslink capability (film or hydrogel forming) due to the abundant number of hydroxyl groups in their side chains (So et al., 2007; Matsumura et al., 2009; Ngawhirunpat et al., 2009; Sailaja et al., 2009).

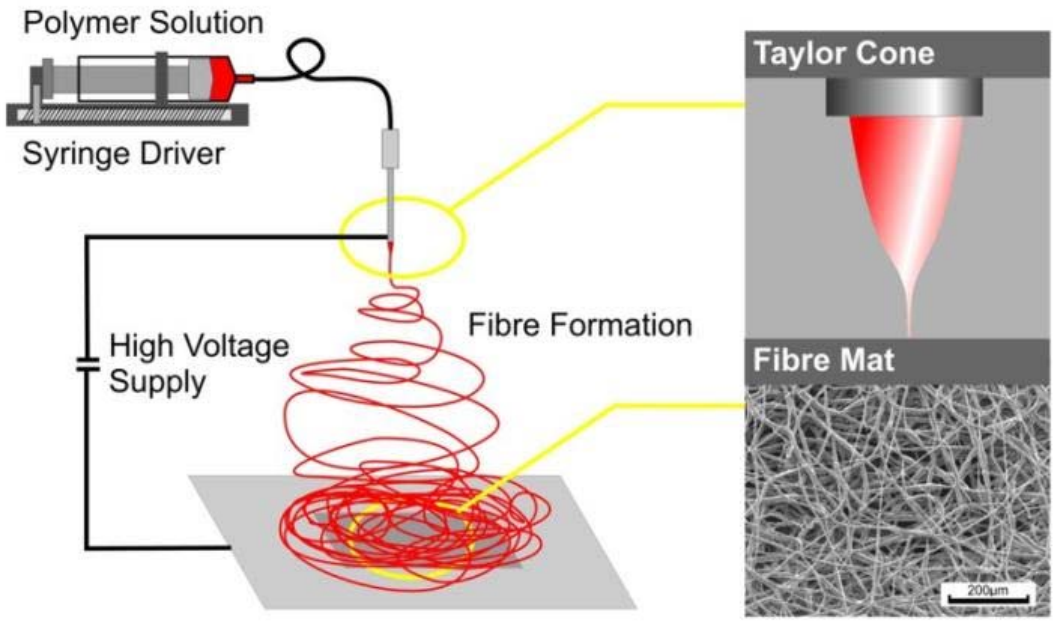

Fig. 16 Illustration of electrospining nanofibers set-up and mechanism of fiber formation

Nanoscale topography of implant surface is critical for the capacity of

osseointegration (Gittens et al., 2011; Mendonca et al., 2009; Dalby et al., 2006). Different topographies, methods and materials have been developed to enhance osseointegration (Dohan Ehrenfest et al., 2010; Tomisa et al., 2011; Gittens et al., 2011; Dohan Ehrenfest et al., 2010; Huang et al., 2008). One alternative approach has been the electrospun nanofibers (Prabhakaran et al., 2009; Asran et al., 2010b; Francis et al., 2010; Schofer et al., 2008). Electrospinning is a process in which a charged polymer jet is collected on a grounded collector; a rapidly rotating collector results in aligned nanofibers while stationary collectors result in randomly oriented fiber mats, as shown in Fig.16. Electrospinning forms superfine fibers with diameters ranging from 10 μm down to 10 nm by forcing a polymer solution with an electric field through a spinneret (Torres-Giner et al., 2009). The advantages of electrospun nanofibers over conventional film-casting techniques include a high surface area, high mass to volume ratio and a small inter-fibrous pore size with high porosity (Ifkovits et al., 2009). These features make electrospun polymeric fibers excellent candidates for fabrication of implant surfaces and for controlled periprosthetic drug delivery (Kim et al., 2008; Sargeant et al., 2008; Asran et al., 2010b; Cho et al., 2009; Ekaputra et al., 2009). Organic solvents or acids are usually required to dissolve either synthetic (PLGA and PLA, etc) or natural (chitosan, gelatin, collagen, etc.) polymers (Duan et al., 2007; Yoshimoto et al., 2003; Huang et al., 2001; Shin et al., 2001; Zhou et al., 2008) prior to electrospinning (Huang et al., 2003). PVA is a water-soluble and has better nanofiber forming capability (Wu et al., 2005; Zhou et al., 2008), in part due to its

sufficiency in electroconductivity (Kenawy et al., 2003; Wu et al., 2005). However, the limitation of PVA nanofibers are obvious, including fast hydrolysis (Yao et al., 2003), and its bioinert nature (Asran et al., 2010a) that hinder the protein and cell adhesion (Schmedlen et al., 2002). Thus, additional efforts are required to incorporate nano HA particles and collagen into PVA nanofibers to mimic natural extracellular bone matrix.

Followed by the idea from previous chapter, we developed a biomimetic nanofiber scaffolds consisting of PVA-Collagen with unidirectionally aligned nano HA particles. The physiochemical properties and degradation profiles have been described. In addition, the behavior of murine osteoblastic MC3T3 cells (adhesion, proliferation and differentiation) growth on the PVA-Col-HA nanofiber scaffolds was examined.

Materials and Methods

Materials

Nano-Hydroxyapatite (HA) (Avg. 20-70 nm, specific surface area: 110 m^2/g, density: 3.0 g/mL) (Berkeley Advanced Biomaterials, INC., Berkeley, CA), Polyvinyl Alcohol (PVA, Mw~205,000, 86.7-88.7 mol% Hydrolysis, 4200~ Polymerization), Albumin fluorescein isothiocyanate conjugate bovine (Albumin-FITC, >7 % mol FITC albumin), Collagen Type I (from rat tail, in 5 wt% acetic acid) (Sigma-Aldrich, St. Louis, MO), Ultrapure water (DNAse, RNAse Free, 0.1 micron filtered) (Invitrogen Corp., Grand Island, NY), Murine MC3T3-E1 preosteoblasts (ATCC, Manassas, VA), α-modified minimum essential medium (α-MEM) (Invitrogen, Carlsbad, CA), Alkaline phosphatase

(ALP) assay kit (ATCC, Manassas, VA), 3-(4,5-Dimethylthiazol-2-yl)-2,5-diphenyltetrazolium bromide (MTT) assay kit (ATCC, Manassas, VA).

Electrospinning of PVA-Col-HA nanofibers

PVA was dissolved in ultrapure water at 90 ºC (10 %, w/v, g/mL). The emulsified solution of HA nanoparticles was added to PVA solution and homogenized at 60 ºC by various HA/PVA ratio (HA/PVA=1/2, 1/4, 1/9, v/v). Albumin FITC was firstly dissolved in ultrapure water (0.1 mg/mL) and then thoroughly mixed with cooled HA-PVA slurry (Albumin, 10 %, v/v) for 10 min. Collagen solution (acetic acid, 5 wt %) was then homogenized with the mixture to finalize the PVA-Col-HA-Albumin FITC blend (Col, 10 %, v/v). The suspension of the blend was immediately loaded in a syringe (5 mL, B-D Scientific, Franklin lakes, NJ) connected to a high purity tubing (IDEX Health and Science, Oak Harbor, WA) with a 26 $G^{1/2}$ needle (B-D Scientific, Franklin lakes, NJ) with blunted tip (0.6 mm inner diameter). The syringe was attached to a syringe pump (R-100E, Razel Scientific Instruments, St. Albans, VT) with a setting flow rate (Q). A high voltage power supplier (ES40P, Gamma High Voltage research, INC., Ormond Beach, FL) was connected to the needle. The electrospinning settings parameters were as follow: Voltage=18 kV, Q=7.8 µL/min, needle tip-to-collector distance=10 cm. A rotational speed of 500 rpm was used to evenly deposit the solute on glass coverslips attached to the stainless steel hexahedron collector linked to the shaft of a motorized stirrer (JR4000, Arrow Engineering Co, INC., Hillside, NJ).. Electrospinning was running in dark for 1 hour to collect fibers. Samples were dried overnight (O/N) before testing.

Characterizations of PVA-Col-HA nanofibers

Scanning electron microscope (SEM)

PVA-Col-HA nanofibers deposited on coverslips were gold-coated (Gold Sputter, Effa Coater, USA) and the morphology of the nanofibers was characterized by Scanning electron microscope (SEM) (JSM-6510LV-LGS, MA, USA). The distribution of fiber diameter was measured from the SEM images using analysis software (Image J, National Institute of Health, USA).

Transmission Electron Microscope (TEM)

The encapsulation of HA nanoparticles in individual fibers was determined by Transmission Electron Microscope (TEM) (JEOL-2010 FasTEM, USA). TEM samples were prepared by directly depositing nanofibers onto Cu-grids covered with ultrathin carbon layers. Dispersive X-Ray spectrometry (EDAX) was used to analyze the chemical composition in area of sample surface of interest.

Optical Microscope

Images of nanofibers were also recorded under 10 × and 40 × through both visible light and fluorescence by an optical microscope (HAL 100, Carl Zeiss Microimaging, INC., Thornwood, NY), supplemented with microscope light source system (X-cite series 120Q, Lumin Dynamics Group Inc., Mississauga, Canada).

The intensity of fluorescence from albumin-FITC incorporated into nanofibers was also quantified by reading the deposited coverslips with the excitation/emission wavelength of 485/528 nm in a UV/VIS Spectrophotometer (BioTek Synergy HT, USA).

Total 9×9 counts were measured to calculate the mean relative fluorescence unit (RFU).

Contact Angle

The sessile drop method was used to measure the contact angle of coverslips surface with deposited nanofibers at ambient temperature. Three 10 µL droplets of distilled water were placed on the different spots of converslips surface until equilibrium and contact angles were measured by a Contact Angle Goniometer (Ramé-Hart, USA) to calculate the mean value.

Atomic Force Microscopy (AFM)

We characterized the surface morphology of nanofibers using a Multimode IIIa AFM (Digital Instruments) and a Dimension 3100 AFM (VEECO). AFM imaging of the nanofibers were conducted using Contact Mode in air. Positioning within micrometer accuracy of the cantilever on top of the nanofibers is achieved by the integrated optical microscope. The data were collected by mapping the fibers within a 20×20 μm^2 sized grid.

The nanomechanical properties of the nanofibers can be studied by AFM force-versus-distance curves in Contact Force Calibration Mode (Blacklock et al., 2010; Mermut et al., 2003). The calculation was done by analyzing data collected on more than 20 spots using 6 specimens. The force curves were fitted to the Hertz model and Hooke's law was used to calculate the loading force (*F*). The nanofibers have a much larger radius of curvature than the AFM tip (~ 20 nm) and can be treated as a planar surface. The measured elastic modulus (*E*) is qualitatively related to Young's modulus.

Rheology Characterization of nanofiber precursor solutions

An AR2000 rheometer (TA Instruments Inc., New Castle, DL) with a standard steel parallel-plate geometry of 20 mm diameter was used for the rheological characterization of all precursor solutions. Test methods of oscillatory stress sweep and frequency sweep were employed. The stress sweep was holding the temperature (25°C) and frequency (2π rad/s) constant while increasing the stress level from 0.001 to 10 Pa. The linear viscoelastic region (LVR) from 0.001 to 10 Pa were determined as safe-region without structural breakage from oscillatory stress. Samples were subjected to a steady stress ramp and the corresponding storage modulus (*G'*) and loss modulus (*G"*) were measured. The frequency sweep was performed at a fixed stress corresponding to the point in the middle of the LVR profile. The oscillatory frequency was increased from 0.1 to 100 rad/s, and the plots of *G'* and *G"* toward frequency were obtained from manufacture provided software. Complex viscosity (η^*) and the tangent of the phase angle ($tan\delta$) (ratio of *G"*/*G'*) were obtained from a flow test to plot against frequency as well.

Degradation of PVA-Col-HA nanofibers

The PVA-Col-HA nanofibers deposited on coverslips were subjected to *in vitro* degradation study at 37 ºC. Briefly, the coverslips were placed into 12-well plate and immersed by ultrapure water in incubator for 236 h. Morphology of nanofibers after water-immersion was timely characterized by optical microscope and SEM.

Cell culture

MC3T3 cells were seeded on the coverslips deposited with electrospun fibers. Briefly, coverslips were placed into 12-wells cell-culturing plate. Murine MC3T3-E1 preosteoblasts (ATCC, Manassas, VA) were cultured in α-modified minimum essential medium (α-MEM, Invitrogen, Carlsbad, CA) supplemented with 10% fetal bovine serum (Invitrogen, Carlsbad, CA), 10 mM β-Glycerophosphate (Sigma, American), and 1 % (v/v) antibiotics mixture of penicillin and streptomycin at 37 ºC in a humidified incubator with 5 % CO2. MC3T3-E1 cells were plated at a density of 1×10^4 cells/ well (12-well plate) onto placed coverslips surfaces with deposited nanofibers.

Cell attachment and proliferation

The mitochondria activities of MC3T3 cells culturing with nanofibers after 48 h and 72 h were determined by colorimetric assay which detected the conversion of 3-(4,5-dimethylthiazol-2yl) -2,5-diphenyltetrazolium bromide (MTT) (ATCC, Manassas, VA) to formazan. 20 µL/well of MTT solution (1 mg/ml in test medium) was added and the wells were incubated at 37 ºC for 4 h to allow the formation of formazan crystals. Then the dimethylsulfoxide (DMSO) (100 µL/well) was added to all wells and mixed thoroughly to dissolve the dark blue crystals. The optical density (OD) of extracted medium was measured in a UV/VIS Spectrophotometer (BioTek Synergy HT, U.S.A.) at 490 nm.

Cell viability was also evaluated using the LIVE/DEAD® Viability/Cytotoxicity staining kit (Invitrogen Corp., Grand Island, NY). Viable cells fluoresce green through the reaction of calcein AM with intracellular esterase, whereas non-viable cells

fluoresce red due to the diffusion of ethidium homodimer across damaged cell membranes and binding with nucleic acids. The cells-nanofibers interaction was visualized under fluorescence microscope (Carl Zeiss microimaging, USA) and AFM (Digital Instruments Nanoscope IIIA, USA).

For the cell differentiation experiment, MC3T3 cells were cultured in osteogenic media (regular media described above plus 10 mM β-glycerophosphate and 50 μg/ml L-ascorbic acid (Sigma)) before they were harvested at 9 d. Culture media were changed every three days. The alkaline phosphatase (ALP) activity of MC3T3 cells after treating with differentiation medium was measured by commercial kit (ATCC, Manassas, VA). 80 μL ALP buffer was added and the plate was incubated at 4 ºC for 4 h. The cell lysate was then centrifuged at a speed of 13,000 g for 3 min and cell debris was discarded. 50 μL of *p*-nitrophenyl phosphate (*p*NPP) was added to react with cell lysate for 60 min in dark at room temperature. 20 μL stop solution was then added to terminate the ALP activity. The standard curve was drawn by using *p*NPP of 0, 4, 8, 12, 16, 20 nmol/well to react with 10 μL of ALP enzyme solution. The O.D. was measured at 405 nm.

Statistical analysis

Data were analyzed with SPSS Version 12.0 (SPSS, chicago, IL). All values are expressed as mean standard deviation. Analysis of variance (ANOVA) was used to analyze the experimental data from all the experiments. Statistical significance was set

to $p < 0.05$.

Results

Optical microscopy of PVA-Col-HA nanofibers

In this study, emulsion of HA nanoparticles was homogenized with PVA solution (10 %, w/v) at various ratio of 1/2, 1/4 and 1/9 (v/v). Randomly oriented electrospun fibers are visualized in Fig.1. Micro-beads can be observed from HA/PVA (1/2) nanofibers, as shown in Fig.1 (a), which were caused by the failure of fiber-formation during spinning. Apparently, excessive amount (HA/PVA=1/2) of incorporated nano-HA disturbed the homogeneity of PVA solution and the stability of electrospinning. In comparison, fibers mesh fabricated from PVA-Col-HA precursor solution with lower amount of nano-HA (1/4 and 1/9) was thicker and more homogenous, as shown in Fig.17, (c, e). The presence of Albumin FITC coupling with HA nanoparticles was visualized in electrospun fibers.(Hlady and Furedimilhofer, 1979; Wassell et al., 1995).

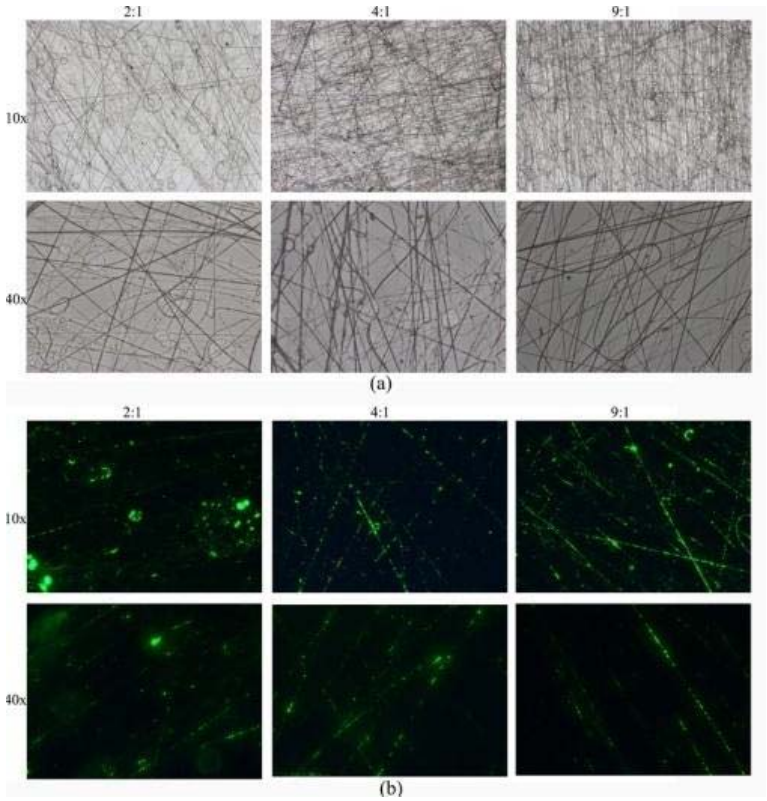

Fig.17 (a) light-visible images of PVA-Col-HA nanofibers with PVA/HA ratio of 2:1, 4:1 and 9:1 (*v/v*). (b) Fluorescence images of the same nanofibers when excited with blue light. Images were observed under 10× and 40× objectives, respectively.

Electron microscopy of PVA-Col-HA nanofibers

The encapsulation of nano-HA in nanofibers was characterized by TEM (Fig.18). The rod-like HA particles were mostly oriented along the axial direction inside individual fiber, whereas a few were perpendicular to the axial direction extruding the fiber. Rough surface caused by these extrusions could provide anchorage sites for cell adhesion during tissue regeneration (Asran et al., 2010a). The elemental composition of nanofibers determined by EDAX reveals the Ca-P components encapsulated within fibers. The morphology of fiber structure was also characterized by SEM (Fig.19 and 20). Large amount of Ca was quantified at the extrusion spots on nanofibers surface.

It is showed that precursor solutions at all HA/PVA ratios (1/2, 1/4 and 1/9) were capable to fabricate fiberous meshes through electrospinning (Fig.19 and 20). The inclusion of collagen during electrospinning showed no effects on fiber formation. The average diameters of fibers without collagen were similar (508, 484 and 514 nm) at different HA/PVA ratios (Fig.3), while the average diameters of fibers with collagen dropped (552, 416 and 362 nm) followed by the decrease of HA/PVA ratio (Fig.20).

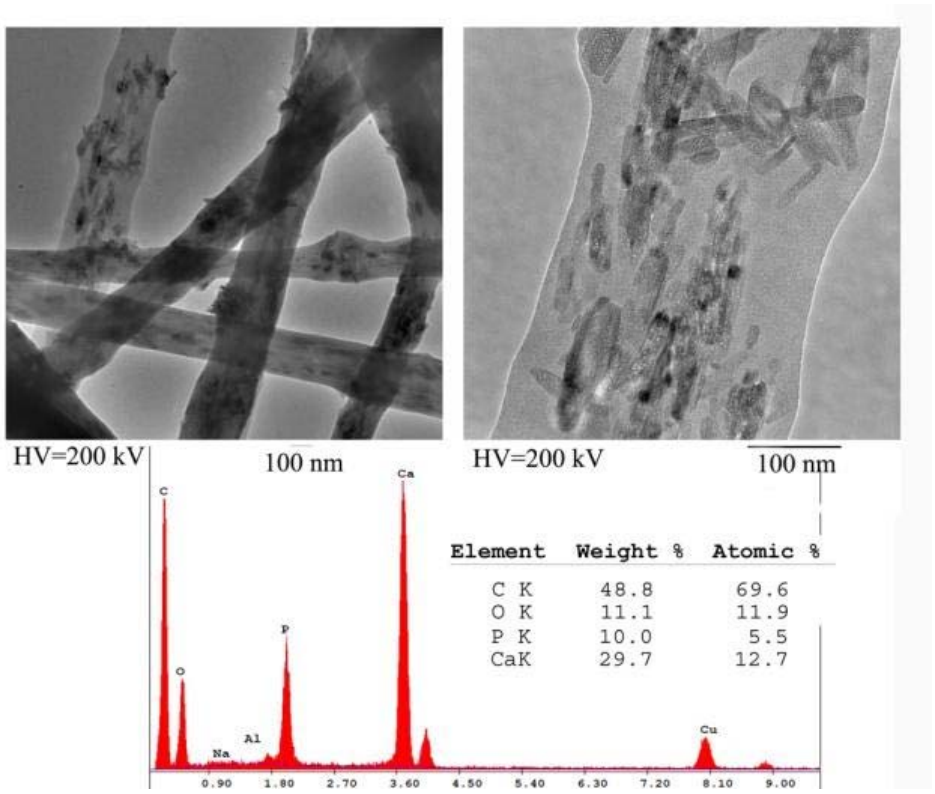

Fig.18 Representative TEM micrograph of PVA-Col-HA nanofibers with PVA/HA ratio of 4:1 (upper panels). Elemental composition of nanofibers obtained from EDAX (bottom panel).

Atomic force microscopy (AFM) of PVA-Col-HA nanofibers

We used AFM to study the morphology and mechanical property of single strand fiber with different ratio of HA/PVA via contact-force model. The tip is kept at a close

distance to the sample surface by a feedback mechanism to return height and deflection images from scanning area. Rough surface of nanofibers was observed from height images as expected as the extrusion of encapsulated HA nanorods (Fig.21 (A) and (B)). Fiber surface turned smoother in consistent with reduced encapsulation of HA.

The obtained Young's modulus (*E*) of nanofibers with encapsulated HA was higher than the pure PVA nanofibers (0.826 MPa), which revealed the increment of the fiber stiffness. *E* significantly increased when higher amount of HA was encapsulated into nanofibers (HA/PVA=1/2) (Fig.21 (C)) compared to others (1/4 and 1/9). The incorporation of collagen showed less influence on the stiffness of nanofibers.

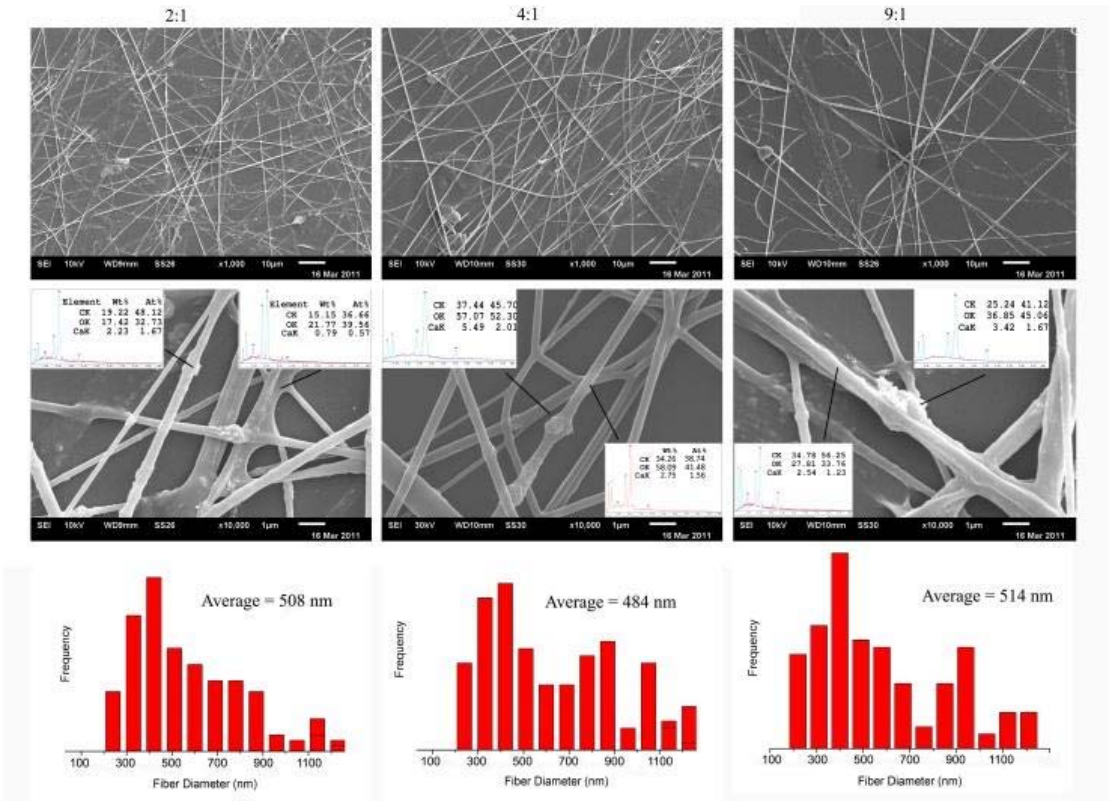

Fig.19 SEM micrograph of PVA-HA nanofibers with PVA/HA ratio of 2:1, 4:1 and 9:1 (upper panel: 1000×; middle panel: 10000×). The diameter histogram of

corresponded nanofibers analyzed from 1000× micrographs (bottom panel).

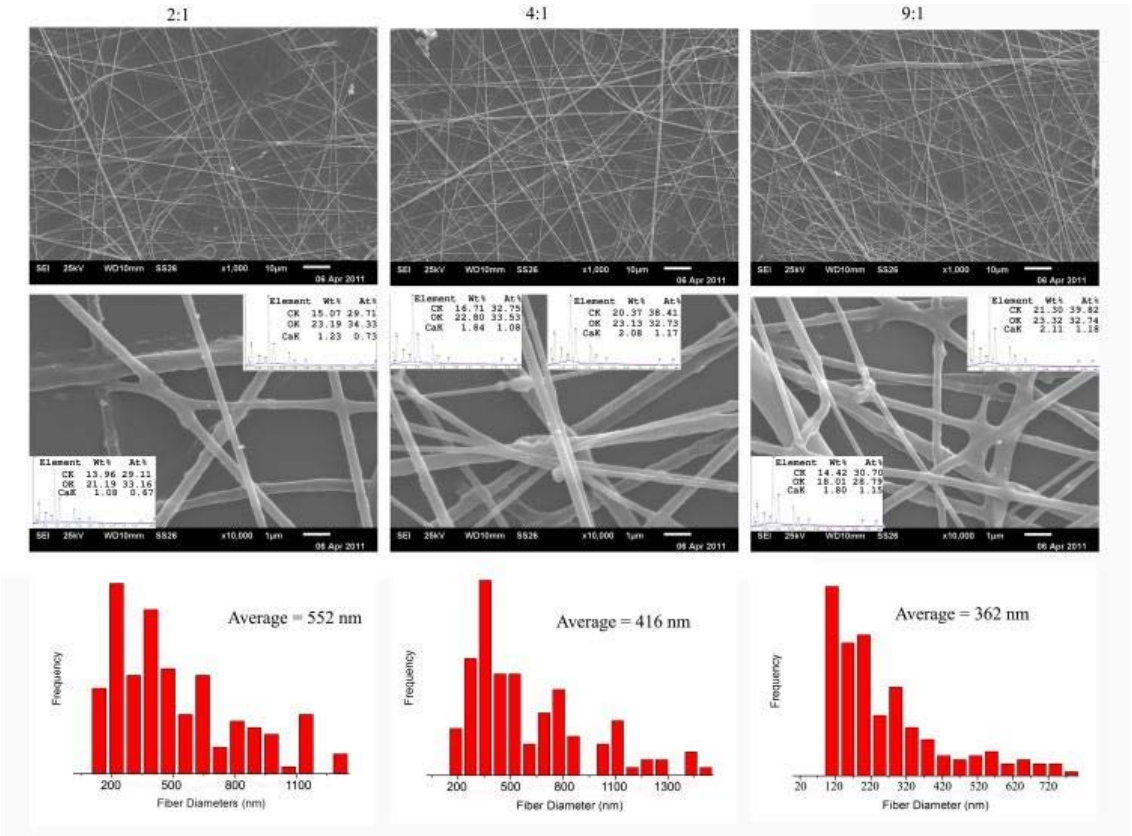

Fig.20 SEM micrograph of PVA-Col-HA nanofibers with PVA/HA ratio of 2:1, 4:1 and 9:1 (upper panel: 1000×; middle panel: 10000×). The diameter histogram of corresponded nanofibers analyzed from 1000× micrographs (bottom panel).

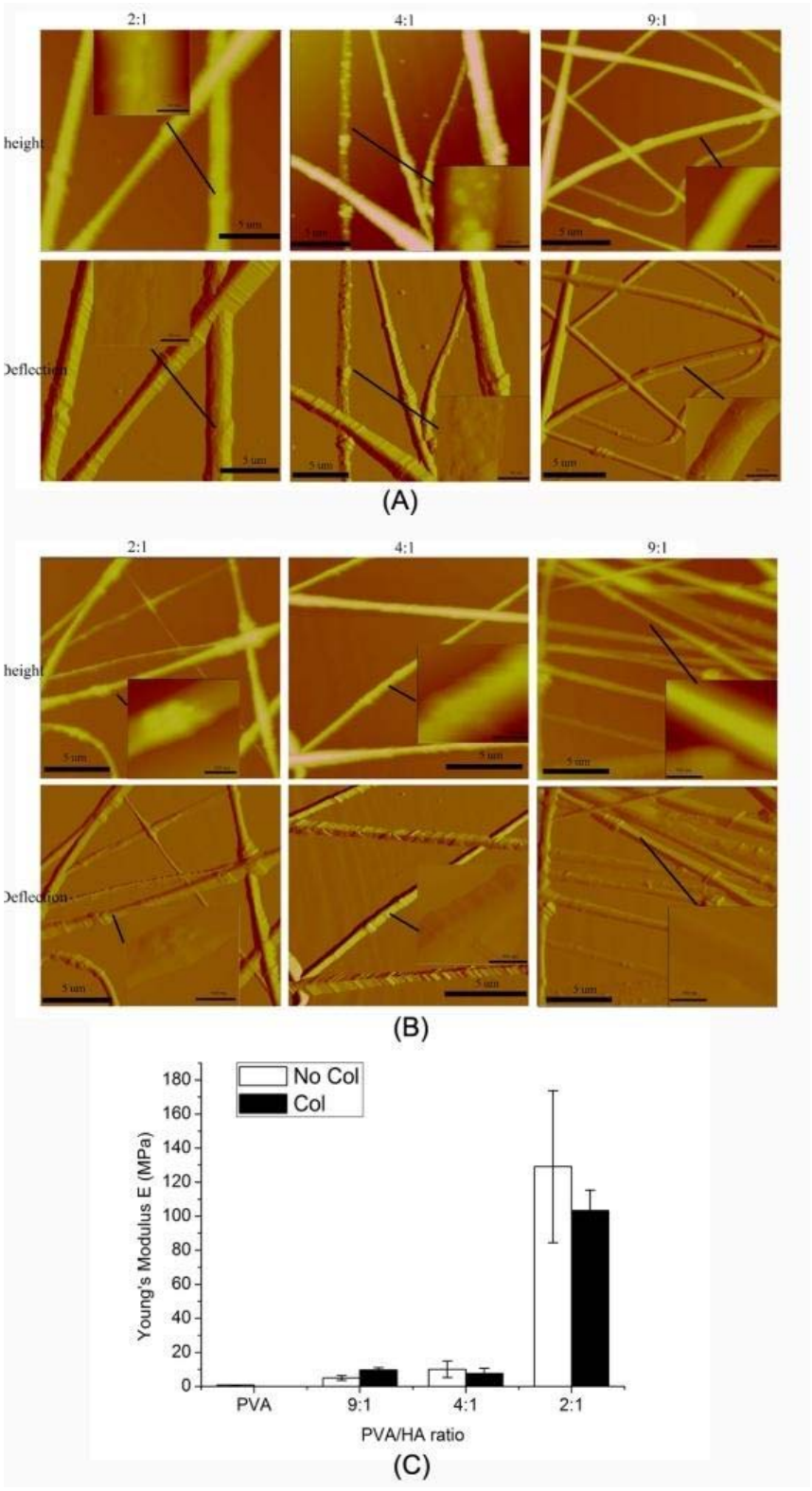

Fig.21 AFM contact mode images of (A) PVA-HA and (B) PVA-Col-HA nanofibers with PVA/HA ratio of 2:1, 4:1 and 9:1 (upper panel: height images; middle panel: deflection images). (C) The mean Young's modulus (*E*) of single nanofibers (*n*=6)

Hydrolytic degradation of PVA-Col-HA nanofibers

In this study, all PVA-Col-HA nanofibers were prepared at the same condition with various ratios of HA/PVA. PVA shows high efficiency in electrospinning for its strong hydrophilicity but high dissolution rate in aqueous solution (Yao et al., 2003). We attempted to incorporate HA nanoparticles to reinforce the mechanical strength and hydrophobicity of PVA nanofibers. Nanofibers with different HA/PVA ratios (1/2, 1/4 and 1/9) were immersed in ultrapure water and timely observed by fluorescence microscope (Fig.22) and SEM (Fig.23, (A)). Within 2h of soaking, the fluorescence intensity of 1/9 nanofibers was low while others were still intense (Fig.6). The fluorescence of nanofibers was gradually decayed following by long-term soaking (48 h and 236 h). The fluorescence of 1/4 nanofibers was most durable, and the mesh structure of 1/4 nanofibers was still observable after 236 h soaking.

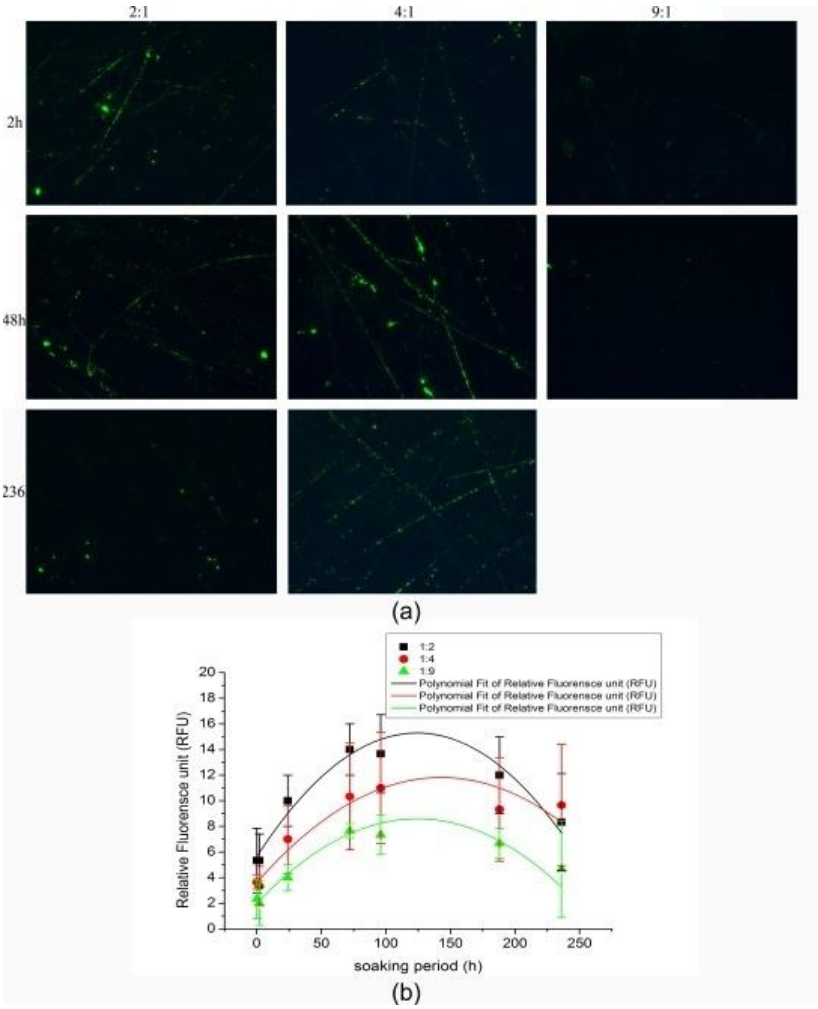

Fig.22 (a) The fluorescence images (10×) of PVA-Col-HA nanofibers with PVA/HA ratio of 2:1, 4:1 and 9:1 soaking in 37ºC water for 2h (upper panel), 48h (middle panel) and 236h (bottom panel). (b) The change of fluorescence intensity for nanofibers during soaking.

The morphologic change of individual fiber after soaking can be visualized in SEM micrograph (Fig.23, (A)). After 48 h of soaking, the fiber structure of 1/2 and 1/4 nanofibers retained (Fig.23, (A)) while 1/9 nanofibers were mostly failed. Precipitates observed around fibers were released HA nanoparticles from nanofibers during degradation. After 236 h of soaking, polymeric components of fibers were mostly degraded, and the encapsulated HA nanoparticles lined along fiber axis.

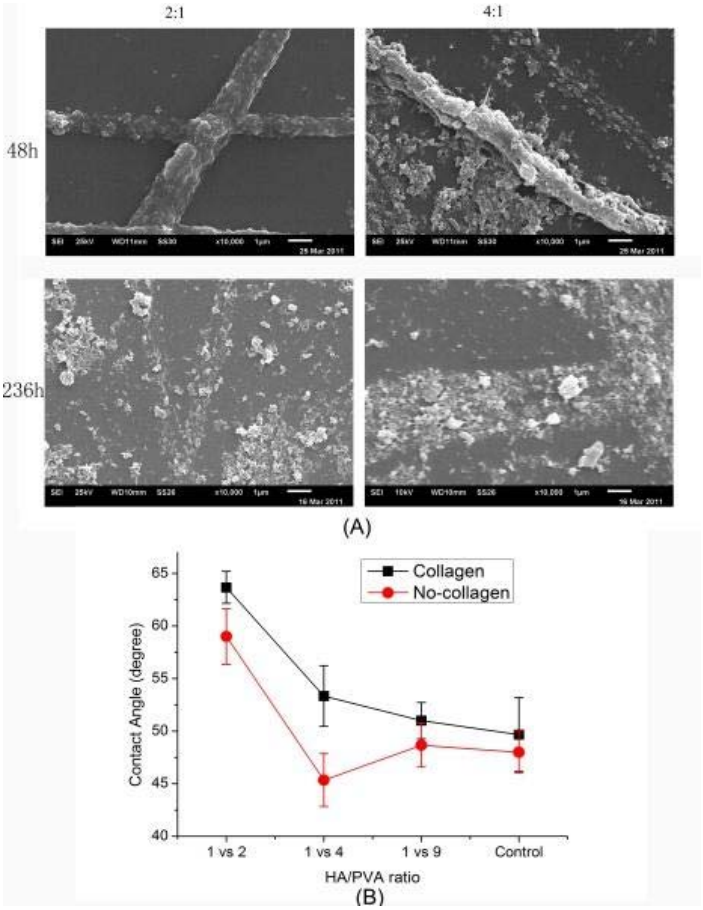

Fig.23 (A) SEM micrograph (10000×) of PVA-Col-HA nanofibers with PVA/HA ratio of 2:1(left) and 4:1(right) soaking in 37ºC water for 48h (upper panel) and 236h (bottom panel); (B) Contact angles of PVA-HA (red) and PVA-Col-HA (black) nanofibers with PVA/HA ratio of 2:1, 4:1 and 9:1. (Control: glass coverslips without nanofibers)

Contact angle of PVA-Col-HA nanofibers

The nano-scaled roughness on substrate surface could alter the hydrophilicity of materials. In this study, encapsulated HA nanoparticles were expected to influence the hydrophilicity of PVA fiber mesh. The contact angles (ϑ) for these nanofiber meshes (1/2, 1/4 and 1/9) were measured to reveal the hydrophilicity (Fig.23, (B)). Generally, the contact angle decreases when the amount of HA encapsulation is smaller for nanofibers with or without collagen. Fibers with collagen have larger ϑ than fibers without collagen might due to its peptide strands. This result indicated that

encapsulated HA nanorods enhanced the hydrophobicity of PVA nanofibers.

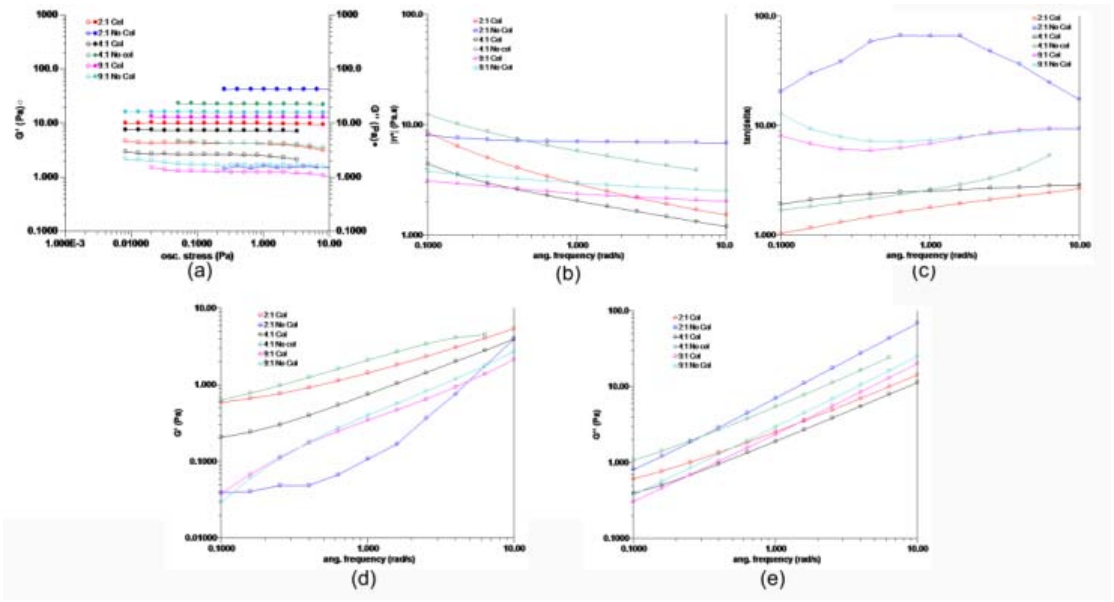

Fig.24 (a) Storage modulus (*G'*) and loss modulus (*G''*) profiles across a oscillatory range of 0.001–10 Pa at 25°C; (b) complex viscosity, (c) tan delta, (d) Storage modulus (*G'*) and (e) loss modulus (*G''*) profiles across a frequency range of 0.1–10 rad/s at 25°C for PVA-HA and PVA-Col-HA precursor solution (PVA:HA=9:1, 4:1 and 2:1)

Rheological properties of PVA-Col-HA nanofibers precursor solution

The predominance of *G''* over *G'* in all precursor solutions can be observed from oscillation stress sweep for the applied non-destructive stress range (Fig.24, (a)), which indicated the prevalence of viscous fluid behaviors for precursor solution in a sol state. The gradual decrease of *G''* followed by the increase of incorporated HA amount showed the influence of HA on rheological property of precursor solutions (Fig.24, (a)). The Col content seemed to minimize the *G"* that might indicate its interaction with other molecules (Fig.24, (a)). An increase in both *G'* and *G''* as the frequency increased was revealed (Fig.24, (c) and (d)). All *G''* (1-100 Pa) are dominant over *G'* (0.1-10 Pa) and the decrease of *G'* slope according to the increase of incorporated HA revealed

the weakly structured system. The complex viscosities (η^*) of all solutions were decreasing across the frequency range suggesting pseudoplastic behaviour (Fig.8, (b)). It is noted that the slope of η^* curve across the frequency range was flattened followed by the decrease of incorporated HA in system (except 1/2 No-Col). This result suggested more bonding interactions were formed by more incorporated HA with PVA, and the dismantling of HA-PVA linkage leaded by higher frequency of shear stress was more significantly revealed by the decrease of η^*. As *tan δ* is a ratio of *G''* to *G'*, a value above 1 indicates a material with dominant liquid-like behavior and a value below 1 indicates a material with dominant elastic (solid-like) behavior (Tanna et al., 2006). All curves of *tan δ* were above 1 indicated the liquid state of precursor solution. However, the addition of nano-HA seemed to assist the transition from sol to gel, as the *tan δ* curve of solution with higher HA content was gradually fell and closely approaching to 1 in lower frequency (except 1/2 No-Col) (Fig.24, (c)). Taken together, the incorporated HA was capable to modify the viscoelasticity of precursor solution by interacting with PVA.

Cell behavior culturing on PVA-Col-HA nanofibers

Live-dead cell staining was utilized to study the cell morphology and interaction with nanofibers after 72 h culturing (Fig.25, (a) and (b)). The attachment and proliferation of live MC3T3 cells (green) seeding on nanofibers mesh can be visualized, showing well compatibility of cell-fibers. Cells grown on both 1/2 and 1/4 nanofibers (Fig.25, (a) and (b)) had much better adhesion and cell spreading pattern, compare to

the cells grown on 1/9 nanofibers after 72 h culturing. No obvious dead cells (red) were observed in all cell colonies seeding on nanofibers with and without collagen. Nevertheless, cells on 1/9 nanofibers were less spread, which is probably due to the earlier failure of the supporting fiber-mesh.

The MTT result from 8 d of culturing was quite consistent with the live-dead staining (Fig.25, (c)). Cells seeded on all groups of nanofibers showed significantly higher proliferation rate than cells seeded on coverslips without nanofibers (Control). It indicated the nano-fibrous mesh promoted the spread and proliferation of osteoblastic cells. The incorporation of collagen can further benefit the cell proliferation along nanofibers, as shown as the higher proliferation rate in MTT results (Fig.25, (c)). The sudden decrease of cell proliferation on 1/9 nanofiber with collagen might be attributed to cell detachment from failed PVA-Collagen fibers. 1/4 nanofiber with collagen was revealed to be most durable and interconnective for cell adhesion and prolifereation, verified by both in live-dead images and MTT results (Fig.25, (a) (b) and (c)). Moreover, the ALP levels normalized with protein levels were measured for each cell groups to analyze the influence of nanofibers on cell functionality (Fig.25, (d)). The results showed that there was no significant difference among cells culturing on different nanofibers. In sum, the nanofibers promote osteoblastic cells adhesion and proliferation without influencing the cell functionality. The cell proliferation rate on nanofibers was dependent on the durability of nanofibers. The interaction of cell-nanofibers was further characterized by AFM via contact mode. Cells were interact

with surrounding fibers and infiltrate into the fibrous mesh to form a sandwich mode.

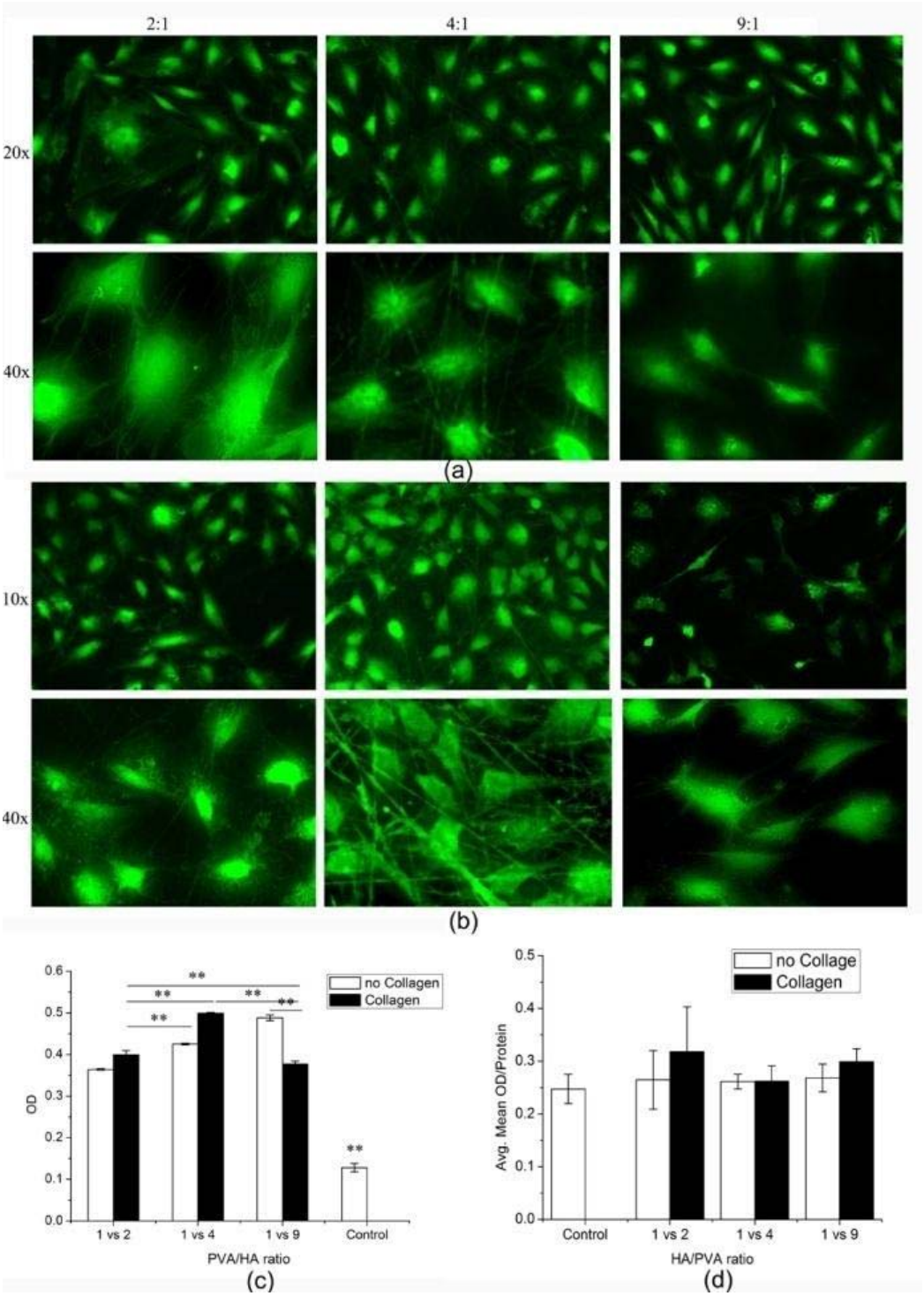

Fig.25 MC-3T3 cell activity assay. The live (green) -dead (red) staining (a, b; objectives, 10× and 40×) of MC3T3 cells cultured on PVA-HA (a) and PVA-Col-HA (b) nanofibers mesh for 72h. MTT results (c) of cells cultured on HA-PVA-albumin FITC (white column) and PVA-Col-HA (black column) nanofibers for 8d. Normalized ALP

activity of cells cultured on PVA-HA (white column) and PVA-Col-HA (black column) nanofibers for 8d. (Control: glass coverslips without nanofibers). (**p<0.005, n=3)

Discussion

Failure of osseointegration (direct anchorage of an implant by bone formation at the bone-implant surface) represents one of the main causes leading to implant failure and loosening(Ramaswamy et al., 2009). One of the important challenges in the field of implant surface fabrication is the development of “bone-like” implant surface substitutes that are ‘‘intelligent” to instruct the in vivo environment to form bone. We propose that a “bone-like” nanofibers implant surface coating mimics the biological, structural and mechanical behavior of natural bone, and enhances the adhesion, growth and differentiation of surrounding bone marrow stromal cells. To imitate the architecture of the natural bone matrix, we developed electrospun PVA nanofibers with embedding of nanoscale HA and type I collagen (Col). We found that 15 % PVA mixed with HA (10 %) and Col (10 %) provides a better cellular response (adhesion, proliferation and differentiation), defined degradation pattern (Fig.22 and 23), and favorable surface roughness as well as mechanical strength (Fig.19-21) with characterized physiochemical properties (Fig.21 and 23). PVA-Col-HA nanofibers were prepared using empirical combinations of electrospinning variables. Several distinct morphologies were observed including fiber diameter distribution, surface roughness, alignment, orientation of nano HAs in the fibers, etc. (Fig. 19-24)

PVA has recently been applied as electrospun nanofibers for its hydrophilicity

and high electroconductivity ensuring its feasibility of spinning. Nevertheless, the rapid hydrolysis rate limits the application of PVA electrospun nanofibers as stable and reliable tissue scaffolds. The attempts to modify the hydrophilicity of PVA nanofibers are numerous. Y. Li, et al.(Yao et al., 2003) stabilized PVA nanofibers in water by methanol treatment to increase the crystallinity of PVA. T. Pisuchpen, et al.(Pisuchpen et al., 2011) enhanced the rigidity and hydrophobicity of PVA nanofibers via the addition of silica. L. Feng and L. Jiang(Feng et al., 2003) showed the highly aligned PVA nanofibers possessed superhydrophobicity attributed to the reorientation of PVA molecules. All of these studies indicate the amphiphilic PVA is chemical amendable in inherent.

The hydrophilic phenomenon of PVA contacting with water is acknowledged as the excessive exposure of hydrophilic hydroxyl groups (-OH) to water molecules and hence the hydrogen-bonding interactions. Hydrophobic alkyl groups (-CH-) as the backbone of PVA are repelled by H_2O molecules to interior(Hassan and Peppas, 2000a). The initial swelling stage of PVA in water can be considered as the process of conformational reorientation for PVA molecules. While the later dissolving stage is the stabilization of reoriented PVA molecules in water phase. In native, -CH- and –OH groups are evenly distributed around PVA surface. However, in certain circumstances, the arrangement of -CH- groups to be dominant on PVA surface with lower free surface energy could dramatically alter its original hydrophilicity in water(Feng et al., 2003).

It has been demonstrated the encapsulated nano-HA and collagen in PVA

nanofibers would form hydrogen bonds with PVA molecules, which significantly changed the crystallinity of PVA (Asran et al., 2010a). The hydrogen bonding in blend system can also be demonstrated from the rheological characterization (Fig.24). Our results indicated that the PVA-Col-HA precursor solutions were in viscous sol-like state that is capable to be electrospun. The interaction of embedded nano-HA and collagen with PVA might result in reduction of free –OH groups while augment of -CH- groups on nanofiber surface, and subsequently affect the wettability of nanofibers. Our study demonstrated the water repelling effect of nanofibers attributed to nano-HA incorporation was increased regarding to the HA ratio (from HA/PVA=1/9 to 1/2), as shown in contact angle results (Fig.23, (B)). More gradual change and larger contact angles could be revealed from nanofibers consisted collagen, which also confirmed the hydrogen- bonding interaction of collagen-PVA. From aspect of nanostructured surface-interface theory (Cassie-Baxter model), rough surface allows air to be trapped between the liquid and the underlying solid surface and repel the water(Pisuchpen et al., 2011). In present study, the encapsulation of HA nanorods within the nanofibers were identified to increase the surface roughness (Fig.19-21). The contact angle of HA-PVA nanofiber surface was increased probably due to the hydrophobic pockets located on the interface.

The promotion of hydrolytic resistance enabled the supportive role of nanofibers allowing the cell infiltration and migration. Studies have been shown cellular growth and functions can be regulated by nanofibers parameters, such as alignment, pore

geometry, surface area, etc. In physiological conditions, ECM fibers provide cells with topographical features that trigger morphogenesis by interact with the cells through their transmembrane integrin receptors to initiate intracellular signaling cascades (Kim et al., 2010; Hynes, 2009). Nanofibers prepared as bone scaffolds revealed to be interacted with bone cells and guided the mineralization(Yoshimoto et al., 2003). We proposed that the encapsulated nano-HA and collagen provided anchorage sites for cell adhesion and mechanically enforced nanofibers to support cells. The interaction of cell-nanofibers can be visualized via cell stainings (Fig.25)

One of the potential applications of this nanofibers scaffold is to provide a “bone-like” implant surface coating to enhance osseointegration by allowing the recruitment of bone marrow osteoblastic cells into the scaffold matrix. But there are some limitations need to be addressed for this study. The efficiency of electrospinning was estimated to be interrupted by adding HA nanoparticles and collagen to PVA precursor solution. Parameters of the precursor solution for electrospinning, such as viscosity, molecular weight, electroconductivity, etc., could dramatically influence the generation of nanofibers. Further investigations on some decisive parameters corresponding with HA and collagen ratio need to be performed in the future. Moreover, the incorporation of HA and collagen extended the degradation of PVA nanofibers to about 10 days. But more durable fibers applied as biomimic tissue-engineering scaffolds could be further-stablized by cross-linking approaches, such as UV treatment, freeze-thawing, etc., and exploration on tunable degradability of

nanofibers need to be elaborated in the future.

Conclusion

PVA-Col-HA nanofibers fabricated by electrospinning revealed excellent biodegradability, biocompatibility and bioactivity. The mechanical strength and hydrolysis resistance of nanofiber are reinforced by incorporation of HA nanoparticles and collagen. The nanofibers enhanced the adhesion and proliferation of interacted bone cells. We propose PVA-Col-HA nanofibers might be promising biomimetic materials modifying the implant surface for orthopedic applications.

CHAPTER 5 COAXIAL-NANOFIBERS FOR SUSTAINED DRUG RELEASE

Introduction

An early and rapid osseointegration requires the recruitment of bone marrow stromal cells (BMSCs) to the periprosthetic site (Lee and Goodman, 2008). After surgery, the gap between the implant surface and surrounding bone needs to be completely bridged by newly formed bone. There is compelling evidence that a defective implant osseointegration (the formation of a piece of fibrous membrane between the implant surface and surrounding bone) leads to implant instability, micromotion, osteolysis and loosening (White et al., 2012a). Kärrholm et al. (Karrholm et al., 1994) reported that the subsidence of the implant is associated with an increased risk of AL. Ryd et al. (Ryd, 1992) proposed that the occurrence of implant instability and micromotion represent two of the risk factors of early implant loosening in both knees and hips. The rate, quantity and quality of osseointegration are closely related to the physiochemical and biological properties of the implant surface (de Jonge et al., 2008). More efforts are required to develop a “bone like” implant surface that shows potential for implant osseointegration.

Natural bone is an organ composed of a complex hierarchical structure with the organic–inorganic constituents combine together (de Jonge et al., 2008). Many implant surface fabrication techniques have been developed with the aim of improving osseointegration (Anselme et al., 2010; Ponche et al., 2010). However, current clinical

studies found no significant improvement in clinical outcomes in patients with a cementless hip replacement as compared to those with a cemented hip replacement (Steens et al., 2010; Yamada et al., 2009). The limitations of HA coating includes (1) a non-physiological surface leads to diminished initial osseointegration (Goosen et al., 2009; Chung et al., 2008); (2) brittle nature (Song et al., 2010a; Leeuwenburgh et al., 2006); (3) poor adhesion strength (Heimann, 1999; de Jonge et al., 2008) and (4) the lack of controllable drug release (Zhang et al., 2004). Current studies demonstrated that the nanoscale topography of the implant surface is critical for earlier osseointegration (Gittens et al., 2011; Dalby et al., 2006) and sustained drug release (Su et al., 2012a).

One of the promising technologies to mimic bone nanoscale extracellular matrix (ECM) structure is electrospinning. Electrospinning forms superfine fibers with diameters ranging from 10 μm down to 10 nm by forcing a polymer solution with an electric field through a spinneret (Baker et al., 2009). A rapidly rotating collector results in aligned NFs while a stationary collector results in randomly oriented NF mats. The advantages of electrospun NFs include a high surface area, high mass to volume ratio and a small inter-fibrous pore size with high porosity (Sundararaghavan et al., 2010). The potential application of electrospun NFs for the enhancement of osseointegration is promising but obviously overlooked. It was demonstrated that the NF structural cues alone can be used to create an osteogenic environment without the use of exogenous factors (Wang et al., 2012). The cell attachment, proliferation, and differentiation of

osteoblastic cells in vitro are significantly influenced by the physiochemical properties of NFs (Wang et al., 2012). More efforts are required to understand the interplay between the physiochemical natures of NF scaffolds and the fate of local osteoblast/osteoclast cells.

Polyvinyl alcohol (PVA) is a biodegradable and biocompatible polymer (Song et al., 2011a). PVA has good electrospun NF-forming capability, because of its excellence in electro-conductivity (Kim et al., 2008). Kim et al. reported that electrospun PVA/HA NFs mimic both the architecture (the morphology) and the chemistry (the composition) of the lowest level of the hierarchical organization of bone (Kim et al., 2008). In our previous study (Song et al., 2012), we described the physicochemical and biological properties of electrospun PVA/Col/HA NFs, and found that the inclusion of HA and Col in the PVA matrix significantly increased the fiber stability and the mechanical strength. The encapsulated nano-HA and Col also enhanced the adhesion and proliferation of osteoblastic MC3T3 cells in vitro. However, these blended PVA/Col/HA NFs cannot be used as a desired drug release device because of their fast dissolution rate. Thus, to develop a kind of nanofibers with capability to support sustainable drug release is our primary goal.

Electrospun NFs can be used as drug release devices by embedding drugs into the NFs. Biological compounds delivered by NF scaffolds included antibiotics(Feng et al., 2010), proteins (Sahoo et al., 2010), DNA (Rujitanaroj et al., 2011), and growth factors. These successes have been achieved either through direct blending of drugs into the

polymer solution before electrospinning, or via the utilization of coaxial electrospinning (Gluck et al., 2011). Coaxial electrospinning is a process where a concentric spinneret can accommodate two different liquids and is regarded as a significant breakthrough in the field, as shown in Fig.26 (Gluck et al., 2011). During the coaxial electrospinning a customized spinneret is employed to trap a secondary fluid layer (containing labile drugs) within the core of the forming NFs (Gluck et al., 2011). The sheath structure of coaxial NFs acts as a guide and encapsulates the core material. We utilized biocompatible and biodegradable poly (ε-caprolactone) (PCL) as sheath structure of coaxial NFs.

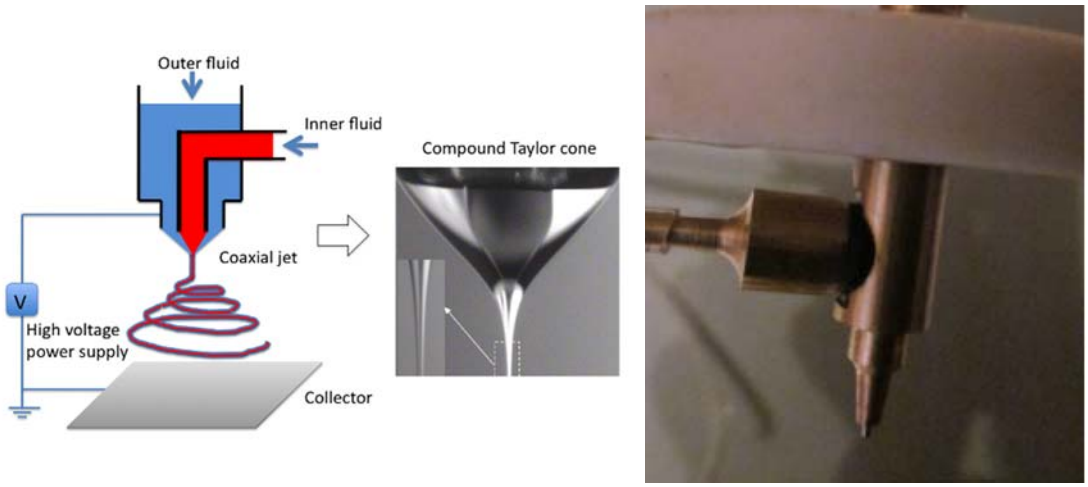

Fig.26 Structure of spinneret for electrospinning coaxial nanofibers

Since we have researched on the monolithic electrospun nanofibers previously and found its limitations in drug delivery, the objective of this study was to develop a "bone-like" implant surface fabricated with coaxial PCL^{Col}/PVA^{HA} core-sheath NFs used for controllable sustained release of embedded drugs. The physiochemical and

biological properties of these NFs were described. The in vitro drug release dynamics of both Doxy and Dex from these NFs were examined. In addition, the bonding strength of PCL^{Col}/PVA^{HA} NFs on the titanium rod surface was confirmed.

Materials and Methods

Coaxial electrospinning

10% (w/v) PCL solution was prepared by dissolving 0.5 g of PCL in 5 ml of dimethylformamide (DMF)/chloroform (1:1, v/v). PCL^{col} solution was prepared by mixing Col (4 mg/ml) with PCL in a ratio of 10:90 (v/v). The PVA^{HA} solution was prepared by mixing HA nanorods (Avg. 20-70 nm) with PVA in a ratio of 10:90 (v/v). Coaxial electrospinning was performed using a custom made coaxial nozzle consisting of a hollow stainless steel t-junction with a fully penetrating 19-gauge core needle. The PVA^{HA} solution (for core fiber) and PCL^{col} solution (for sheath) were uploaded to the syringes. The syringes were attached to syringe pumps set at a flow rate (Q) of 1 mL/h for PCL^{col} and 0.47 mL/h for PVA^{HA}. An 18 kV voltage was applied to the needle from the power supply. The distance from needle tip to collector was 10 cm. A rotational speed of 500 rpm was used to evenly deposit the solute on a glass coverslip attached to the stainless steel hexahedron collector, which was linked to the shaft of a motorized stirrer. For drug loading purpose, Doxycycline (Doxy), a member of the tetracycline antibiotics group, and is commonly used to treat a variety of infections, is utilized in this study. Doxy was firstly dissolved in H_2O and then homogenized with PVA^{HA} solution

or PCL^{col} solution (350 μg/mL). The mixtures were then electrospun to generate Doxy-loaded NFs.

Scanning Electron Microscopy

The coaxial nanofiber scaffold was firstly gold-coated (Gold Sputter, EFFA Coater, Redding, CA, USA) and the morphology of the nanofibers was characterized by Scanning electron microscope (SEM) (JSM-6510LV-LGS, MA, USA). Morphologies were viewed at a 25 kV accelerating voltage.

Transmission Electron Microscope (TEM)

Transmission Electron Microscope (TEM) (JEOL-2010 FasTEM, USA) was utilized to characterize the structure of coaxial NFs. NFs were directly depositing onto Cu-grids covered with ultrathin carbon layers and observed under an accelerating voltage of 200 kV. Dispersive X-Ray spectrometry (EDAX) was used to analyze the chemical composition in area of sample surface of interest. Image J 1.41 software (National Institutes of Health, Bethesda, MD) was used to determine the average fiber diameter and pore size by taking measurements from SEM micrographs

Optical Microscope

The core-sheath structure of nanofibers were also observed under an optical microscope (HAL 100, Carl Zeiss Microimaging, INC., Thornwood, NY), facilitated with microscope light source system (X-cite series 120Q, Lumin Dynamics Group Inc., Mississauga, Canada). The fluorescence image of nanofibers embedded with albumin-fluorescein isothiocyanate (FITC) was captured also to elucidate the core-sheath

structure of NFs.

Contact Angle

The hydrophilicity of coaxial NFs was determined by the contact angle measurement. A sessile drop method was applied to measure the contact angle of nanofibers mesh surface at ambient temperature. The droplets of distilled water were placed on fibrous surface until equilibrium and contact angles were measured by a Contact Angle Goniometer (Ramé-Hart, USA).

Atomic Force Microscopy (AFM)

The surface morphology of nanofibers was characterized by a Multimode IIIa AFM (Digital Instruments) and a Dimension 3100 AFM (VEECO) as described previously (26). A Contact Mode was applied to obtain AFM imaging. The integrated optical microscope was used to position the cantilever on the top of the NFs within micrometer accuracy. Data were collected by mapping the NFs within a 20×20 μm^2 sized grid. The cantilever tip deflection was used as a feedback signal to maintain a constant force over the scanned area. The nanomechanical properties of the nanofibers can be studied by AFM force-versus-distance curves in Contact Force Calibration Mode (Blacklock et al., 2010; Mermut et al., 2003). The calculation was done by analyzing data collected on more than 20 spots using 6 specimens. The force curves were fitted to the Hertz model and Hooke's law was used to calculate the loading force (F) and Young's modulus. The Young's modulus (E) for each sample (n=3) was calculated by finding the slope of the stress (σ) and strain (ε) curve ($E=\sigma/\varepsilon$). The

ultimate strain and stress were determined at the peak load point of the stress-strain curve.

Rheological characterization of coaxial NFs

An AR-G2 rheometer (TA Instruments Inc., New Castle, DL) with an environmental temperature chamber (ETC) and torsion clamp geometry was used for the rheological characterization of nanofibers scaffolds. Oscillatory stress sweep and frequency sweep were firstly employed to determine the linear viscoelastic region (LVR). Then, an oscillatory temperature ramp was performed to study the thermal behaviors of nanofibers and determine the heat distortion temperature (HDT). The samples were scanned in a temperature ramp in oscillatory mode from 40°C to 75°C at a rate of approximately 2 °C/min with a constant oscillatory stress of 1000 Pa and a constant frequency of 2π rad/s. Storage modulus (G'), and loss modulus (G'') were recorded at an interval of 30 s. The results were shown in supporting information.

Cell culture

Pre-grown murine MC3T3-E1 preosteoblast cells (ATCC) were used for the cell culture. Briefly, coaxial nanofiber scaffolds were placed into petri-dish. MC3T3 cells were cultured in α-MEM (Invitrogen) supplemented with 10% fetal bovine serum (Invitrogen), 10 mM β- glycerophosphate (Sigma), and a 1% (v/v) antibiotic mixture of penicillin and streptomycin at 37°C in a humidified incubator with 5% CO_2. MC3T3-E1 cells were seeded at a density of 1.0×10^4 cells/dish onto placed scaffold surfaces (n=3). The mitochondrial activity of MC3T3 cells cultured on nanofibers after 8 days was

determined by MTT assay. Cell viability was also evaluated using the LIVE/DEAD viability/cytotoxicity staining kit (Invitrogen).

Drug release study

A modified *S. aureus* growth inhibition assay was used to measure the bactericidal activity of Doxy eluted from NFs, as we have described previously (24). Briefly, 40 mg of NFs (encapsulating ~1 mg Doxy) were soaked in 2 ml of Mueller–Hinton broth inoculated with *S. aureus* (ATCC#49320, 1×10^2 CFU) and cultured at 37°C. At each time point, the broth was removed and replaced with the same amount of broth. The optical density (OD) of collected broth was measured at 625 nm. All the tests were performed in triplicate and repeated two times. In addition to the bactericidal activity assay, the release profile of Doxy from NFs has been measured. Briefly, 140 mg of Doxy-encapsulated NFs were soaked in 2 mL D-H_2O at 37°C. The Doxy concentration in supernatant was timely measured via spectrometer at 256 nm. Similarly, 140 mg of Dex-encapsulated-NFs were soaked in 2 mL D-H_2O and the release profile of Dex was also plotted.

Bonding strength of implant

To determine whether the NF coating remained intact during implantation, we developed an ex vivo porcine bone implantation model. Since the bone mineral density of porcine proximal tibia (1.42 g/cm^2) is closer in value to young human proximal tibia (1.30 g/cm^2) (Nagarkatti et al., 2001), we selected porcine proximal tibia bone for Ti rod implantation. We purchased fresh-frozen porcine knee specimens

from a local slaughterhouse and stored them at -20^{o}C. The specimens were thawed overnight and all soft tissues were removed before testing. A flat dissected bony surface was obtained after removing all superficial articular tissues. The tibial bone holes (diameter = 2.54 mm; depth = 15 mm) were made. We deposited electrospun PCL^{col}/PVA^{HA} NFs directly on the surface of Ti rods (diameter = 2.5 mm, length = 60 mm) covering the entire surface of the Ti rod stem. The thickness of the NFs coating is ~ 50μm. We slowly inserted NFs coated Ti rods into the bony holes using an Instron model 8841 Universal Materials Test Machine at the speed of 10 mm/min. The porcine bones with Ti rod implantation were then soaked in sterilized PBS at 37^{o}C for 2 or 7 days. At each time point, the Ti rods were pulled out from the bone holes (n=3).

Results and Discussion

PCL^{col}/PVA^{HA} core-sheath NF scaffolds for controlled drug release:

We developed a novel core-sheath NF composed of PCL and PVA through coaxial electrospinning. Since PCL lacks biological recognition sites, we incorporated Col into the PCL sheath (PCL^{col}) to increase its cytocompatibility. The exposure of the internal amino acid sequence (Arginine-Glycine-Aspartic acid, RGD), due to the partial denaturing of Col in the organic solvent of PCL solution, provided numerous binding sites for the enhancement of cell adhesion and proliferation (Ekaputra et al., 2009; Taubenberger et al., 2010). The slow-degrading PCL^{Col} sheath provided a physical barrier for the slow drug release (Natu et al., 2011). We incorporated HA into the PVA

core (PVA^{HA}) to increase the surface roughness and mechanical strength of NFs. The exposure of some HA nanorods outside of the NF surface provide numerous functional anchoring sites for cell adhesion and proliferation. The PVA^{HA} core was used to mimic the bone structure and used as a reservoir for drug loading.

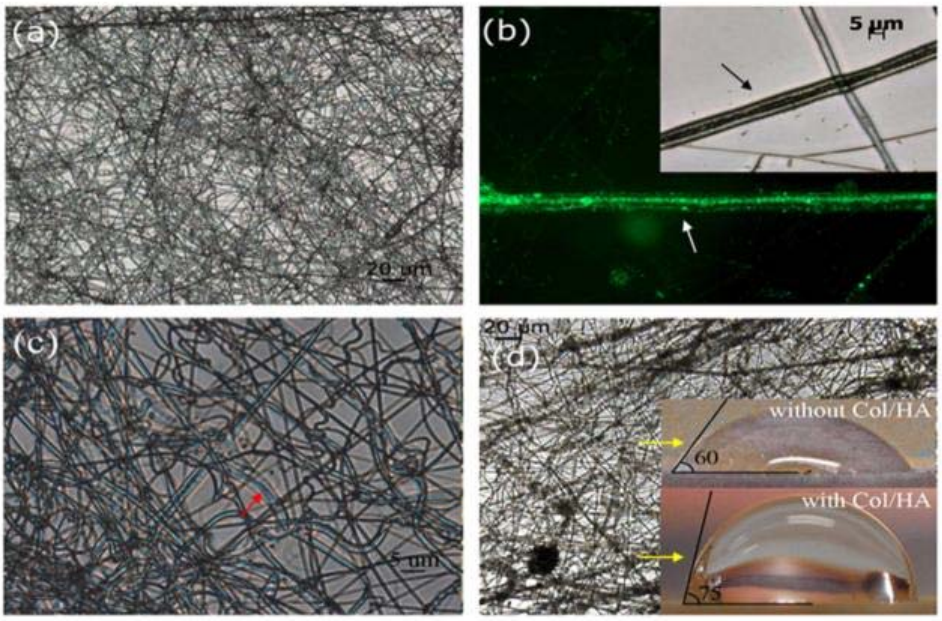

Fig. 27 Morphology of core-sheath NFs consisting of PCL^{Col} sheath and PVA^{HA} core. (a, c) Electrospun NF mesh on coverslips (original magnification, 100x and 400x, respectively).The red arrow indicates the embedded HA nanorods in the core fiber (c); (b) A representative fluorescence/visible image of core-sheath structure of NFs (Albumin-FITC encapsulated in the PVA^{HA} core as indicators, original magnification, 400x). The black arrow indicates a distinguishable core-sheath NF structure. The white arrow shows a distribution of albumin-FITC in both the core and sheath site in some segments, suggesting a diffusion of albumin from core to the sheath during electrospinning. The incorporation of both Col and HA nanorods formed a rough surface and numerous micro-projections, which are expected to increase the surface area of NFs and provide a favorable condition for cell growth; and (d) Representative image of PCL^{Col} / PVA^{HA} NFs 24 h after being soaked in water (original magnification, 100x). The integrity of the NF structure was still intact. The insert shows the contact angles on the surface of NFs with and without incorporation of Col and HA. A slight increase of the contact angle was observed by incorporation of Col and HA (yellow arrow).

Characterization of PCL^{col}/PVA^{HA} core-sheath NFs:

As shown in Fig.27, a distinguishable core-sheath structure of NFs was identified. Some of NFs showed a co-continuous (multi core-sheath) structure instead of a typical core-sheath structure. The finding of a distribution of albumin-FITC in both the core and sheath site in some segments of NFs suggested a diffusion of albumin from core to the sheath during electrospinning (Fig.27, b). The embedding of Col and HA formed a rough surface and numerous micro-projections, which are expected to increase the surface area of NFs and provide a favorable condition for cell growth. Surface wettability of NFs is critical for cell adhesion, proliferation, and migration (Kim et al., 2006a). Using a Contact Angle Goniometer, we found that the incorporation of Col in PCL and HA in PVA increased the contact angles of NFs (Fig. 27d, insert). SEM analysis (Fig.28) demonstrated that the mean average fiber diameter was 948 ± 179 nm. The average pore size was 96 ± 30 μm. The dimension of fibers is capable to encapsulate nano-HA rods in average size of 20-70 nm. The elemental composition analysis of NFs by EDAX showed the presence of Ca (from HA), C and O (from PVA, PCL), and N (from albumin and Col). A sharp boundary between the sheath and core fibers was observed by TEM (Fig.29). The formation of distinguishable core-sheath NF structures results from the immiscibility of the two polymer solutions during electrospinning. We noticed that HA nanorods were properly embedded in the PVA core and some HA nanorods protruded through the PCL sheath layer. The core-sheath fiber ratio is ~1:5.

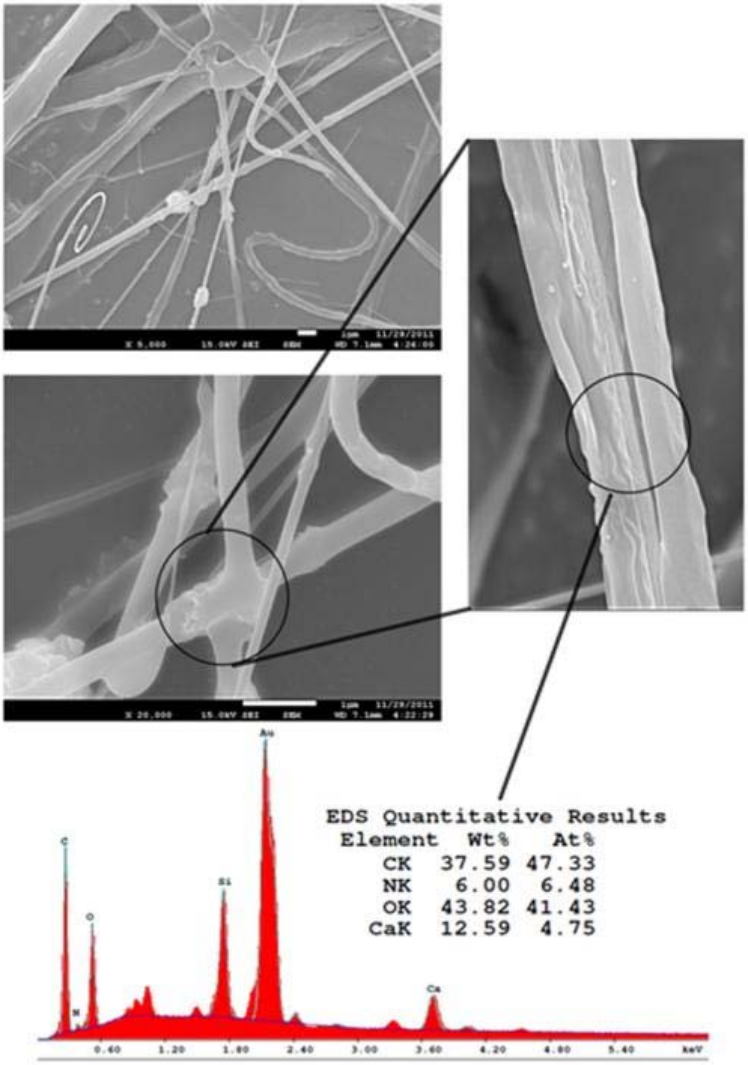

Fig. 28 SEM micrograph of PCL^{Col}/PVA^{HA} coaxial NFs (upper panel) and elemental composition of NFs by EDAX analysis on single NF (bottom panel).

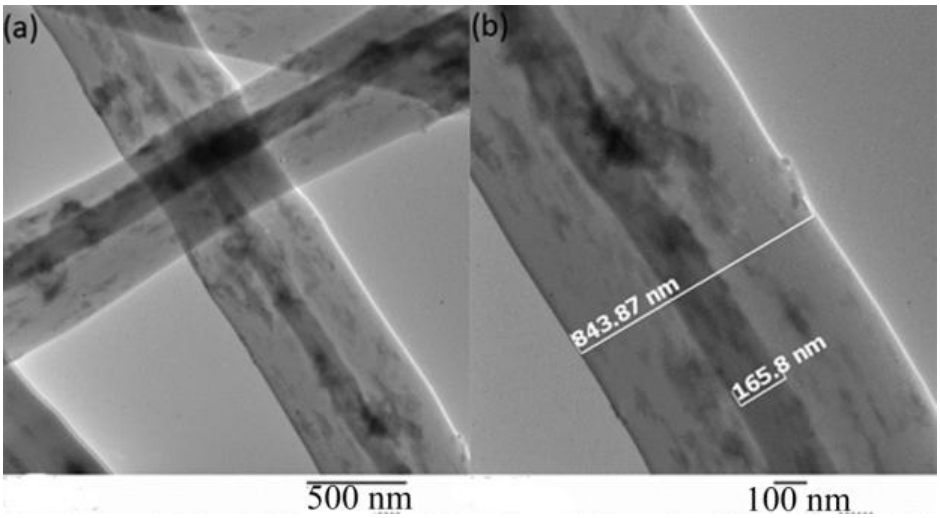

Fig. 29 Representative TEM images of PCL^{Col}/PVA^{HA} coaxial NFs (a) Overlapping NFs showing distinguishable core-sheath structure, and (b) The ratio of sheath/core fiber diameter is approximately 4:1.

Atomic force microscopy (AFM) of PCL^{Col}/PVA^{HA} NFs:

We investigated the morphology and mechanical property of both blended PVA NFs and The surface roughness of NFs was measured from the height images on the encapsulated HA nanorods (Fig. 30, A) in PCL^{Col}/PVA^{HA} NFs. In agreement with AFM images the Young's modulus (*E*) of PCL^{Col}/PVA^{HA} NFs (3.12 MPa) was significantly higher than that of the pure PVA NFs (0.83 MPa, $p< 0.05$) (Fig. 30, C). Our data indicate that the stiffness of PCL^{Col}/PVA^{HA} NFs is higher than blended PVA NFs. The potential impacts of NFs stiffness on cell behaviors will be carefully investigated.

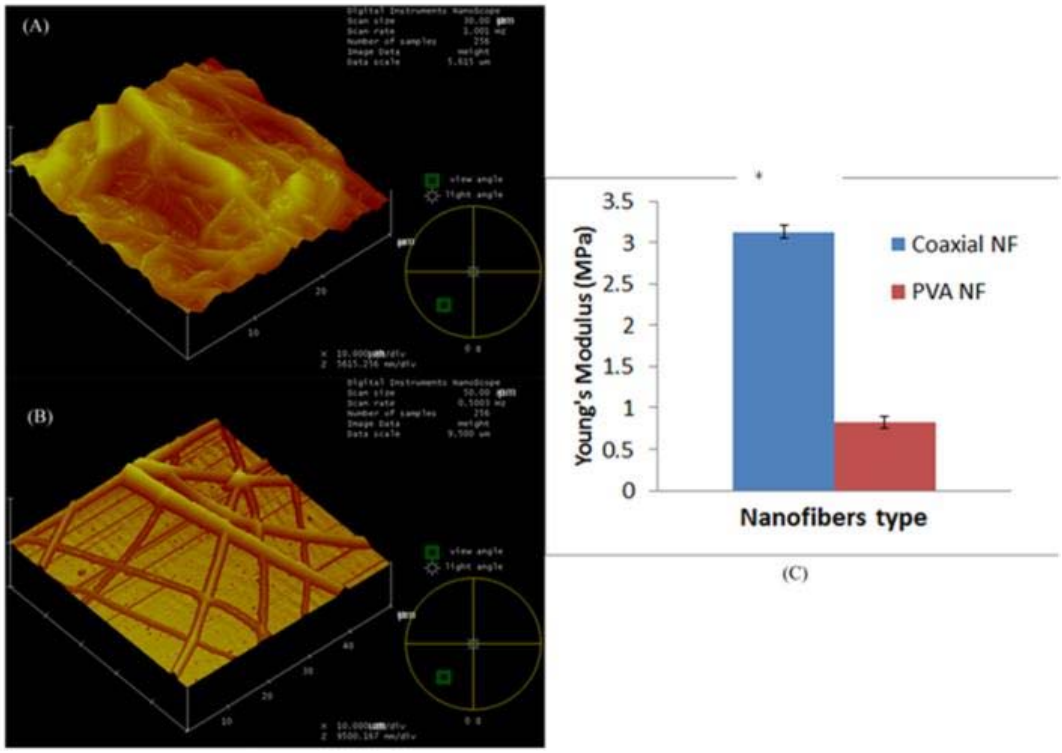

Fig. 30 3D AFM contact mode height images of (A) PCL^{Col} / PVA^{HA} coaxial NFs and (B) PVA NFs on Ti disc. (C) The mean Young's modulus (E) of single NF (n=6). *p < 0.05

Sustained release of Doxycycline (Doxy) and dexamethasone (Dex) loaded in PCL/PVA NFs:

The release of Doxy and Dex from both blended and coaxial core-sheath NFs was studied and the results are shown in Fig.31. NFs (blended or core-sheath) with Doxy loading were prepared. As shown in Fig.31 (B), blended PVA^{Doxy} NFs showed a burst release of Doxy within 10 h, and the release was complete within 48 h. When the PCL sheath was added to create the coaxial PCL/PVA^{Doxy} NFs, an extended Doxy release for over 700 h was observed, due to the protection of the slow-degrading PCL sheath. When Doxy was also loaded in the PCL sheath fibers (PCL^{Doxy}/PVA), both the burst release and the extended bacterial growth inhibition were increased when compared

to PCL/ PVA^{Doxy} NFs, as shown in Fig.31 (A). This might be due to the early erosion of the PCL sheath fiber. With the loading of Doxy in PCL sheath fibers bacterial growth inhibition is increased at first stage, as compared to PCL/PVA^{Doxy} NFs. Taken together, Doxy embedded in NFs during coaxial electrospinning is stable and its bactericidal activity is effective in a long term. We found that the blended PCL NFs (no Doxy loading) showed a gradual increase of bacterial growth inhibition, which might be due to the potential effects of PCL degradation products on *S. aureus* growth. Beyond 152 h (phase II), all PCL-containing NFs (with or without Doxy loading) showed a similar extent of bacterial growth inhibition, indicating complete Doxy release after 152 h. In conclusion, coaxial PCL/PVA core-sheath NF scaffolds represent a better device for a sustained and sufficient (> minimal inhibitory concentration) antibiotic release for at least 152 h. The Dex release profile is similar to the release of Doxy (Fig. 31). NFs weighing about 40 mg (encapsulating ~ 0.1 mg Dex) were soaked in 20 ml of sterilized distilled water in glass vials and incubated at 37^{o}C. At each time point, 1 ml of the supernatant was removed from the vial, and replaced by an equal volume of fresh water. The concentrations of Dex (at OD of 242 nm) in the supernatant were then determined using a UV–vis spectrophotometer. Similar to Doxy, blended PVA^{Dex} NFs showed a burst release within 10 h, and Dex was completely released within 48 h. Coaxial PCL/PVA^{Dex} NFs significantly extended Dex release for over 150 h. A slight increase of Dex burst release was found when Dex was added in PCL sheath (PCL^{Dex}/PVA^{Dex}).

Numerous studies have dealt with applying coaxial electrospinning for encapsulation of drugs in either the core or sheath or both (Huang et al., 2006). The sheath structure represents a physical barrier to reduce the initial burst release and protects the drugs in the core fiber. Drug release from NFs mainly relies on diffusion (Szentivanyi et al., 2011). The concentration gradient inside the core polymer matrix is the driving force for diffusion. In diffusion across a barrier (sheath), the driving concentration gradient is between the reservoir (core) and the release environment, which are separated by a barrier (sheath). In such a core-sheath system, a drug release rate is affected by both the concentration gradient and the degradation rate of the barrier. Therefore, control of the drug release rate can be achieved by preparation of various formulations and thicknesses of slow/fast-degradation sheath fibers and/or modification of physiochemical properties of NFs. We propose that the release of Doxy seems to be via diffusion and an erosion-coupled mechanism. The initial Doxy release, mainly due to the diffusion and surface erosion of the PCL sheath, provides an instant protection against bacterial adhesion and growth. Subsequently with the slow-degradation and hydrolysis of the PCL sheath, a controllable and sustained Doxy release is expected through a diffusion of Doxy from the core fiber crossing a degrading PCL sheath barrier, until the release is completed. In conclusion, coaxial core-sheath NF scaffolds are capable of providing controllable and sustained drug release, which is crucial for the implant osseointegration, because BMSCs require sufficient and sustained osteogenic signals for their differentiation and maturation, leading to new

bone formation.

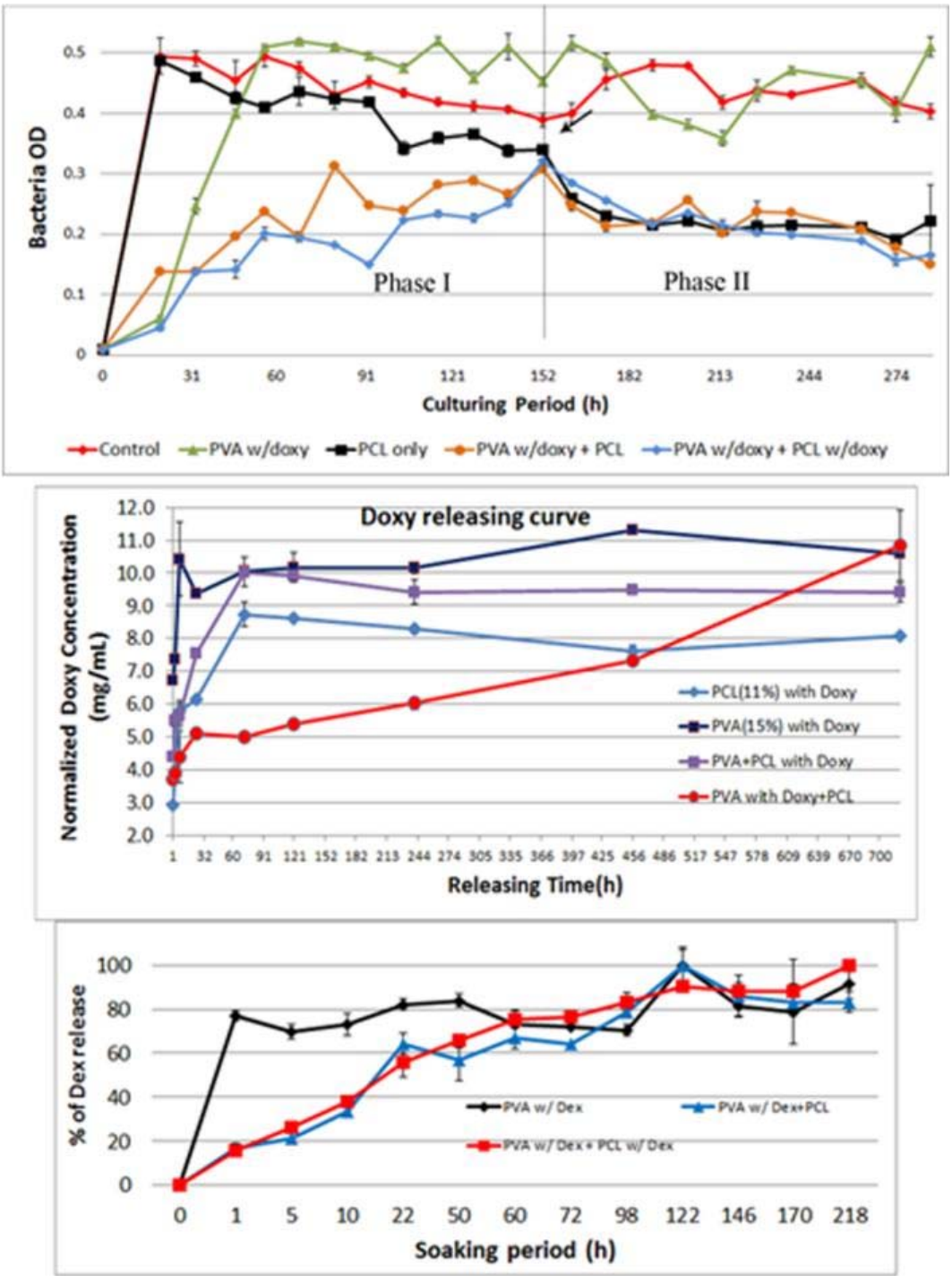

Fig.31 Drug release profiles. (A) A semi-quantitative *S. aureus* growth inhibition for release solution from NFs (blended or coaxial core-sheath) with/without Doxy incorporation at predetermined time points; (B) The cumulative concentration of Doxy released from NFs soaking in distilled water up to 700 h. (C) The cumulative concentration of Dex released from NFs soaking in distilled water up to 218 h. n=3.

Viability and proliferation of MC3T3 cells grown on PCL^{Col}/PVA^{HA} NFs:

Live–dead cell staining was utilized to determine the cellular response to PCL^{Col}/PVA^{HA} NFs by simultaneous monitoring of viable and dead cells after culturing for 3 days. No difference for red-stained dead cells was found between cells cultured on coverslips with (Fig. 32B) and without (Fig. 32C) PCL^{Col}/PVA^{HA} NFs. Results of the MTT assay showed that MC3T3 cells cultured on PCL^{Col}/PVA^{HA} NFs had a higher proliferation rate than that of cells cultured on coverslips. However, there is no statistical significance ($p>0.05$). It is well recognized that the cell behavior is largely influenced by the physiochemical properties of NFs. We found that the embedding of HA nanorods in electrospun PVA NFs significantly increased the surface roughness and mechanical strength of NFs, leading to the enhancement of cell adhesion, proliferation and differentiation. It is likely that a wide variability in NF diameters or the presence of a certain amount of large spaces might lead to the inferior cell adhesion and/or proliferation, because of the reduction of surface area. The cell adhesion and growth on the NF scaffolds can be enhanced by the embedded biological compounds, such as HA and Doxy. The loosely interlaced fibrous structures provide minimal obstruction and matched mechanical properties for cell migration. The living cells entering into the NF matrix by amoeboid movement migrate through the pores by pushing the surrounding fibers aside, because nanoscale NFs offer little resistance to the cell movement.

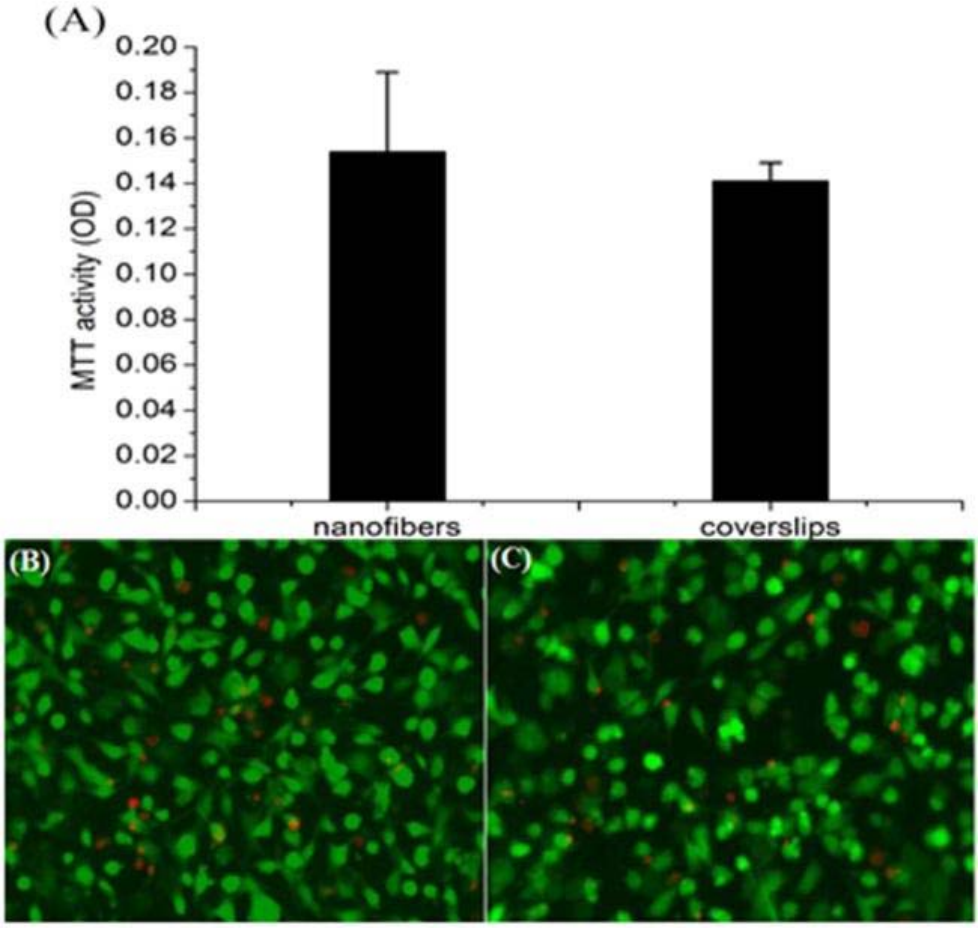

Fig.32 Viability and proliferation of MC3T3 cells grown on coverslips with and without coating of PCL^{Col}/PVA^{HA} NF scaffolds. (a) MTT activity assay for proliferation of MC3T3 cells for 8 days (Control: glass coverslips without NFs); (b, c) The live (green)-dead (red) staining (original magnification, 200×) of MC3T3 cells cultured on coverslips with (b) and without (c) coating of PCL^{Col}/PVA^{HA} NF scaffolds for 3 days. n=3

Characterization of bonding strength of PCL^{Col}/PVA^{HA} NFs to the titanium implant:

To determine whether the NF coating remained intact during implantation, we developed an ex vivo porcine bone implantation model. The maximum shear force required for insertion of NFs coated Ti rod was 20 N (shear stress = 0.17 MPa). The porcine bones with Ti rod implantation were then soaked in sterilized PBS at 37°C for 2 or 7 days. At each time point, the Ti rods were pulled out from the bone holes. The

force required to pull out the Ti rods from bone holes at 2 days was 10 N (shear stress = 0.085 MPa). We found that NFs coating remained intact on the surface of Ti rods after pullout. No disruption or delamination could be observed in the distal part of Ti rods (inside of bone), as compared to the proximal part of Ti rods (outside of bone). Our data showed that the bonding strength of NFs to the smooth surface of the Ti rods was higher than 0.17 MPa of shear stress.

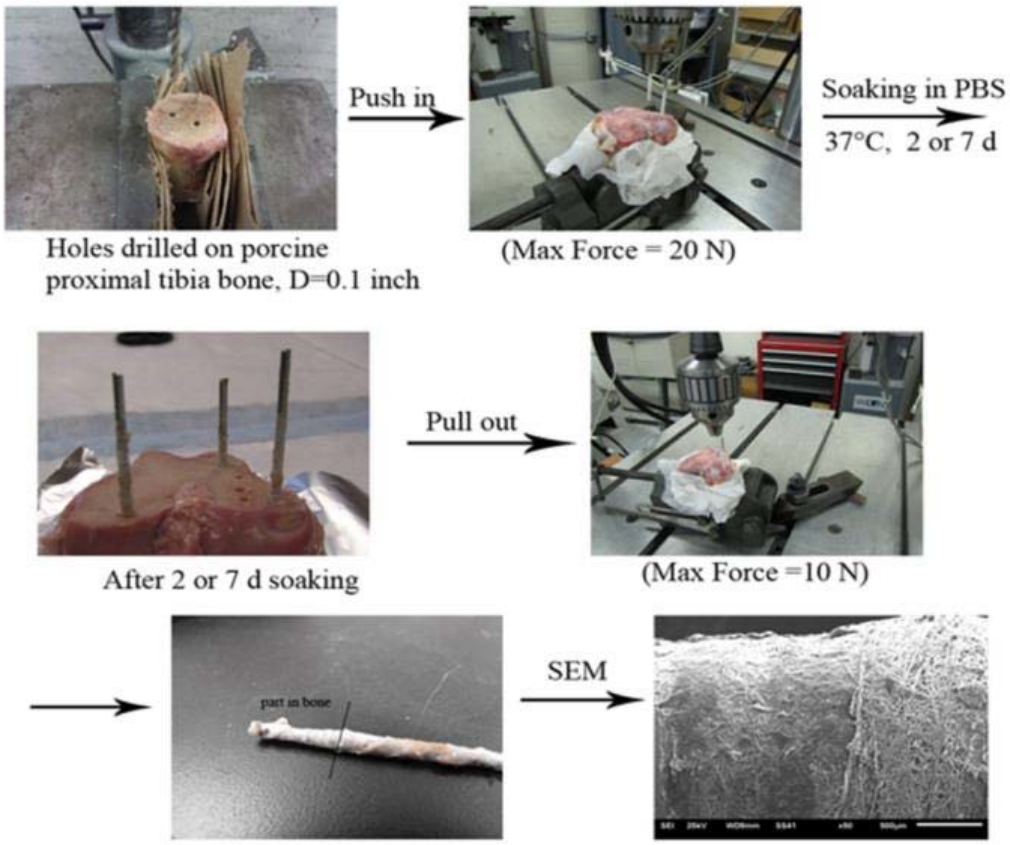

Fig.33 A flow chart of the Ti rod implantation and pullout procedure in a porcine bone implantation model. Holes were drilled in the dissected surface of porcine proximal tibia (diameter= 2.54 mm, depth= 15 mm). Ti rods (diameter = 2.5 mm, length= 60 mm) deposited with PCL^{Col}/ PVA^{HA} coaxial NFs (thickness= 50 µm) were slowly inserted into the drilled holes (rate= 10 mm/min) and the shear force was recorded. Ti rods inserted into tibia bone were soaked in sterilized PBS at 37°C for 2 or 7 days. Rods were subjected to a pullout test with the same rate and the shear force was recorded (n=3). Pulled out Ti rods were analyzed by SEM. The line drawn across the rod shows the border of Ti rod after pullout (in/out bone tissue).

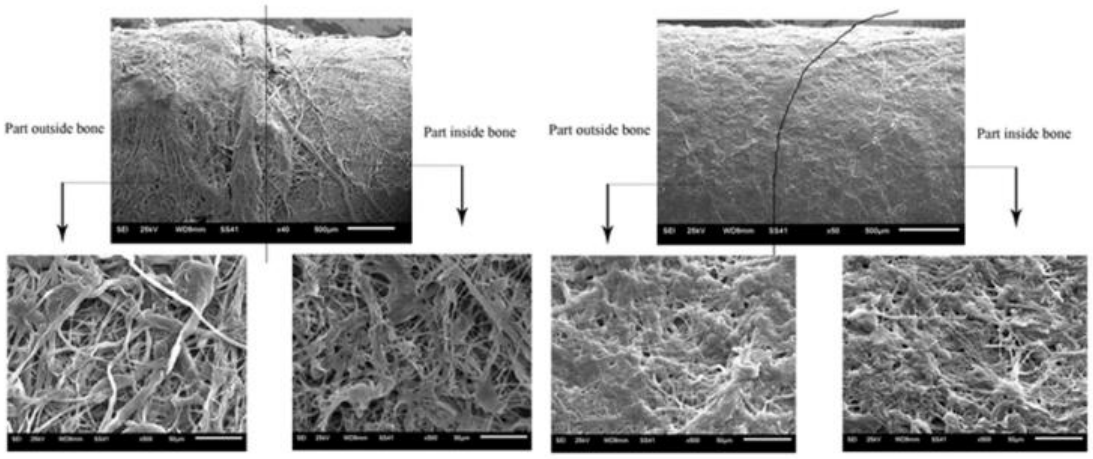

Fig.34 SEM micrograph of PCL^{col}/PVA^{HA} core-sheath NFs deposited on the surface of Ti rods by coaxial electrospinning. The Ti rods were pulled out from bone holes after incubation in sterilized PBS at 37°C for 2 and 7 days, respectively (10000 X). Dark line in the picture showing the interface of inside/outside of bone holes .

In separate experiments, SEM was used to measure the microstructure changes at the NFs/Ti interface of Ti rods pullout. As shown in Fig. 34, SEM images showed that the NFs network matrix remained intact and distributed evenly on the Ti rod surface. Partial degradation of NFs (both in and out of bone holes) could be found, especially after 7 days of incubation in PBS at 37°C. The partial degradation of NFs did not induce a significant change of NF diameters. Shear force applied (during insert and pullout) did not cause any visible disruption, delamination or folding of the NFs on the Ti rod surface. As compared to the NFs on the proximal part of Ti rods (outside of bone), the NFs matrix on the distal part of Ti rods (inside of bone) was less swollen, probably due to the defined space within the bone holes during soaking period. The NFs in the bone holes showed a much rougher surface than the NFs outside of bone. It might be due to the precipitation of biological apatite nanocrystals released from surrounding

bone onto the NF surface. In vivo, NFs with biological apatite layer incorporates proteins and promotes the adhesion of osteoprogenitor cells that would produce the extracellular matrix of bone tissue. Taken together, our data ensured that the NFs coating remains intact during implantation. This is important for the proposed study, because the drug loaded on the NFs coating layer will not be disrupted and the desired drug release dynamics can be expected.

The goal of this study is to demonstrate whether coaxial PCL/PVA NFs represent dual functional devices in enhancing implant osseointegration and eliminating bone infection. We have demonstrated NFs coating was capable to support local drug delivery in a sustained manner and effectively inhibit MRSA infection *in vitro*. In future study, a rat implantation model with MRSA infection will be utilized to further elucidate the impact of incorporation of antibiotics in the coaxial NFs on bactericidal activity and cellular responses (adhesion, growth and differentiation) *in vivo.* Additionally, a rat tibia implantation model is planned to be utilized for NFs coated Ti rod. The osseointegrationon NFs coatings would be characterized via a sodium fluoride (F18-NAF) PET imaging technology to identify the new bone formation. Histology imaging would also be applied to support the evidence of osseointegration.

Conclusion

In this study, we developed PCL^{Col}/PVA^{HA} coaxial electrospun NFs with defined

physiochemical and biological properties in order to enhance implant osseointegration. We demonstrated that the coaxial NFs encapsulated Doxy were able to Inhibit MRSA colonization and subsequent infection via controlled release of Doxy. The viability of loaded drug in PVA core phase was greatly improved by the barrier protection of PCL sheath structure. PCL^{Col}/PVA^{HA} coaxial NFs showed good biocompatibility and osteoconductivity. Taken together, PCL^{Col}/PVA^{HA} coaxial NFs could be applied as promising nanofabricated coatings with drug biomolecules/drugs loading capacity to promote earlier and sufficient implant osseointegration and prevent implant infections.

CHAPTER 6 IMPLANT SURFACE FABRICATION WITH COAXIAL NANOFIBER COATING TO ENHANCE EARLY IMPLANT OSSEOINTEGRATION IN A RAT MODEL

Introduction

Our previous study has demonstrated coaxial electrospun PCL/PVA nanofibers have excellent potential to be applied as implant surface modification materials. The purpose of this study was to evaluate its ability of inducing osseointegration and bacteria inhibition in vivo.

Many implant surface fabrication techniques have been developed with the aim of improving osseointegration (Anselme et al., 2010). However, current clinical studies found no significant improvement in clinical outcomes in patients (Steens et al., 2010). The weakness in adhesion, brittleness and burst drug release largely limits the current coating technology for further application, as addressed in previous chapters. Our previous study (Ren et al., 2010) showed that around 75% of the total amount of erythromycin loaded onto a titanium rod with HA coating was released within 24 h. Current studies demonstrated that the nanoscale topography of the implant surface is critical for earlier osseointegration (Gittens et al., 2011) and sustained drug release (Su et al., 2012b).

We have demonstrated that electrospinning was one of the promising technologies to fabricate nanofibers that can mimic bone nanoscale extracellular matrix (ECM) structure, as shown in previous studies. The potential application of

electrospun NFs for the enhancement of osseointegration is promising but obviously overlooked. We found three papers(Wang et al., 2011; Kohgo et al., 2011; Huang et al., 2008) demonstrating that the NF structural cues alone can be used to create an osteogenic environment without the use of exogenous factors(Wang et al., 2011). The cell attachment, proliferation, and differentiation of osteoblastic cells in vitro are significantly influenced by the physiochemical properties of NFs (Wang et al., 2011; Huang et al., 2008). More efforts are required to understand the interplay between the physiochemical natures of NF scaffolds and the fate of local osteoblast/osteoclast cells.

Animal models for studies of implant osseointegration typically involve the use of large animals such as dogs, sheep and rabbits. Although these models have the advantages of large bone/joint size and the ability to use a realistic prosthetic implant, the cost and ethical issues prevent broad employment of large animals. In this study, we used a rat tibia implantation model (Ren et al., 2012). Titanium (Ti) pins were inserted into the proximal tibia. This model is simple and highly reproducible. This model has been widely used for the evaluation of implant osseointegration by local drug delivery and implant surface modification (Li and Nilsson, 2001; Xu et al., 2011; Mekraldi et al., 2003).

Positron Emission Tomography (PET) provides information on distribution and kinetics of injected radiotracers in vivo. ^{18}F-Fluoride (^{18}F-NaF) was used as a bone imaging agent nearly 40 years ago. After diffusion through bone capillaries into bone

extracellular fluid, F- ion exchanges with hydroxyl groups in the hydroxyapatite crystal to form fluoroapatite. F- is preferentially deposited at the bone surface where turnover is greatest. ^{18}F-NaF has been used as a clinical routine to detect cancer metastatic lesions to the bone that is important for diagnosis and staging. Whereas the clinical value of ^{18}F-NaF in detecting metastatic bone disease is validated, its clinical value to assess implant osseointegration has not been firmly established.

The objective of this study was to determine the therapeutic efficacy of these NF scaffolds in vivo for the implant osseointegration using a rat model. We propose that Ti with NF coating significantly enhanced implant osseointegration and PET ^{18}F-NaF can be used to quantitatively and noninvasively evaluate the implant osseointegration in vivo.

Materials and Methods

Study design

To determine whether Ti with nanofiber coating increased implant osseointegration in vivo, total six rats were included in this study. Rats were divided into two groups: Ti pin with (n=3) and without (n=3) nanofiber coating. Rats were PET scanned at 2, 4 and 8 weeks after Ti pin rat tibia implantation.

Preparation of coaxial nanofibers and Titanium coating

10% (w/v) PCL solution was prepared by dissolving 0.5 g of PCL in 5 ml of dimethylformamide (DMF)/chloroform (1:1,v/v). The 10% PVA solution was

prepared by dissolving PVA in distilled water. Coaxial electrospinning was performed using a custom made coaxial nozzle consisting of a hollow stainless steel t-junction with a fully penetrating 19-gauge core needle. The PVA solution (for core fiber) and PCL solution (for sheath) were uploaded to the syringes. The syringes were attached to syringe pumps set at a flow rate (Q) of 0.5 ml/h. An 18 kV voltage was applied to the needle from the power supply. The distance from needle tip to collector was 10 cm. A rotational speed of 500 rpm was used to evenly deposit the formed nanofiber on the Ti pin attached to the stainless steel hexahedron collector, which was linked to the shaft of a motorized stirrer. For this in vivo study, we deposited electrospun PCL/PVA NFs directly on the surface of Ti pin (diameter = 1 mm, length = 10 mm) covering the entire surface of the Ti pin stem. The thickness of the NFs coating is ~ 50 μm, measured by a micrometer and SEM. Ti pins with NFs coating were sterilized by UV light overnight right before implantation. We found that UV irradiation is a very effective sterilization method and has least effects on the morphology and structural properties of NF structures.

Rat tibia implantation model

All research protocols of animal use were approved by the Institutional Animal Care and Use Committee of Providence Hospital and Wayne State University. Sprague Dawley (SD) rats (female, body weight of 200g-300g) were anesthetized by intra-peritoneal injection of ketamine (75 mg/kg) and xylazine (8 mg/kg). The right hind limb area was shaved and sterilized with 70% alcohol. The center of tibial plateau was

reamed to form a circular indent of 1.5 mm diameter and 0.5 mm depth. The proximal 5 mm of the tibial intramedullary canal was reamed with a 0.8 mm dental drill through the center of the plateau. A titanium (Ti) pin (diameter 1 mm, length: 10 mm, Stryker Orthopaedics, NJ) with/without nanofiber coating was implanted into the proximal tibia to form part of a knee joint, as shown in Fig.39. The wound was cleaned and rinsed with sterilized saline containing Penicillin G (500 unit/ml) and Streptomycin (500 μg/ml) before being closed by suture in layers.

Histomorphometry

We followed the methods, as described by Dr. Jiang (Jiang et al., 1997; Jiang et al., 2003). During the distal tibia bone segments (including part of the Ti pin) were fixed and dehydrated in graded ethanol (70-99%) and defatted in acetone. Specimens were then placed in 99% propanol before being embedded in cold poly(methylmethacrylate) (PMMA) without decalcification. Perpendicular to the tibia shaft, each specimen was sectioned in 100-μm thick slices using a rotary diamond saw. The sections were ground to a thickness of ~ 30 μm by Leica SP2600 (Germany), and then stained with 1% toluidine blue. Bone-to-implant contact (BC) was calculated as the linear percentage of the interface with direct bone-to-implant contact to total interface of the implant in the cancellous bone. Bone area ratio (BA) was measured as the area percentage of bone tissue to the whole area, which will be defined as a ring extending 200 μm from the implant surface.

μPET scanning protocol.

Imaging was performed using the μPET R4 tomography (Concorde Microsystems, Knoxville, TN). Rats were anesthetized with a mixture of ketamine (100 mg/kg) and Xylazine (7 mg/kg) using a nose cone and positioned in spread supine position on the μPET bed. In order to achieve reproducible positioning of the rat in the μPET and μCT scanner gantry, we used an in-house developed whole body holder. The holder consists of a short plate on which the animal's body rests and is secured with multiple Velcro straps as well as with head positioning screws. Attached to the holder are three fixed plastic receptacles of 5mm diameter in which porous beads can be inserted. These beads are visible in both the μPET (radioactivity) as well as in the μCT (plastic) images and were used for co-registration of the two imaging modalities. Initially, a 17 min transmission scan was acquired to correct for attenuation of 511 keV photons. Following the transmission scan, the rats were injected with the tracer ^{18}F-NaF (10 MBq) and a 60 min list mode scan was acquired. A subset of mice will be kept overnight and the ^{18}F-NaF scan was repeated, following injection of unlabeled tetracycline (10 μg/ml) in order to determine the amount ^{18}F-NaF displacement with cold TC. The list mode data were recombined into a frame sequence (6 x 10s, 4 x 30s, 2 x 120s 3 x 300s, 4 x 600s) and all images were subsequently reconstructed using measured attenuation, scatter correction, and the OSEM2D iterative algorithm, yielding images with an isotropic resolution of about 2mm FWHM. At the conclusion of the ^{18}F-NaF scan the animals were sacrificed, and knee joint tissues (implanted and un-implanted controls)

were collected for histological and SEM analysis.

μPET data analysis

A calibration factor was routinely established in our micro-PET facility, which is subsequently used to convert counts/pixel/min to units of μCi/cc for the PET tracers. All images were processed using the AMIDE data analysis software. Initially, regions of interest (ROIs) were defined bilaterally at the location of the tibia joint in μCT images and copied to the co-registered PET images. In addition, a small ROI was defined at the location of the left ventricle (LV) in early PET image frames (showing the bolus activity) in order to obtain the arterial input function. Subsequently, time-activity curves were obtained and used to estimate kinetic parameters using a two-tissue (parameters K1, k2, k3) kinetic model. This model has been shown to accurately characterize ^{18}F-NaF tracer uptake. A semi-quantitative analysis of tracer uptake was performed using the standard uptake value (SUV), which is defined as the tracer concentration in tissue (μCi/cc) normalized to the injected activity (μCi) per weight (g). Tracer concentration was obtained by averaging 10-30 minutes of the dynamic acquisition.

SEM methodology

The harvested Ti pin sample from rat tibia was firstly fixed in 4% paraformaldehyde for 30 min. Then samples were orderly dehydrated in 50%, 60%, 70%, 80%, 90%, 100% ethanol for 10 min, respectively. Before SEM observation, samples were gold-coated (Gold Sputter, EFFA Coater, Redding, CA, USA) and the morphology of Ti pin surface was characterized by Scanning electron microscope (SEM)

(JSM-6510LV-LGS, MA, USA). Morphologies were viewed at a 25 kV accelerating voltage.

Push-in test

The proximal parts (with Ti pin) of tibia samples used for push-in testing. Soft tissue around the tibia was removed to expose the surface of the implanted Ti pin head and proximal tibia. The dorsi side of the tibia sample was then fixed into a self-manufactured aluminum fixture with a central cylindrical hole, as shown in Fig.36 (c). The inserted tibia was stabilized by facilitated screws from four directions. Approximate alignment was achieved by positioning the tibia parallel to push-in probe with the loading axis of the Instron model 8841 Universal Materials Test Machine. Proper specimen alignment was obtained by adjusting the two rotational axes of the fixture while using continuous fluoroscopy to confirm perpendicularity of the pins with respect to the fixture base. Once the fixture is attached to the load cell, the fixture aligned along the x-axis and y-axis cross slides to obtain alignment between the extraction pin and the implants. Under position control, the Instron 8841 actuator pushed the Ti pins into the bone marrow at a rate of 1 mm/minute. Actuator position and load recorded by a PC using software. The Ultimate Shear Strength (the peak push-in force) and energy for complete pin push in (integration of push-in force and displacement) was used to reflect the osseointegration of interface.

Statistical Analysis

Initially, regions of interest (ROIs) were defined bilaterally at the location of the knee joint in microCT images and copied to the co-registered PET images. Subsequently, the BP and SUV values were derived from the operated (R) and non-operated (L) knee joint and used to calculate the asymmetry index (AI) defined as

$$AI(\%) = 100\frac{(R-L)}{0.5(R+L)}$$

yielding for the two groups the AI(BP) and AI(SUV). A comparison of these two AIs within each group was conducted using the Wilcoxon sign rank test for non-parametric data, whereas comparison between the two groups was made using the Mann-Whitney U test. A *p* value of less than 0.05 was considered to be a significant difference. All data was analyzed using the SPSS software package (version 7.5; Chicago, IL).

Results

SEM analysis

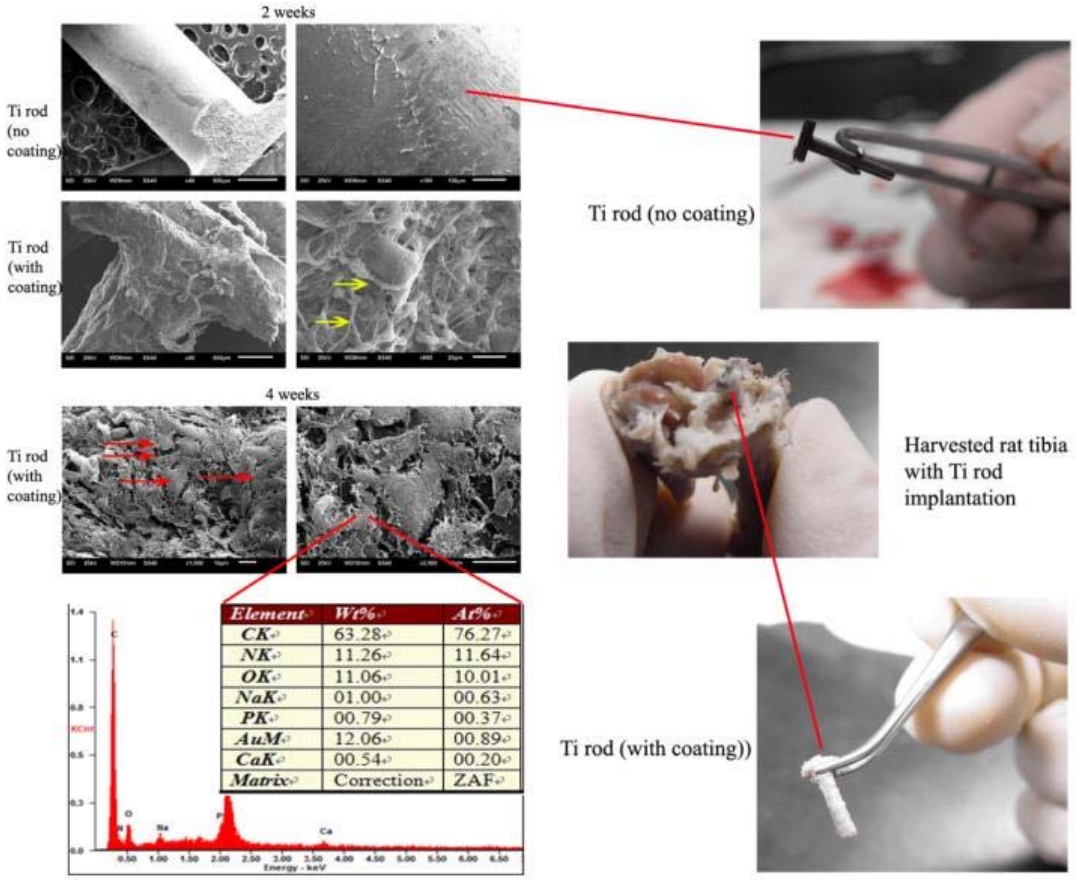

Fig. 35 SEM micrograph of NF-coated Ti-pin implanted in rat tibia and the surface elemental analysis by EDAX. Red arrows: cells; Yellow arrows: nanofibers.

As shown in Fig. 35, the surface morphology of NF-coated Ti pin harvested from Rat tibia after 2 and 4 weeks of implantation was obtained from SEM micrograph. In comparison with Ti pin without NF coating at 2 week time point, NF-coated Ti pin has rough surface created by NFs. The nanostructure of NF can still be observed (yellow arrow) and the NF coating remained firmly attached to the Ti pin surface after 2 weeks of implantation. This result indicated the delamination of NF coating contacted with surrounding bone tissue was not occurred during implantation. At 4 week time point, bone cells attached to NF matrix can be clearly viewed, and the cell showed a well

spread and proliferative morphology, which indicated bone cells started migration and proliferation on NF coated-Ti pin surface within 2-4 weeks. Ti pin without NF coating showed no attached cells, which indicated its bio-inert property. EDAX elemental analysis on area of interest with large amount of cells was performed. The spectrum showed high amount of N that does not come from either Ti pin or NF coating. The only possible source of N is from extracellular matrix. This result confirmed the bone cells laid down high content of extracellular matrix (possibly collagen) within 4 weeks, which is crucial for initiation of bone remodeling. The implanted NF-coated Ti pin showed magnificent biocompatibility and osteoconductivity, which presents improvement for enhancing Ti-based implant osseointegration.

Mechanical testing

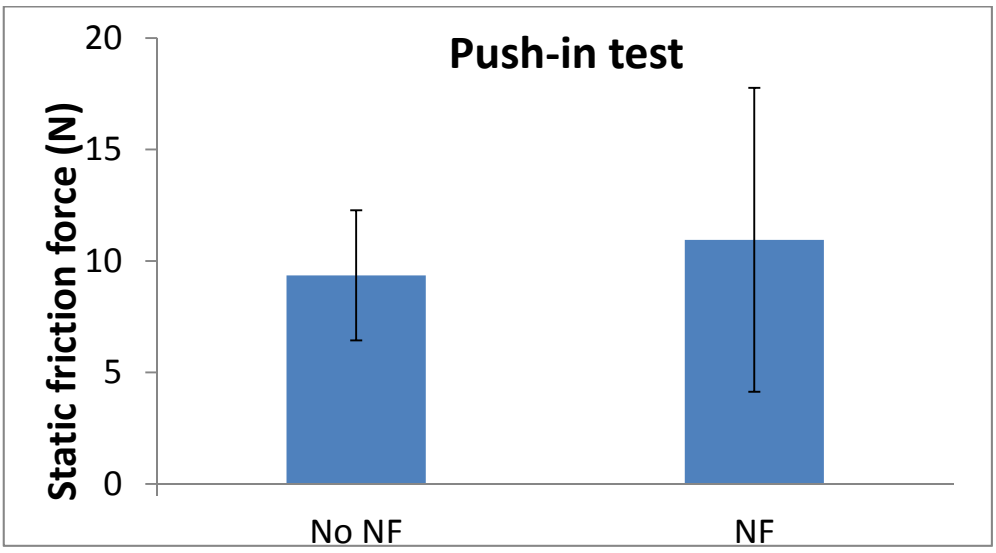

(a)

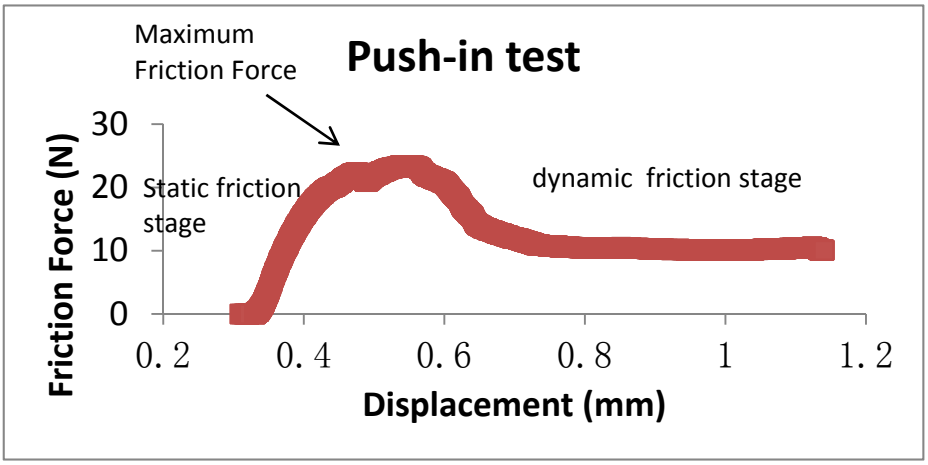

(b)

Fig 36(a) a pilot study of Rat tibia implanted Ti-pin push-in test. Rat tibias were harvested after implantation for 8 weeks. n= 5. (b) representative force vs displacement curve for push-in test. The static friction force was determined as Push-in force.

Fig.36 shows that the present study gives push-in forces that are within the range reported by previous studies (Yang et al., 2007). For Ti pin inserted into rat tibia, the presently measured range of composite bone push-in loads 5-20 N. When push in load was vertically applied to Ti-pin in y direction, friction force was generated from interface between NF coating and surrounding bone tissue. Ideally, the static friction force was constantly increased until the maximum static friction force was reached. In general, this progress takes about 0.1 mm of displacement to achieve due to the plastic behavior of polymer based NF matrix and then the Ti pin will start to move. A constant dynamic friction force will be recorded. The maximum friction force was determined to be the push in force to reflect the bonding force between NF coating and surrounding bone tissue. After 8 weeks of implantation, bonding strength of Ti-bone was detected in a range of 10 N (control), which indicated the osseointegration was occurred. The push in force of NF groups is a little higher than Non-NF group though

not significantly, which indicates the NF coating provides some positive effect on bonding strength between bone and implant. We hypothesize that longer duration of implantation might show larger difference between NF groups and Non-NF groups.

PET data analysis

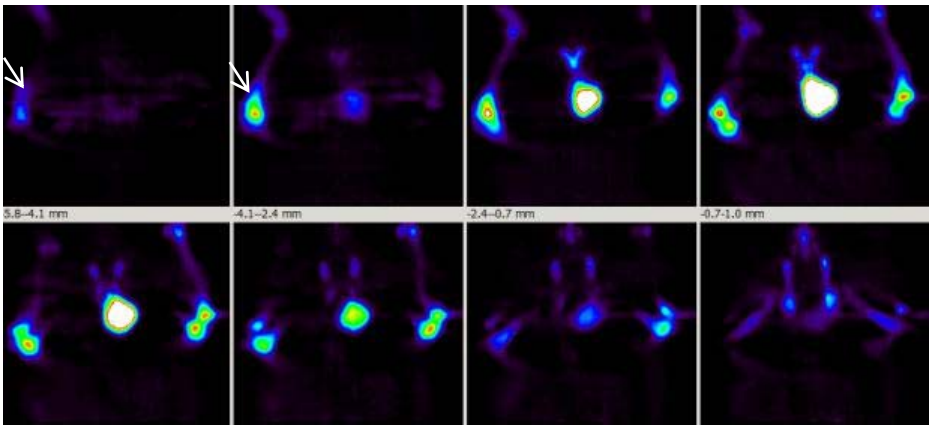

(a)

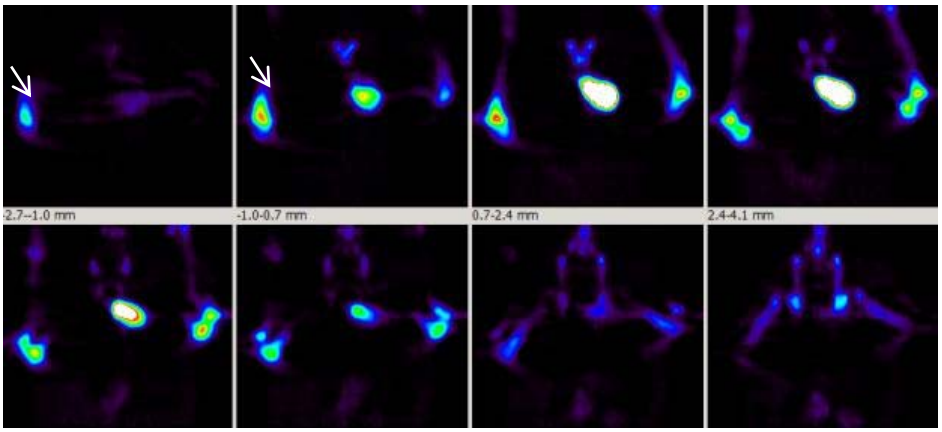

(b)

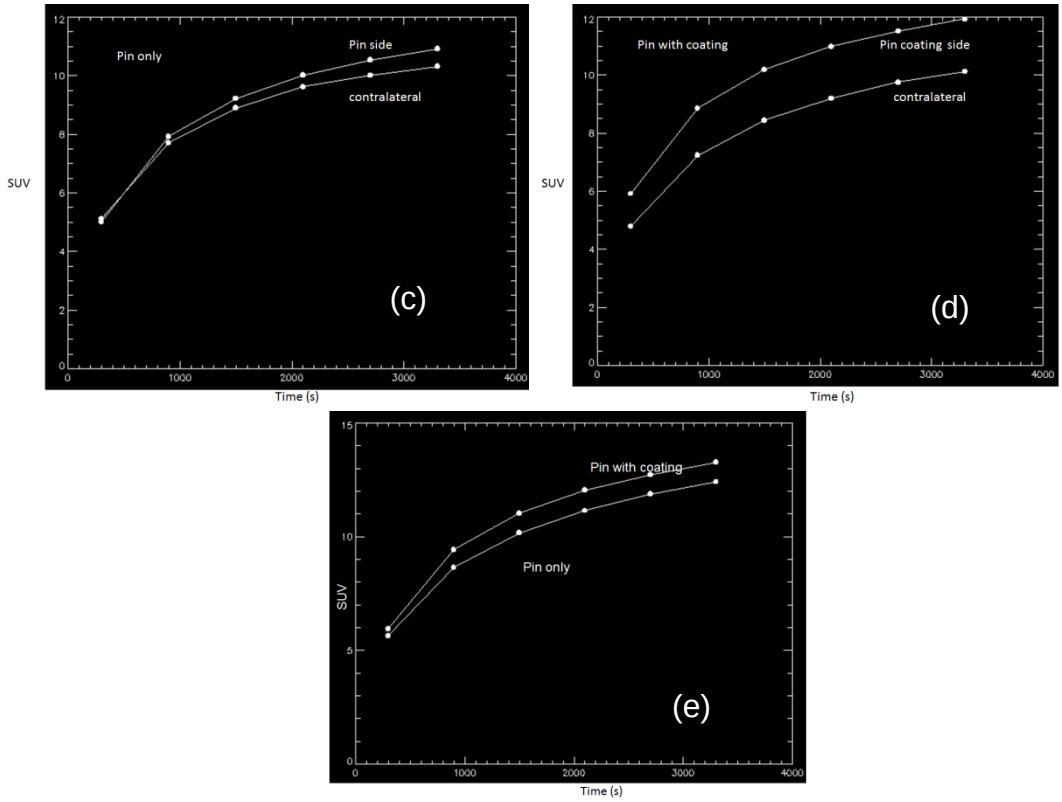

Fig. 37 F18-fluoride PET images of a rat with non-NF-Ti pin (a) and NF-Ti pin (b). Uptake of tracer shows significant asymmetry between the operated (left, arrow indicated) and control (right) tibia. A standard uptake value (SUV) from (c) non-NF Ti pin implantation side (left) and control (right); (d) NF Ti pin implantation side (left) and control (right); (e) comparison of non-NF Ti pin implantation and NF Ti pin implantation.

Representative PET images are shown in Fig. 37. As shown in Fig. 37, for both non-NF-Ti pin (a) and NF-Ti pin group, the operated (left) tibia SUV values were obviously higher than control (right) group. It also can be observed that the gap of non-NF-Ti pin tibia to control is much smaller than NF-Ti pin tibia to control. Accordingly in comparison, SUV of NF-Ti pin group was also higher than non-NF-Ti pin group values. It confirmed that Ti-pin implantation enhance the new bone formation. Moreover, NF coated Ti pin further improved the osseointegration to Ti-pin surface.

Hard tissue sectioning

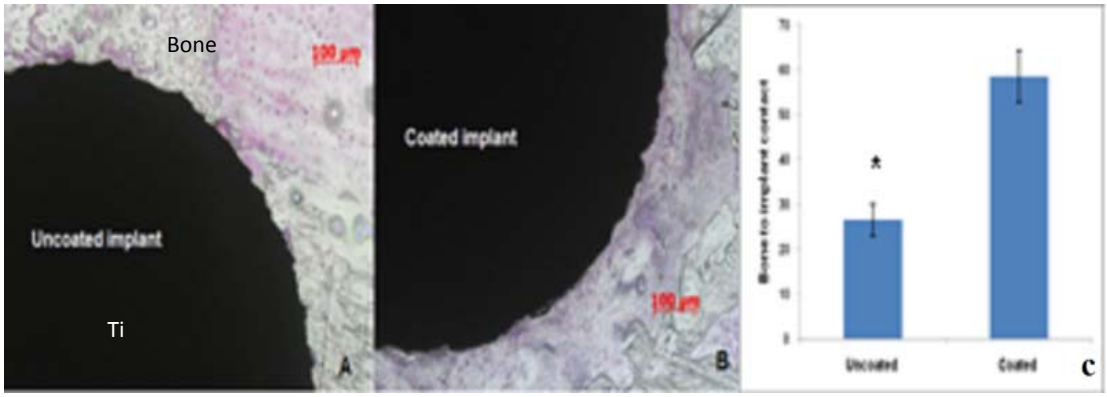

Fig. 38 Histological images of the bone/Ti pin interface 8 weeks after implantation (a, Uncoated; b, coated; H&E stain, original magnification ×100); and results of the BC (c) in histomorphometry. Data are expressed as mean ±SD, n =3 per group. *p< 0.05.

As shown in Fig.38, image analysis of tissue sections stained with hematoxylin and eosin showed that new bone formation around implant were characterized by increased (H&E +, red) osteoblast proliferation. It was observed that NF coated Ti pin significantly increased osteoblasts proliferation and activity as compared with uncoated Ti pin. Quantitative image analysis, as shown in Fig.38 (c), revealed that NF coatings significantly induced osteogenesis (P < 0.05).

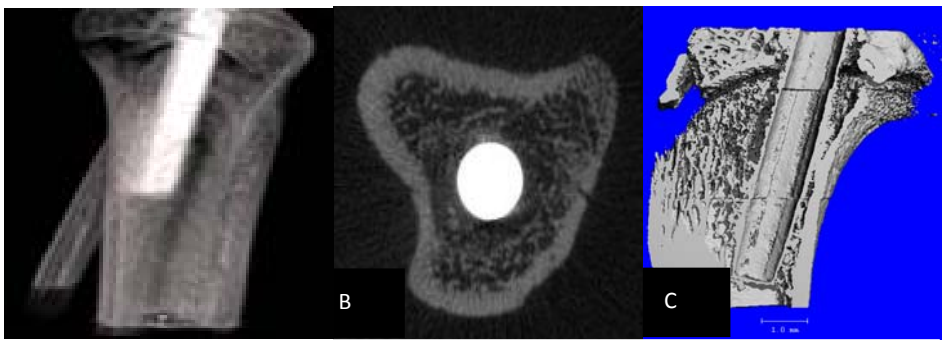

Fig.39 µCT: (A) Ti pin implantation at implant/bone interface; (B) cross-section and (C) reconstructed longitudinal section.

Discussion

In previous study, we found that the PCL/PVA NFs are biocompatible and enhance the adhesion and proliferation of murine osteoblastic cells. The release of Doxy from coaxial PCL/PVA NFs showed more controlled release compared with the blended NFs. Using an ex vivo porcine bone implantation model we found that the PCL/PVA NFs bind firmly on the Ti pin surface and the NFs coating remained intact on the surface of Ti pin after push-in. We propose that PCL/PVA NFs encapsulating drugs have great potential in enhancing implant osseointegration in vivo. In this continuing study, we used a rat tibia implantation model (Ren et al., 2010) to determine the effects of Ti pin with PCL/PVA NF coating on the implant osseointegration in vivo. Pins were inserted into the proximal tibia. This model is simple and highly reproducible. This model has been widely used for the evaluation of implant osseointegration by local drug delivery(Back et al., 2012) and implant surface modification(Cheng et al., 2012). The tibia implantation model is designed so that cyclical loading is transmitted to the bone-implant interface to mimic post-operative mechanical environment. Our data demonstrated that Ti pin with nanofiber coating increased implant osseointegration as compared to that of uncoated Ti pins up to 8 weeks.

To date, reliable visualization of the intensity and distribution of new bone adjacent to an implant soon after surgery is still lacking. There is clearly a need to establish noninvasive, accurate and specific diagnostic tools for the monitoring the status of implant osseointegration. This is of particular importance, as the prognosis

and treatment plan is completely different for those with dysfunctional implant osseointegration. PET imaging has been established as a major research tool in many areas of life science, clinically relevant applications of molecular imaging in the orthopedic field have been limited (Su et al., 2012a). ^{18}F-fluoride (^{18}F-NaF) is a nonspecific bone tracer that has been used for skeletal imaging since the late 1960's. Diffusion through capillaries into bone extracellular fluid leads to a slow exchange of fluoride ions with hydroxyapatite crystals forming fluoroapatite. Due to the fact that remodeling and bone turnover is greatest at the surface, it is mainly stored there (Gluck et al., 2011). Moreover, the “first-pass” extraction of ^{18}F-NaF from blood through the capillary membrane into the bone is almost 100%. The use of ^{18}F-NaF in the evaluation of implant osseointegration has been so far limited(Su et al., 2012a; Kim et al., 2008; Ren et al., 2010). Uilmark et al. (Back et al., 2012) used ^{18}F-NaF PET to monitor new bone formation in periacetabular bone adjacent to the implant in 16 bilateral THA patients 1 week, 4 months and 12 months after surgery and concluded that ^{18}F-NaF PET is a valuable tool to analyze bone formation and secondary stabilization of acetabular cups. In another study (Cheng et al., 2012), these same investigators found ^{18}F-NaF PET imaging to be a useful method for evaluating the healing of morselized bone allograft, impacted in large osteolytic acetabular defects at revision arthroplasty. Nevertheless, the number of publications describing the use of ^{18}F-NaF PET imaging for orthopeadic application is rather modest. In this study, we found that ^{18}F-NaF PET imaging is helpful to semi-quantitatively evaluate the status of

implant osseointegration. There is a general correlation between ^{18}F-NaF tracer uptake and histomorphometric parameters and SEM description.

Consistent with the PET imaging findings, the SEM analysis demonstrated the evidence of implant osseointegration at both 2 and 4 weeks after implantation. In addition, histology data showed that there was an improvement of implant ossoeintegration in the Ti pins with nanofiber coating, as compared to that of Ti pin without NF coating 8 weeks after implantation.

One of the limitations in this study is that the sample size is small and was conducted as a proof-of-concept experiment. Though we demonstrated a higher implant osseointegration in the rats with coated Ti pins at any given time points as compared to that of uncoated Ti pins, no significant difference could be established, thus follow-up studies with larger sample size are warranted.

CHAPTER 7 IMPLANT SURFACE WITH DOXYCYCLINE-DOPED NANOFIBER COATING TO TREAT IMPLANT INFECTION IN RAT MODEL

Introduction

The purpose of this investigation is to determine whether NFs doped with certain amounts of Doxycycline (Doxy) are functional in eliminating SA infection using a rat tibia SA infection model (Ren et al., 2012). Specifically, we determined whether NF coatings at current Doxy loading and drug release dynamics are sufficient to inhibit SA infection over a period of up to 8 weeks. We propose that Doxy released from NF coatings can be delivered to the infected surface of the implants and exerts its antibacterial activity for up to 8 weeks. We prepared electrospun Doxy-doped NF scaffolds on the surface of Ti pin that were used in this rat tibia SA infection model.

Doxy is a tetracycline class broad-spectrum antimicrobial agent effective against variety of bacteria, including SA (Zhang et al., 2007). The effects of Doxy on bone modeling have been investigated (Zhang et al., 2007; Park, 2012). Doxy inhibits osteoclast activity. We previously demonstrated that Doxy effectively inhibited implant wear- induced osteoclast activity and osteolysis in a mouse model(Zhang et al., 2007). Franco et al.(Franco et al., 2011) studied the mechanism of action of Doxy in this regard, and found that Doxy reduces RANKL- induced osteoclast formation by its inhibitory effect on matrix metalloproteinase (MMP-9) activity that is independent of the MAPK-NFATc1 signaling cascade. Doxy promotes osteoblast differentiation (Park, 2012) and

enhances bone healing. Waleed et al.(Al-Ali et al., 1989) reported that an augmentation of new bone formation was achieved in a dog ligature-induced bone defect model when a combination of Doxy and tricalcium phosphate was applied. Park et al.(Park, 2012) investigated the effect of Doxy on the viability, differentiation, and mineralization of murine preostoblastic MC3T3-E1 cells. They found that Doxy treatment has no effects on the morphology, viability and growth of these cells. However, a marked increase of alkaline phosphatase (ALP) activity was noticed in Doxy- treated cells as compared to cells without Doxy treatment. In addition, Doxy increased the production of bone morphogenetic protein-2 and phospho-Smad1/5 expression. To avoid the side effects of Doxy, such as gastrointestinal disturbance, candidiasis, and vestibular concerns, a lasting and controllable local Doxy delivery is highly desired. We propose that a local delivery of Doxy through the core-sheath NFs represents a new approach for the prevention of implant infection and augmentation of implant osseointegration. It was reported that a high dose of Doxy (>0.5 mg/ml) inhibited the growth of osteoblasts(Almazin et al., 2009). Therefore, we incorporated a lower amounts of Doxy (100 μg/ml) into the core-sheath NFs. We determined the appropriate dose and release dynamics of Doxy from these NFs and the therapeutic efficacy of Doxy-doped NFs in treating SA-infected implants in a rat tibia implantation model.

In this study, we used a rat tibia implantation model (Allen et al., 1996; Ren et al., 2010). Titanium (Ti) pin was inserted into the proximal tibia. This model is simple and

highly reproducible. This model has been widely used for the evaluation of implant osseointegration by local drug delivery (Back et al., 2012; Song et al., 2010b) and implant surface modification (Cheng et al., 2012; Diefenbeck et al., 2011; Raquez et al., 2011).

Rat tibia implantation model with bacterial infection is an established model to mimic periprosthetic infection (Monzon et al., 2001; Lucke et al., 2003; Schmidmaier et al., 2006). Periprosthetic infection can be initiated by the inoculation of a bacterial suspension at the site of infection in order to produce biofilms (Power et al., 1990) or the use of a pre-colonized implant (Ward et al., 1992). Mixed-models, involving the use of both a pre-colonized implant and a bacterial suspension (Gracia et al., 1998) were reported to reproduce the clinical use of infected implants and bacterial suspensions of washing solutions at surgery and systemic infections. One limitation of the mixed models was difficult to distinguish the biofilm formed on the implant from that of the inoculated bacterial suspension. Therefore, we used a pre-colonized implant approach (Monzon et al., 2001) in reproducing a chronic biofilm infection in implant and bone, thus being suitable comparative studies on antibiotic performance. An appropriate bacteria inoculation (colony-forming units, CFU) is to maintain the rat infected without significant systemic toxicity. Previous studies showed that inoculation of S. aureus in the dosage between 10^2– 10^6 CFU showed similar histological changes (Lucke et al., 2003). In some of these models the number of bacteria used in the inoculated biofilms can be as high as 10^8 CFU (Gracia et al., 1998) in the tibia implant site without

significant systemic symptoms (Ren et al., 2012)

Materials and methods

Preparation of Ti pins with NF coating

We prepared coaxial electrospun PCL/PVA NFs on the surface of the Ti pin (diameter 1 mm, length 10 mm) with defined thickness (~ 50 μm), covering the entire surface of Ti pin stem. Ti pins coated with Doxy (100 μg/ml) - doped NF scaffolds (both at core and sheath layers) were sterilized under UV light overnight, and stored in 70% ethanol briefly and air dried right before surgery.

In details, 10% (w/v) PCL solution was prepared by dissolving 0.5 g of PCL in 5 ml of dimethylformamide (DMF)/chloroform (1:1,v/v). The 10% PVA solution was prepared by dissolving PVA in distilled water. To encapsulate the Doxy into the nanofiber, a stock solution (50 mg/ml in distilled water) of doxycycline hyclate was prepared. Doxy solution was mixed with both PCL (sheath) and PVA (core) gel solution right before electrospinning (final concentration 100 μg/mL in both solutions). Coaxial electrospinning was performed using a custom made coaxial nozzle consisting of a hollow stainless steel t-junction with a fully penetrating 19-gauge core needle. The PVA solution (for core fiber) and PCL solution (for sheath) were uploaded to the syringes. The syringes were attached to syringe pumps set at a flow rate (Q) of 0.5 ml/h. An 18 kV voltage was applied to the needle from the power supply. The distance from needle tip to collector was 10 cm. A rotational speed of 500 rpm was used to

evenly deposit the formed nanofiber on the Ti pin attached to the stainless steel hexahedron collector, which was linked to the shaft of a motorized stirrer. For this in vivo study, we deposited electrospun PCL/PVA NFs directly on the surface of Ti pins (diameter 1 mm, length 10 mm) covering the entire surface of the Ti pin stem. The thickness of the NFs coating is ~ 50 μm, measured by a micrometer and SEM. Ti pin with NFs coating were sterilized by UV light overnight right before implantation. We found that UV irradiation is a very effective sterilization method and has least effects on the morphology and structural properties of NF structures.

SA inoculation

Ti pin placed in tubes containing 2 ml of a stationary culture of SA (1 X10^4 CFU). Bacterial colonization was developed on the surface of the Ti pin for 12 h at 37°C. Colonized Ti pins were recovered under sterility and washed with sterilized PBS to remove unbound bacteria right before implantation. The number of clonorized bacteria was determined in the control Ti pin which weren't-implanted. Ti pin without inoculation of SA included as controls. To quantify a possible loss of viable bacteria after freeze–thaw cycles the CFU was reconfirmed after each cycle of defrosting.

Rat groups

Group	n	Description
I	24	NF, no SA (control)
II	24	NF, with SA
III	24	Doxy-NF, with SA

Experimental design

A total of 72 rats (300g-400g) were

used in this study. Rats were divided into 3 groups (Table). Each group included 24 rats (8 rats for each time point). Under anesthesia, the right knee region was shaved and sterilized with 70% ethanol. A 10 mm medial parapatellar incision was made to expose the patellar tendon. The patella was dislocated laterally to expose the tibia plateau. A pilot hole was drilled through the intercondylar eminence and a 1.0-mm titanium pin was gradually twisted to make a channel from the proximal tibial metaphysis into the medullary canal. Right before Ti pin implantation, an inoculation of SA (1 $X10^4$ CFU in 10 μl of saline) or the same amount of saline only (control) was delivered into the bone marrow cavity. Our previous studies showed that inoculation of SA in the dosage between 1 $x10^2$– 1 $x10^6$ CFU showed similar histological changes of osteomyelitis and bone loss. The CFU was confirmed by several plate counts with the use of a spiralplater. Suspensions was split into portions and deep frozen at -80°C until the day of surgery. To quantify a possible loss of viable bacteria following the freeze–thaw cycle the CFU was reconfirmed after each cycle of defrosting. In addition, a 10 μL sample of inoculants was analyzed to determine the bacterial concentration in each rat inoculation. Ti pin deposited with PCL/PVA NFs was inserted into the channel until beneath the growth plate. After implantation of Ti pin into the proximal tibia, wounds were cleaned before being closed by suture in layers. μCT scans was performed right after surgery to provide baseline information of periprosthetic bone volume. Rats sacrificed at 4, 8 and 16 weeks after surgery, respectively. We propose that Doxy released from NFs remains its bactericidal activity for 4 weeks or longer in

the presence of slow-degrading PCL sheath fibers. We propose to extend our investigation up to 16 weeks. It is crucial to understand whether Doxy-loaded NF scaffolds are still effective in inhibiting infection up to 16 weeks during bone remodeling phase. During the entire experiment, rats were monitored for the signs of systemic infection and side effects. The outcome measures include microbiologic testing, histology, mechanical pullout test and μCT/PET scan. Rectal body temperature was measured with a digital thermometer and body weight was determined every two days. We recorded the clinical signs of infection (swelling and reddening of the right hind leg, loss of passive motion in knee and ankle joints).

Sample preparation

Rat tibia samples were collected and fixed in 70% ethanol immediately. After fixation, samples were scanned with μCT. Then the specimens were cut transversely using a diamond saw into two equal parts covering the entire length of the implanted Ti pins (approximately 0.5 cm for each part). The proximal part (with rod head) was used for the push-in test. The distal part was used for the microbiological and histomorphometrical evaluation. The specimens were randomly allocated a code number, which was unknown to the observers for the treatment of the specimen during tests and analysis.

Histomorphometry

The distal tibia bone segments (including part of the Ti pin) were fixed and

dehydrated in graded ethanol (70-99%). Specimens then were placed in 99% propanol before being embedded in cold PMMA without decalcification. Perpendicular to the tibia shaft, each specimen was sectioned in 100-um thick slices using a rotary diamond saw. The sections were ground to a thickness of approximately 30 μm, and then stained with 1% toluidine blue. Bone-to-implant contact (BC) was calculated as the linear percentage of the interface with direct bone-to-implant contact to total interface of the implant in the cancellous bone. Bone area ratio (BA) was measured as the area percentage of bone tissue to the whole area, which was defined as a ring extending 200 μm from the implant surface.

MicroCT (μCT)

Rats were scanned right after surgery (baseline) and repeated at sacrifice at different time points (4, 8 and 16 weeks after surgery) using a μCT scanner (vivaCT 40). The scanning system was set to 70 kV, 114 μA, 700 ms integration time at 40 μm resolution, for maximal signal-to-noise ratio and maximal X-ray transmission through the Ti pins. A procedure for multi-level threshold data acquisition (threshold for bone -205 and threshold for implant -700) was applied to discriminate bone from other tissues. The reconstructed three-dimensional (3-D) images were utilized for quantitative evaluation of osseointegration. The volume of interest (VOI) included the trabecular compartment around the implant starting from 2.0 mm below the growth plate and extending distally for 100 slices; it also include a ring with a radius of 200 μm from the implant surface. After segmentation, the bone volume per total volume

(BV/TV), the mean trabecular thickness (Tb.Th), the mean trabecular number (Tb.N), the mean trabecular separation (Tb.Sp), and the mean connective density (Conn.D) were assessed within the VOI zone. The % VOI was calculated as the ratio between bone and total voxels in direct contact with the implant.

Reduction of metallic artifacts

Ti pin- induced metallic artifacts around periprosthetic bone tissue are a challenging. To reduce the metallic artifacts in reconstructed CT images, we (1) repeated the CT scan after the removal of the Ti pin by the pullout test, and (2) Analyzed μCT data on defined sections of bone (1 mm) distal to the tip of the Ti pins in the tibia, as we have described before (Ren et al., 2010).

Push-in test

The proximal parts (with Ti pin head) of tibia samples used for push-in testing. Soft tissue around the tibia was removed to expose the surface of the implanted Ti pin head and proximal tibia. The dorsi side of the tibia sample was then fixed into a self-manufactured aluminum fixture with a central cylindrical hole, as shown in Fig.36 (c). The inserted tibia was stabilized by facilitated screws from four directions. Approximate alignment was achieved by positioning the tibia parallel to push-in probe with the loading axis of the Instron model 8841 Universal Materials Test Machine. Proper specimen alignment was obtained by adjusting the two rotational axes of the fixture while using continuous fluoroscopy to confirm perpendicularity of the rods with respect to the fixture base. Once the fixture is attached to the load cell, the fixture

aligned along the x-axis and y-axis cross slides to obtain alignment between the extraction pin and the implants. Under position control, the Instron 8841 actuator pushed the Ti pin into the bone marrow at a rate of 1 mm/minute. Actuator position and load were recorded by a PC using software. The Ultimate Shear Strength (the peak push-in force) and energy for complete pin push in (integration of push-in force and displacement) was used to reflect the osseointegration of interface.

Microbiological analysis

Ti pin was removed and washed with 0.5 ml sterile saline before SEM analysis. Bone marrow cavity was washed with sterilized PBS three times and the washouts were collected. To determine the bone SA contamination, a piece of tibia bone was chilled with liquid nitrogen, followed by pulverization in a sterile bone mill. 150 mg of bone powder was agitated in 1.5 ml of sterile PBS for 2 min by vortex and the suspension was centrifuged for 10 s (10,000 rpm). 100 μl of the supernatant was used for the bacterial assay. Washouts from bone marrow, Ti pins and extracts from bone tissue were used for microbiologic analysis. A quantitative bacteria growth assay was used to measure bacteria growth. We used SEM to determine whether the ingrowths of SA on the Ti pin surface are inhibited by Doxy treatment.

Data Processing and Analysis

The following assumptions, based on our previous publication, are applied to the power calculation: (a) bactericidal activity (OD at 625 nm of bacterial culture medium)

varies from zero to 0.8 among groups; (b) the variations of histomorphometric variables (Bone-to-implant contact and Bone area ratio) are >30%; (c) the changes of the ultimate shear strength of the interface found at a pullout test (peak push in force (N) and energy for complete pin movement (N-mm)) varies between 30-70%, and (d) the variables of μCT (BV/TV, Tb.Th, Tb.N, Tb.Sp, Conn.D, and the % VOI) varies from 25% to 70%. Each group contained 8 rats per time point. Data was expressed as mean± standard error of the mean for each group. A p-value of less than 0.05 was considered as a significant difference. Procedure mixed (PROC MIXED) in SAS used for data analysis. When the assumptions of repeated measures ANOVA are not realized for some response variables, the generalized estimating equation was used.

Results:

Push-in test

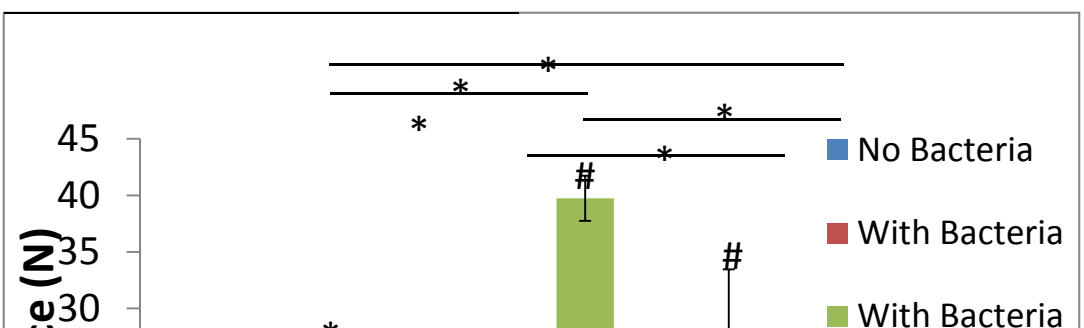

Fig.40 Rat tibia implanted Ti-pin push-in test. (a) Push-in force. Rat tibias were harvested from different time points (4, 8, 16 weeks). n= 5. *p**< 0.05 represents significant difference between different time points within group. *p*#< 0.05 represents significant difference between different groups within the same time point. Representative image of (b) push-in test and (c) harvested rat femur with Ti-pin.

As shown in Fig.40, at 4 week time point, non-Doxy groups w/ SA group showed the lowest push-in force, showing a weak bonding between NF and surrounding bone tissue, which was considered as the result of SA- induced osteomyelitis. Doxy groups

w/ SA obtained the significant highest push-in force, showing a promising bactericidal effect to prevent loosening. At 8 week time point, push-in forces of all groups were significantly increased (p<0.05). Doxy group w/ SA still has the highest push-in force, and non-Doxy group w/ SA was the lowest. The incorporation of Doxy significantly inhibited the SA-induced osteomyelitis (p<0.05) in 8 weeks. However, the situation changed at 16 week time point. Non-SA group (control) showed the highest push-in force, and other two groups with SA inoculation decreased drastically (p <0.05). This result indicated the incorporated Doxy was either completely released or failed after 16 week, which caused remaining SA grew back to affect the bonding. Though SA-induced osteomyelitis was observed in both groups at 16 weeks, Doxy group showed stronger bonding with bone in comparison with non-Doxy group (p< 0.05). This test confirmed that Doxy incorporated NFs was able to maintain the stability and local delivery efficiency of antibiotics, which inhibited SA activity for 8 weeks. The bactericidal activity of Doxy incorporated NF could prevent the infection induced osteomyelitis in early stage (within 8 weeks).

MicroCT analysis

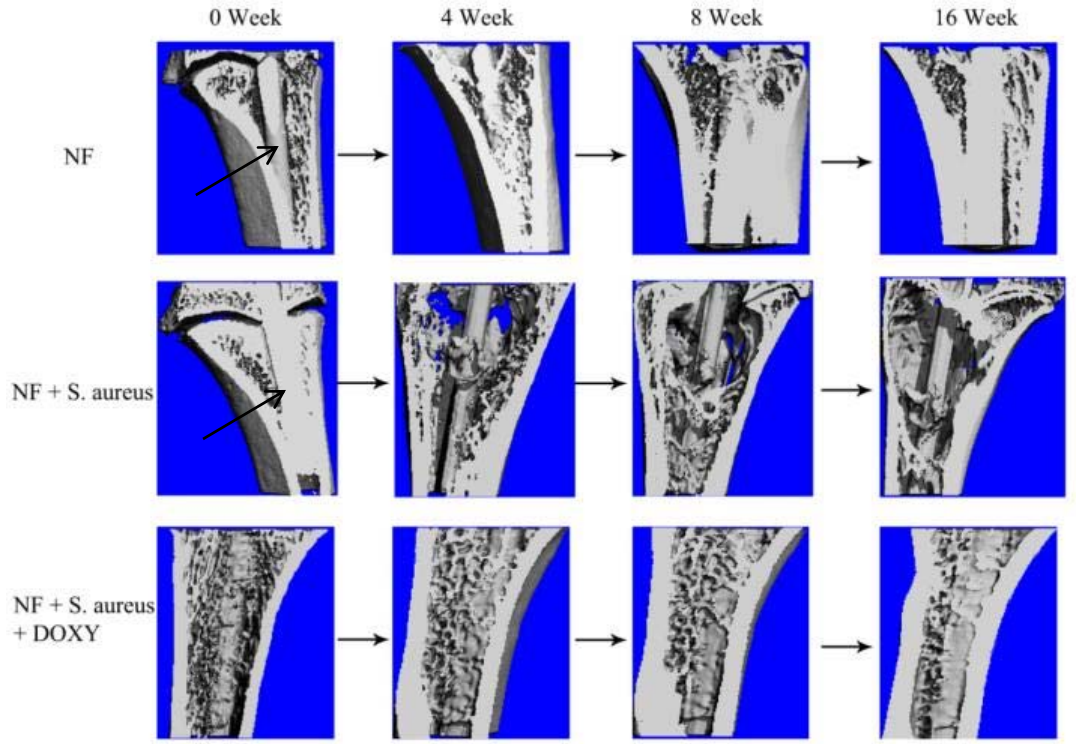

(a)

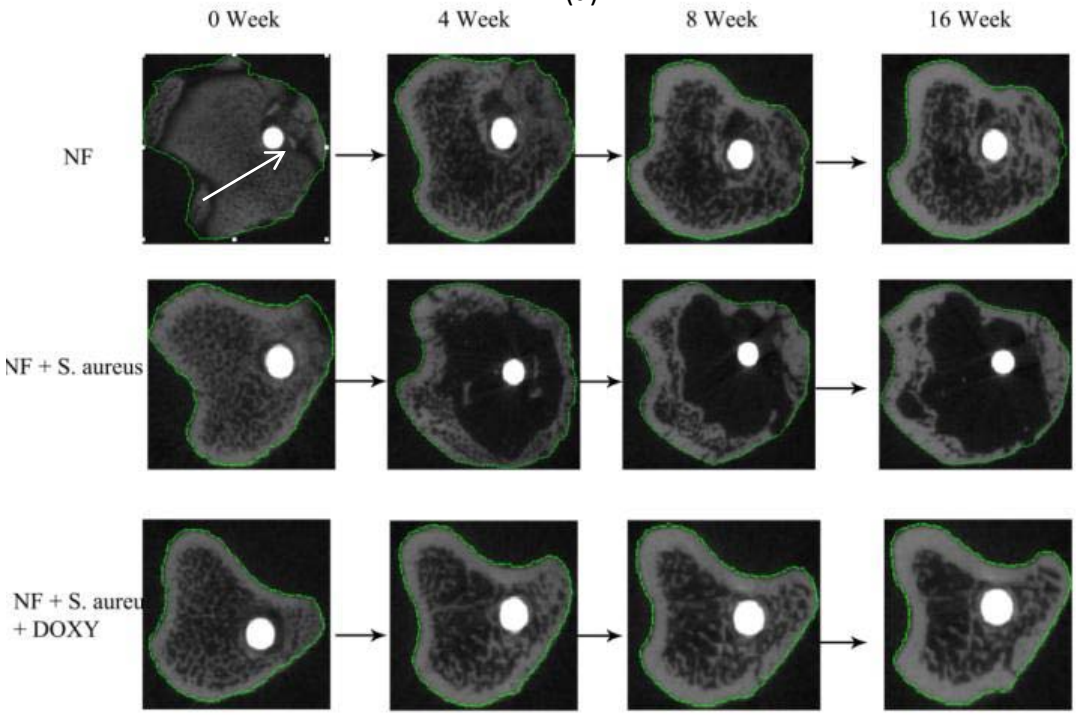

(b)

Fig.41 Representative (a) 3D and (b) 2D reconstructed images of rat tibia bone morphologic change during implantation. Arrows: Ti pin.

The interface of NF coated Ti pin and surrounding bone tissue was analyzed by MicroCT (Scanco Viva CT 40, Scanco Medical, Switzerland). The 3D morphology of the tibia was reconstructed using built-in software and key parameters including bone volume fraction (BV/TV) and Trabeculae separation (Tb.Sp) were measured to characterize the SA-induced osteomyelitis and the therapeutic effect of NF-coatings with incorporated Doxy. In consistence with the push-in test, micro CT showed similar result. Representative 3D and 2D images with morphological change of rat tibia implantation in time course were shown in Fig. 41 (a) and (b), respectively. A typical plane cut in vertical direction to expose the implanted Ti-pin and surrounding bone tissue was adopted during 3D reconstruction. For NF (control) group, a gradual improvement of bone volume around Ti pin and bonding between bone mineral and Ti around the interface can be observed from 0 week to 16 week. This change can be viewed more clearly from 2D image (Fig. 41 (b)). It indicated the self- remodeling mechanism of bone when defect was occurred. In other hand, NF + SA group showed a huge morphological change from 0 week to 4 week. At 4 week, the bone volume in implanted area was significantly reduced in 3D image, and a huge gap between Ti and bone tissue can be viewed in 2D image. After 16 weeks, the bone loss hasn't been recovered and Ti pin was shown to be loosening and have very week bonding with surrounding bone. For NF + SA + Doxy group, the SA induced osteomyelitis was largely alleviated. After implantation for 4 weeks, new trabeculae bone was started to form around Ti pin and the bone volume was constantly increased. The gap between Ti and

bone is not observed during implantation. More quantified parameters were shown to elucidate the effect of Doxy incorporation against SA-induced infections as below.

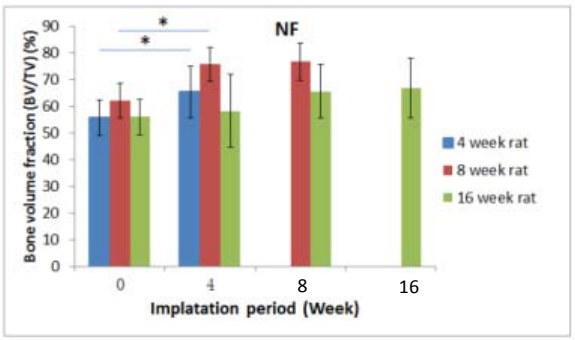

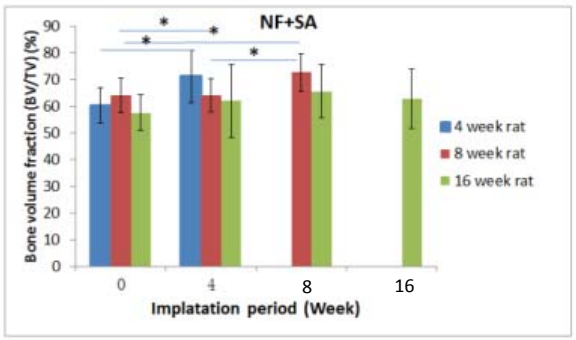

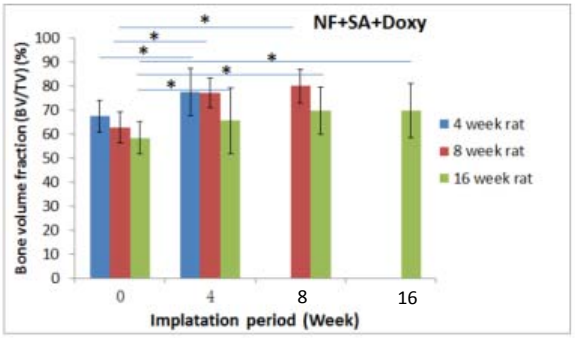

	Bone volume change slope		
Treatment	4 week	8 week	16 week
NF	2.3925	1.8358	0.7116
NF+ SA	2.6788	1.0738	0.2882
NF+SA+Doxy	2.5353	2.1641	0.6548

Fig. 42 Quantitative results of micro-CT scans for rat tibia implanted with NF-coated Ti-pin (NF, control), NF-coated Ti-pin with inoculation of S. aurous (NF + SA) and doxycycline incorporated NF-coated Ti-pin with inoculation of S. aurous (NF+SA+ Doxy). All rats were scanned every 4 weeks. Bone volume fraction was presented via percentage of bone volume/ total volume (BV/TV %). BV/TV change slope was obtained by linearly fit the data. n= 8. p*< 0.05 represents significant difference.

As shown in Fig.42 (a), Non-SA group (control) presented a recovery progress in bone volume from 4 week to 16 week after implantation. Non-Doxy with SA group (NF + SA) showed similar trend, however, with much slower recovery rate (table). As shown in Fig. (c), Doxy with SA group (control) presented a rapid recovery progress in bone volume from 4 week to 16 week after implantation. BV/TV values at 8 weeks and 16 weeks shows significant elevation in comparison with 4 weeks (p<0.05). From the linear fitting result as shown in table in Fig. 42, NF + SA group only obtained a slope of

BV/TV change of 1.0738 at 8 weeks and 0.2882 at 16 week, which is much lower than both control group (1.8358 at 8 weeks and 0.7116 at 16 week) and NF + SA + Doxy group (2.1641 at 8 weeks and 0.6548 at 16 week). With the influence of incorporated Doxy, the recovery rate of bone volume in the presence of SA is significantly accelerated, which is closed to the normal bone defect recovery (control)

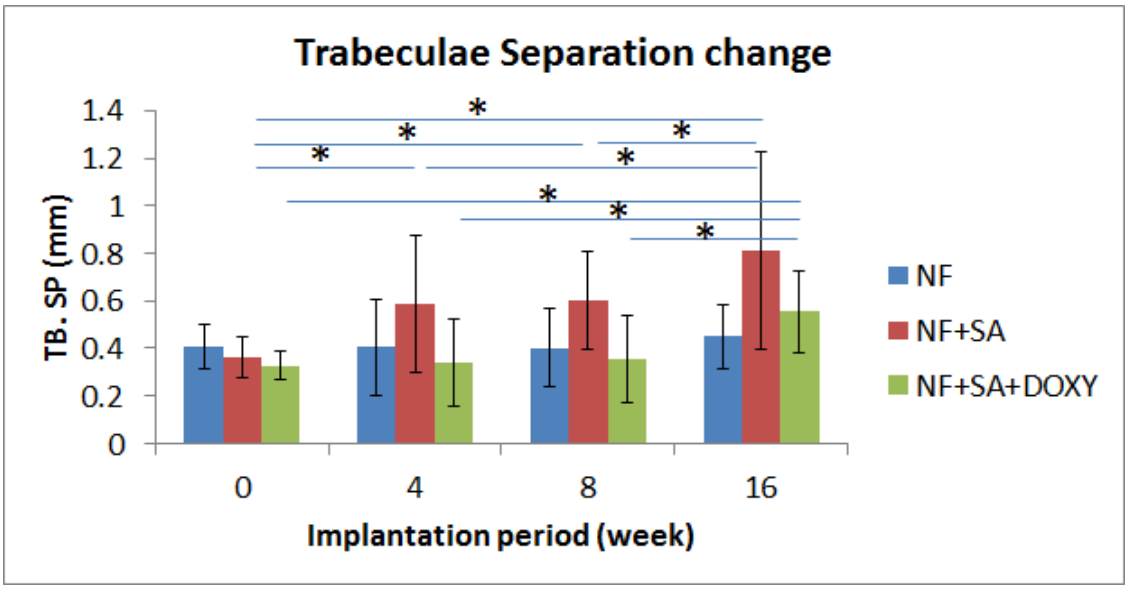

Fig. 43 Quantitative results of micro-CT scans for rat femur implanted with NF-coated Ti-pin (NF, control), NF-coated Ti-pin with inoculation of S. aurous (NF + SA) and doxycycline incorporated NF-coated Ti-pin with inoculation of S. aurous (NF+SA+ Doxy). All rats were scanned every 4 weeks. Trabecular Separation (Tb.Sp) which is the measurement of the space between the trabeculae was quantified and plot against implantation time points. n= 8. $p^*< 0.05$ represents significant difference.

Trabecular Separation (Tb.Sp), which is the measurement of the space between the trabeculae, was also used to evaluate bone volume changes. Higher value of Tb. Sp means the larger space between trabeculae, showing another evidence of loosening and resorption in bone volume. As shown in Fig. 43, NF + SA group has a significant elevation in Tb. SP after every 4 weeks during implantation ($p<0.05$), whereas no difference was found for control groups during entire implantation period.

Moreover, NF + SA group obtained the highest value in each time point after 4 weeks of implantation. This result also confirmed that SA induced significantly bone loss and weak bone structure, which consisted with the data from prior push in test. For NF + SA + Doxy group, however, no difference in Tb. Sp was found up to 16 weeks. This result is also consistent with push in test for the sudden descending force at 16 week time point, which has been discussed as the reason of doxy failure. Nevertheless, incorporated Doxy was able to prevent SA-induced osteomyelitis up to 8 weeks, which prevents the bone loss and implant failure in early stage.

Microbiology analysis

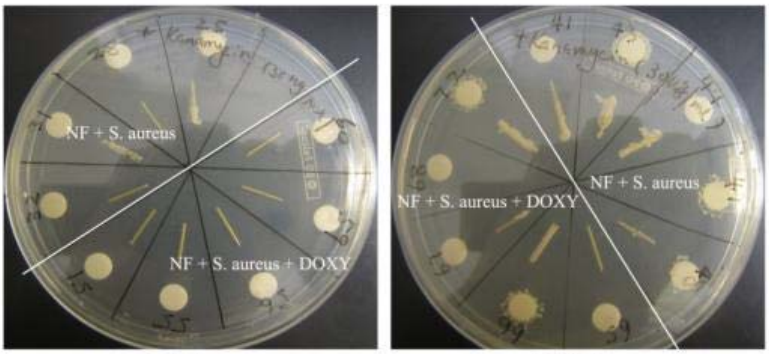

8 Week 16 Week

(a)

	4 Week	8 Week	16 Week
NF + S. aureus	+/- - - -	+ +/- - -	+++++
NF + S. aureus + DOXY	- - - - -	- - - - -	++/- - -

(b)

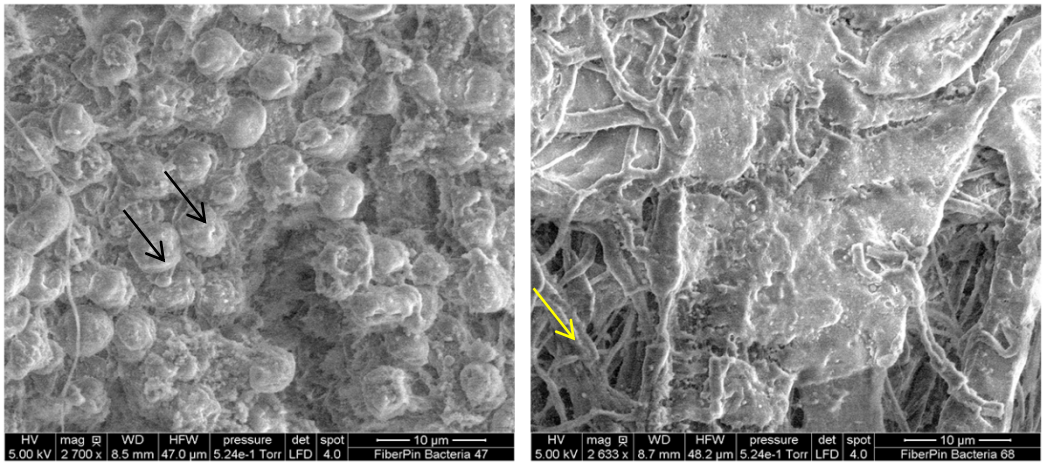

(c)

Fig. 44 Microbiology assay. (a) SA growth on harvested Ti-pin implanted in Rat tiba. (b) SA growth in washout medium. +, positive growth; -, negative growth. (c) SEM morphology of SA growth on harvested NFs from Pin surface (16 week). Left: NF + SA; Right: NF+ SA + Doxy. Black arrows: SA formed biofilm; Yellow arrow: NFs

We performed microbiological assay on harvested Ti pin and washout solution from bone marrow in order to further confirm the bactericidal effect from Doxy-incorporated NF coatings. As shown in Fig.44, at 8 week time point, Ti pin harvested from NF + SA groups showed obvious bacteria growth in agar plate, whereas NF + SA + Doxy groups have no sign of bacteria growth. The semi-quantitative result of washout test was quite consistent, as shown in Table in Fig.44. A 2 out of 5 positive result of positive bacteria activity was obtained from bone marrow washout of NF + SA group, whereas no positive result was given from NF + SA + Doxy group. At 16 week time point, more bacteria growth could be observed in surrounding of Ti pin from NF + SA group, whereas much less of bacteria was found for NF + SA + Doxy group. Assay on washout showed similar result. All 5 samples were positive for NF + SA group, whereas only 2 out of 5 were positive for NF + SA + Doxy group. This result further

demonstrated Doxy incorporated NF coating was very effective to inhibit bacterial infection for 8 to 16 weeks. Moreover, the morphology of SA from SEM also confirmed the formation of biofilm from richer and outnumbered SA colonies on Non-Doxy NFs, as shown in Fig. 44 (c). Doxy contained NFs were still easy to differentiate due to less adhered bacteria.

A bacteria activity assay on SA on Ti-pin samples in vitro was performed to confirm the viability of SA after growing in dried condition at room temperature for 45 d, as shown in Fig.45. The positive results of SA activity on Ti sample indicated the viability of SA is affirmative for a long-term period.

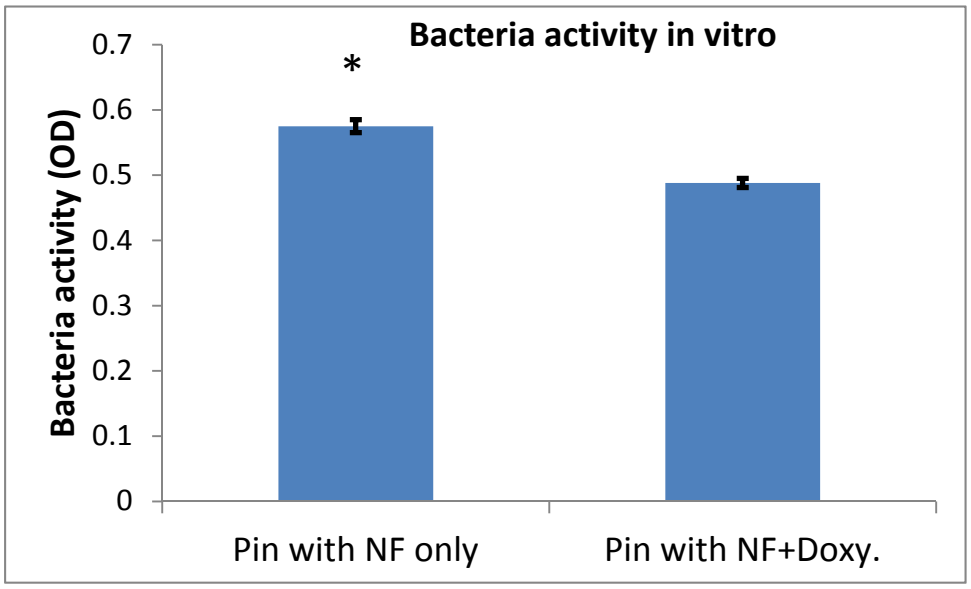

Fig. 45 The activity of SA seeded on Ti pin surface was evaluated: SA seeded Ti pin + NF and SA seeded Ti pin + NF + Doxy were dried and placed at room temperature for 45 d. Then the Bacteria activity (OD) was measured to exclude the possibility of SA self-apoptosis. *P<0.05.

Discussion

S. aureus is one of the most common pathogens found in periprosthetic infection. Surgical procedure of treating periprosthetic infection and osteomyelitis is to remove infected bone and soft tissue, which leaves large space that eventually cause instability of implant. In our push-in test, this situation was observed in NF + SA group that bonding between implant and bone is extremely weak. Numerous attempts have been made by researchers in order to overcome this problem. The most efficient way is developing a local delivery system that enables the implant to release antibiotics in a sustainable manner. Sustainable release of antibiotics from local delivery device could effectively prevent bacterial colonization in the early stage and is advantageous in releasing drug directly to the implanting area in prolonged period, which alleviates systemic toxicity. The challenge in clinical treatment on osteomyelitis is to determine an optimal therapeutic outcome with effective drug dosage. In this study, we explored an approach by incorporating certain amount of antibiotics to effectively prevent osteomyelitis in early stage of implantation without interrupting the self- bone remodeling.

A desired local drug delivery system should deliver antibiotics well above their minimum inhibitory concentration (MIC) in a sustainable manner (Mourino and Boccaccini, 2010; Lepretre et al., 2009). A period of up to 6 weeks is required for a full vascularization of bone grafts implanted in segmental defects to occur(Geiger et al., 2005). Therefore, a sustained antibiotics release exceeding the MIC for at least 6

weeks is highly desirable for the treatment of osteomyelitis(Simchi et al., 2011b). There is a big challenge to develop bactericidal bone scaffolds with controllable sustained release of active antibiotics(Mourino and Boccaccini, 2010). Several attempts have been made to reach a desired local drug delivery(Simchi et al., 2011b; Baroli, 2009).

According to the preliminary studies, Doxy incorporated PCL/PVA coaxial nanofiber has shown to be effective in inhibiting bacteria growth in vitro. Incorporated Doxy followed a zero-order sustainable release that can continue for over 30 days (Fig.31) and enable to inhibit bacteria growth for over 10 days. Our result from the rat tibia implantation model study further supported the in vitro data. The bactericidal effect from Doxy incorporated NF coating was sustained for 8 weeks, which already exceeded the standard requirement of total duration of 4-6 weeks of parenteral therapy for osteomyelitis. There was no obvious systemic toxicity caused by Doxy during the implantation. In our experimental design, 100 μg/mL of Doxy for preparing NF coating is quite modest. There has more potency to incorporate higher dose of Doxy that possess longer therapeutic effect against osteomyelitis.

Micro CT imaging technology is particular useful in study the biological process of bone remodeling. The reconstructed 3D and 2D images in combined with quantitative data (BV/TV, Tb. Sp) were used to evaluate the bone mineral change at the site of proximal tibia in containing of infected Ti pin. In contrast, Doxy incorporated NF induced a higher bone density and new trabaculae formation surrounding implant

within 8 weeks duration of experiment. It is noted that timely measurements of micro CT represent a cost-effective and accurate approach to monitor each individual rat for the infected bone density change.

One thing need to be noted is the growth back of bacteria after 8 week of implantation. As we discussed previously, the release of Doxy from PCL/PVA coaxial NFs could sustained for over 30d, which was in consistent with the in vivo study that bacteria activity was suppressed for 4-8 weeks. Doxy released from NFs could still be active for a period to inhibit bacteria activity. However, the dose of Doxy applied in NFs from this study may not be sufficient for extending to over 8 weeks. Therefore, SA was growing back from expiration of Doxy after 8-16 week of implantation. In future study, more Doxy could be incorporated to further explore the optimal inhibitory efficacy against SA infection.

In summary, Doxy incorporated PCL/PVA coaxial NFs could sustainably and locally deliver Doxy and effectively prevent the bacteria adhesion on Ti implant surface. This bactericidal efficacy of surface coating NFs last for over 8 weeks and successfully avoid the osteomyelitis, which demonstrated to be a very efficient alternative to overcome the infection of orthopaedic prosthesis.

Chapter 8 Conclusions

Since the total joint replacement (TJR) has been widely applied for about century, TJR surgery currently has very high successful rate. Each year, over 700,000 total joint replacement (TJR) operations (hip and knee) are performed in the US, and this number is still constantly increasing due to the elevated requirements of pursuing high quality life from patients. However, the TJR is far away from perfection, especially from a long-term perspective, as already addressed in our study. Multi-factors induced loosening (mainly categorized into septic and aseptic) caused a large proportion of TJR implant failure. The revision surgery or secondary replacement represents a high cost and suffering to patients, which urges researchers to explore new technologies for overcome these problematic issues. Current approaches, including cemented, cementless, press-fit fixation, biological coatings with antibiotics cannot completely prevent implant loosening, especially during long-term implantation. Lack of osseointegration for interface between implant and surrounding bone, wear debris of implant materials and osteomyelitis are major issues to induce implant loosening. Therefore, developing a biocompatible, bioactive and bactericidal interface between bone and implant becomes a crucial approach for preventing implant failure.

We initially proposed a hydrogel system incorporated bone components (PVA-Col-HA gel) with local delivery capability as a coating material on implant surface. It has been demonstrated that PVA-Col-HA gel system is tunable in physiochemical

properties and advantageous as follow:

- Excellent biocompatibility that induced bone cells adhesion and proliferation
- Great capability to load and sustainable delivery of antibiotic that effectively inhibit bacteria growth and osteoclastogenesis

Components (PVA, HA, Col) used in this study were proven to be excellent candidates for implant surface modification. However, the limitations of this system are obvious:

- The bonding between PVA gel and bone is still weak
- The dense or nonporous structure of the gel prevented cell infiltration, which hindered the later osseointegration.
- The distribution of HA and Col is inhomogeneous, and the particle scale is not well matched for cell interaction.

Thus, in order to improve the surface modification method, we proposed electrospun nanofibers as surface coating matrix in our study. Electrospinning technology for manufacturing fibrous mat in nano scale has been introduced in biomedical field for decades. However, the application in orthopaedic field is rare. Our idea to utilize this new technology for solving old problems in TJR surgery is quite innovative. We firstly fabricated monolithic PVA-Col-HA electrospun nanofibers, for which components are all introduced from previous hydrogel study. The improvements of these monolithic NFs are significant:

- Tunable highly interconnected porous structure in this fibrous scaffold

- Capable of incorporation nano-HA and Col, and the distribution of embedded components are more homogeneous.
- Improvement in cell adhesion and proliferation

However, we still found limitation from monolithic PVA-Col-HA electrospun nanofibers:

- The fast hydrolysis or degradation of PVA fibers ruled out the possibility of sustained delivery of drugs to inhibit bacteria growth in a long-term period.

Therefore, we further developed a coaxial electrospun nanofibers (NFs) system (PCL/PVA) with a hydrophobic sheath (PCL) and hydrophilic core (PVA) structure to prolong the degradation of nanofibers. The unique physiochemical properties and bioactivities have demonstrated that coaxial NFs an excellent surface modification material on implant surface:

- Prolonged degradation of PCL sheath enables the controllable and sustainable release of incorporated drugs.
- Stiffer surface modulus enhanced bone cell adhesion that benefits osseointegration
- Significance in bactericidal effect to prevent bacteria colonization in vitro

Once we thoroughly studied the physiochemical properties and bioactivities of coaxial NFs in vitro, a series of in vivo study were carried on. A well-established rat tibia

implantation model was utilized to evaluate the feasibility of coaxial NFs as a coating material on implants. The results of this in vivo study show PCL/PVA coaxial NFs as promising coating materials for TJR implants as follow:

- Coaxial NFs enhanced the osseointegration from surrounding bone to implant
- The bonding between implant and bone was reinforced
- Osteomyelitis was prevented since antibiotics can sustainably release from NFs to inhibit bacteria growth in early stage of implantation

REFERENCES

Al-Ali, W., Bissada, N. F., Greenwell, H., (1989). The Effect of Local Doxycycline With and Without Tricalcium Phosphate on the Regenerative Healing Potential of Periodontal Osseous Defects in Dogs. Journal of Periodontology 60**,** 582-590.

Allen, M., Brett, F., Millett, P., Rushton, N., (1996). The effects of particulate polyethylene at a weight-bearing bone-implant interface. A study in rats. Journal of Bone & Joint Surgery - British Volume 78**,** 32-37.

Almazin, S. M., Dziak, R., Andreana, S., Ciancio, S. G., (2009). The effect of doxycycline hyclate, chlorhexidine gluconate, and minocycline hydrochloride on osteoblastic proliferation and differentiation in vitro. J Periodontol 80**,** 999-1005.

Anselme, K., Ponche, A., Bigerelle, M., (2010). Relative influence of surface topography and surface chemistry on cell response to bone implant materials. Part 2: biological aspects. Proc.Inst.Mech.Eng H. 224**,** 1487-1507.

Asran, A. S., Henning, S., Michler, G. H., (2010a). Polyvinyl alcohol-collagen-hydroxyapatite biocomposite nanofibrous scaffold: Mimicking the key features of natural bone at the nanoscale level. Polymer 51**,** 868-876.

Asran, A. S., Henning, S., Michler, G. H., (2010b). Polyvinyl alcohol-collagen-hydroxyapatite biocomposite nanofibrous scaffold: Mimicking the key features of natural bone at the nanoscale level. Polymer 51**,** 868-876.

Back, D., Pauly, S., Rommel, L., Haas, N., Schmidmaier, G., Wildemann, B., Greiner, S., (2012). Effect of local zoledronate on implant osseointegration in a rat model. BMC Musculoskeletal Disorders 13**,**

42.

Bahraminasab, M., Sahari, B. B., Edwards, K. L., Farahmand, F., Arumugam, M., Hong, T. S., (2012). Aseptic loosening of femoral components - A review of current and future trends in materials used. Materials & Design 42**,** 459-470.

Baker, B. M., Handorf, A. M., Ionescu, L. C., Li, W. J., Mauck, R. L., (2009). New directions in nanofibrous scaffolds for soft tissue engineering and regeneration. Expert.Rev.Med.Devices 6**,** 515-532.

Baroli, B., (2009). From natural bone grafts to tissue engineering therapeutics: Brainstorming on pharmaceutical formulative requirements and challenges. Journal of Pharmaceutical Sciences 98**,** 1317-1375.

Berry, D. J., Harmsen, W. S., Cabanela, M. E., Morrey, B. F., (2002). Twenty-five-Year Survivorship of Two Thousand Consecutive Primary Charnley Total Hip Replacements : Factors Affecting Survivorship of Acetabular and Femoral Components. Journal of Bone and Joint Surgery 84**,** 171-177.

Blacklock, J., Sievers, T. K., Handa, H., You, Y. Z., Oupicky, D., Mao, G., Mohwald, H., (2010). Cross-linked bioreducible layer-by-layer films for increased cell adhesion and transgene expression. J.Phys.Chem B 114**,** 5283-5291.

Boos, C., Fink, K., Stomberg, P., Koeller, W., Igl, B. W., Russlies, M., (2008). The influence of bone quality and the fixation procedure on the primary stability of cementless implanted tibial plateaus. Biomed.Tech.(Berl) 53**,** 70-76.

Borsari, V., Fini, M., Giavaresi, G., Rimondini, L., Consolo, U., Chiusoli, L., Salito, A., Volpert, A., Chiesa, R., Giardino, R., (2007). Osteointegration of titanium and hydroxyapatite rough surfaces in healthy and compromised cortical and trabecular bone: in vivo comparative study on young, aged, and

estrogen-deficient sheep. J.Orthop Res. 25**,** 1250-1260.

Bosnjakovic, A., Mishra, M. K., Ren, W. P., Kurtoglu, Y. E., Shi, T., Fan, D. N., Kannan, R. M., (2011). Poly(amidoamine) dendrimer-erythromycin conjugates for drug delivery to macrophages involved in periprosthetic inflammation. Nanomedicine-Nanotechnology Biology and Medicine 7**,** 284-294.

Boxma, H., Broekhuizen, T., Patka, P., Oosting, H., (1996). Randomised controlled trial of single-dose antibiotic prophylaxis in surgical treatment of closed fractures: the Dutch Trauma Trial. Lancet 347**,** 1133-1137.

Bozic, K. J., Kurtz, S. M., Lau, E., Ong, K., Vail, T. P., Berry, D. J., (2009). The epidemiology of revision total hip arthroplasty in the United States. J.Bone Joint Surg.Am. 91**,** 128-133.

Bullough, P. G., Dicarlo, E. F., Hansraj, K. K., Neves, M. C., (1988). Pathologic-Studies of Total Joint Replacement. Orthopedic Clinics of North America 19**,** 611-625.

Carr, B. C., Goswami, T., (2009). Knee implants - Review of models and biomechanics. Materials & Design 30**,** 398-413.

Cheng, Z., Guo, C., Dong, W., He, F. m., Zhao, S. f., Yang, G. l., (2012). Effect of thin nano-hydroxyapatite coating on implant osseointegration in ovariectomized rats. Oral Surgery, Oral Medicine, Oral Pathology and Oral Radiology 113**,** e48-e53.

Cho, W. J., Kim, J. H., Oh, S. H., Nam, H. H., Kim, J. M., Lee, J. H., (2009). Hydrophilized polycaprolactone nanofiber mesh-embedded poly(glycolic-co-lactic acid) membrane for effective guided bone regeneration. J.Biomed.Mater.Res.A 91**,** 400-407.

Chung, Y. Y., Kim, J., Lim, C. H., Kim, K. S., Lee, Y. S., (2008). Measurement of extent of bone ongrowth and hydroxyapatite absorption in retrieved acetabular cups. J.Orthop.Sci. 13**,** 198-201.

Classen, D. C., Evans, R. S., Pestotnik, S. L., Horn, S. D., Menlove, R. L., Burke, J. P., (1992). The timing of prophylactic administration of antibiotics and the risk of surgical-wound infection. N.Engl.J.Med. 326**,** 281-286.

Dalby, M. J., McCloy, D., Robertson, M., Wilkinson, C. D., Oreffo, R. O., (2006). Osteoprogenitor response to defined topographies with nanoscale depths. Biomaterials 27**,** 1306-1315.

Dawson, J. I., Wahl, D. A., Lanham, S. A., Kanczler, J. M., Czernuszka, J. T., Oreffo, R. O., (2008). Development of specific collagen scaffolds to support the osteogenic and chondrogenic differentiation of human bone marrow stromal cells. Biomaterials 29**,** 3105-3116.

de Jonge, L. T., Leeuwenburgh, S. C., Wolke, J. G., Jansen, J. A., (2008). Organic-inorganic surface modifications for titanium implant surfaces. Pharm.Res. 25**,** 2357-2369.

De, R. M., Carteni', M., Petillo, O., Calarco, A., Margarucci, S., Rosso, F., De, R. A., Farina, E., Grippo, P., Peluso, G., (2004). Cationic polyelectrolyte hydrogel fosters fibroblast spreading, proliferation, and extracellular matrix production: Implications for tissue engineering. J.Cell Physiol 198**,** 133-143.

Dearnley, P. A., (1999). A review of metallic, ceramic and surface-treated metals used for bearing surfaces in human joint replacements. Proc.Inst.Mech.Eng H. 213**,** 107-135.

Diefenbeck, M., M++ckley, T., Schrader, C., Schmidt, J. +., Zankovych, S., Bossert, J. +., Jandt, K. D., Faucon, M., Finger, U., (2011). The effect of plasma chemical oxidation of titanium alloy on bone-implant contact in rats. Biomaterials 32**,** 8041-8047.

Dohan Ehrenfest, D. M., Coelho, P. G., Kang, B. S., Sul, Y. T., Albrektsson, T., (2010). Classification of osseointegrated implant surfaces: materials, chemistry and topography. Trends Biotechnol. 28**,** 198-206.

Duan, B., Wu, L. L., Li, X. R., Yuan, X. Y., Li, X. L., Zhang, Y., Yao, K. D., (2007). Degradation of electrospun PLGA-chitosan/PVA membranes and their cytocompatibility in vitro. Journal of Biomaterials Science-Polymer Edition 18**,** 95-115.

Ekaputra, A. K., Zhou, Y., Cool, S. M., Hutmacher, D. W., (2009). Composite electrospun scaffolds for engineering tubular bone grafts. Tissue Eng Part A 15**,** 3779-3788.

Estey, T., Kang, J., Schwendeman, S. P., Carpenter, J. F., (2006). BSA degradation under acidic conditions: A model for protein instability during release from PLGA delivery systems. Journal of Pharmaceutical Sciences 95**,** 1626-1639.

Fan, Y., Duan, K., Wang, R., (2005). A composite coating by electrolysis-induced collagen self-assembly and calcium phosphate mineralization. Biomaterials 26**,** 1623-1632.

Feng, K., Sun, H., Bradley, M. A., Dupler, E. J., Giannobile, W. V., Ma, P. X., (2010). Novel antibacterial nanofibrous PLLA scaffolds. J.Control Release 146**,** 363-369.

Feng, L., Song, Y. L., Zhai, J., Liu, B. Q., Xu, J., Jiang, L., Zhu, D. B., (2003). Creation of a superhydrophobic surface from an amphiphilic polymer. Angewandte Chemie-International Edition 42**,** 800-802.

Francis, L., Venugopal, J., Prabhakaran, M. P., Thavasi, V., Marsano, E., Ramakrishna, S., (2010). Simultaneous electrospin-electrosprayed biocomposite nanofibrous scaffolds for bone tissue regeneration. Acta Biomater. 6**,** 4100-4109.

Franco, G. C., Kajiya, M., Nakanishi, T., Ohta, K., Rosalen, P. L., Groppo, F. C., Ernst, C. W., Boyesen, J. L., Bartlett, J. D., Stashenko, P., Taubman, M. A., Kawai, T., (2011). Inhibition of matrix metalloproteinase-9 activity by doxycycline ameliorates RANK ligand-induced osteoclast differentiation in vitro and in vivo. Exp.Cell Res. 317**,** 1454-1464.

Fry, D. E., Barie, P. S., (2011). The changing face of Staphylococcus aureus: a continuing surgical challenge. Surg.Infect.(Larchmt.) 12**,** 191-203.

Fu, K., Pack, D. W., Klibanov, A. M., Langer, R., (2000). Visual evidence of acidic environment within degrading poly(lactic-co-glycolic acid) (PLGA) microspheres. Pharmaceutical Research 17**,** 100-106.

Geesink, R. G., de, G. K., Klein, C. P., (1987). Chemical implant fixation using hydroxyl-apatite coatings. The development of a human total hip prosthesis for chemical fixation to bone using hydroxyl-apatite coatings on titanium substrates. Clin.Orthop.Relat Res. 147-170.

Geiger, F., Bertram, H., Berger, I., Lorenz, H., Wall, O., Eckhardt, C., Simank, H. G., Richter, W., (2005). Vascular endothelial growth factor gene-activated matrix (VEGF165-GAM) enhances osteogenesis and angiogenesis in large segmental bone defects. J Bone Miner.Res. 20**,** 2028-2035.

Gittens, R. A., McLachlan, T., Olivares-Navarrete, R., Cai, Y., Berner, S., Tannenbaum, R., Schwartz, Z., Sandhage, K. H., Boyan, B. D., (2011). The effects of combined micron-/submicron-scale surface roughness and nanoscale features on cell proliferation and differentiation. Biomaterials 32**,** 3395-3403.

Gluck, J. M., Rahgozar, P., Ingle, N. P., Rofail, F., Petrosian, A., Cline, M. G., Jordan, M. C., Roos, K. P., MacLellan, W. R., Shemin, R. J., Heydarkhan-Hagvall, S., (2011). Hybrid coaxial electrospun nanofibrous scaffolds with limited immunological response created for tissue engineering. Journal of Biomedical Materials Research Part B: Applied Biomaterials 99B**,** 180-190.

Goosen, J. H., Kums, A. J., Kollen, B. J., Verheyen, C. C., (2009). Porous-coated femoral components with or without hydroxyapatite in primary uncemented total hip arthroplasty: a systematic review of randomized controlled trials. Arch.Orthop.Trauma Surg. 129**,** 1165-1169.

Gracia, E., Lacleriga, A., Monzon, M., Leiva, J., Oteiza, C., Amorena, B., (1998). Application of a rat osteomyelitis model to compare in vivo and in vitro the antibiotic efficacy against bacteria with high capacity to form biofilms. J.Surg.Res. 79**,** 146-153.

Gracia, L., Ibarz, E., Puertolas, S., Cegonino, J., Lopez-Prats, F., Panisello, J. J., Herrera, A., (2010). Study of bone remodeling of two models of femoral cementless stems by means of DEXA and finite elements. Biomed.Eng Online. 9**,** 22.

Green, L. C., Wagner, D. A., Glogowski, J., Skipper, P. L., Wishnok, J. S., Tannenbaum, S. R., (1982). Analysis of Nitrate, Nitrite, and [N-15]-Labeled Nitrate in Biological-Fluids. Analytical Biochemistry 126**,** 131-138.

Haboush, E. J., (1996). A new operation for arthroplasty of the hip based on biomechanics, photoelasticity, fast-setting dental acrylic, and other considerations. 1953 [classicle article]. Bulletin - Hospital for Joint Diseases 55**,** 95-111.

Harris, W. H., Schiller, A. L., Scholler, J. M., Freiberg, R. A., Scott, R., (1976). Extensive localized bone resorption in the femur following total hip replacement. J.Bone Joint Surg.Am. 58**,** 612-618.

Hassan, C. M., Peppas, N. A., (2000a). Structure and applications of poly(vinyl alcohol) hydrogels produced by conventional crosslinking or by freezing/thawing methods. Biopolymers/Pva Hydrogels/Anionic Polymerisation Nanocomposites 153**,** 37-65.

Hassan, C. M., Peppas, N. A., (2000b). Structure and morphology of freeze/thawed PVA hydrogels. Macromolecules 33**,** 2472-2479.

Heimann, R., (1999). Design of novel plasma sprayed hydroxyapatite-bond coat bioceramic systems. Journal of Thermal Spray Technology 8**,** 597-603.

Hermida, J. C., Bergula, A., Dimaano, F., Hawkins, M., Colwell, C. W., Jr., D'Lima, D. D., (2010). An in vivo evaluation of bone response to three implant surfaces using a rabbit intramedullary rod model. J.Orthop.Surg.Res. 5**,** 57.

Hlady, V., Furedimilhofer, H., (1979). Adsorption of Human-Serum Albumin on Precipitated Hydroxyapatite. Journal of Colloid and Interface Science 69**,** 460-468.

Howie, D. W., Haynes, D. R., Rogers, S. D., McGee, M. A., Pearcy, M. J., (1993). The response to particulate debris. Orthop.Clin.North Am. 24**,** 571-581.

Huang, L., Nagapudi, K., Apkarian, R. P., Chaikof, E. L., (2001). Engineered collagen-PEO nanofibers and fabrics. Journal of Biomaterials Science-Polymer Edition 12**,** 979-993.

Huang, Z., Daniels, R. H., Enzerink, R. J., Hardev, V., Sahi, V., Goodman, S. B., (2008). Effect of nanofiber-coated surfaces on the proliferation and differentiation of osteoprogenitors in vitro. Tissue Eng Part A 14**,** 1853-1859.

Huang, Z. M., Zhang, Y. Z., Kotaki, M., Ramakrishna, S., (2003). A review on polymer nanofibers by electrospinning and their applications in nanocomposites. Composites Science and Technology 63**,** 2223-2253.

Huang, Z. M., He, C. L., Yang, A., Zhang, Y., Han, X. J., Yin, J., Wu, Q., (2006). Encapsulating drugs in biodegradable ultrafine fibers through co-axial electrospinning. Journal of Biomedical Materials Research Part A 77A**,** 169-179.

Hynes, R. O., (2009). The Extracellular Matrix: Not Just Pretty Fibrils. Science 326**,** 1216-1219.

Ifkovits, J. L., Sundararaghavan, H. G., Burdick, J. A., (2009). Electrospinning fibrous polymer scaffolds for tissue engineering and cell culture. J.Vis.Exp. 1589-1593.

Jensen, B. E. B., Smith, A. A. A., Fejerskov, B., Postma, A., Senn, P., Reimhult, E., Pla-Roca, M., Isa, L., Sutherland, D. S., Stadler, B., Zelikin, A. N., (2011). Poly(vinyl alcohol) Physical Hydrogels: Noncryogenic Stabilization Allows Nano- and Microscale Materials Design. Langmuir 27**,** 10216-10223.

Jiang, Y., Zhao, J., Genant, H. K., Dequeker, J., Geusens, P., (1997). Long-term changes in bone mineral and biomechanical properties of vertebrae and femur in aging, dietary calcium restricted, and/or estrogen-deprived/-replaced rats. Journal of Bone and Mineral Research 12**,** 820-831.

Jiang, Y., Zhao, J. J., Mitlak, B. H., Wang, O., Genant, H. K., Eriksen, E. F., (2003). Recombinant human parathyroid hormone (1-34) [teriparatide] improves both cortical and cancellous bone structure. Journal of Bone and Mineral Research 18**,** 1932-1941.

Junker, R., Dimakis, A., Thoneick, M., Jansen, J. A., (2009). Effects of implant surface coatings and composition on bone integration: a systematic review. Clin.Oral Implants.Res. 20 Suppl 4**,** 185-206.

Kankilic, B., Bayramli, E., Kilic, E., Dagdeviren, S., Korkusuz, F., (2011). Vancomycin Containing PLLA/beta-TCP Controls MRSA In Vitro. Clin.Orthop Relat Res. 469**,** 3222-3228.

Karrholm, J., Borssen, B., Lowenhielm, G., Snorrason, F., (1994). Does early micromotion of femoral stem prostheses matter? 4-7-year stereoradiographic follow-up of 84 cemented prostheses. J Bone Joint Surg.Br. 76**,** 912-917.

Kenawy, E. R., Layman, J. M., Watkins, J. R., Bowlin, G. L., Matthews, J. A., Simpson, D. G., Wnek, G. E., (2003). Electrospinning of poly(ethylene-co-vinyl alcohol) fibers. Biomaterials 24**,** 907-913.

Kendal, A. R., Prieto-Alhambra, D., Arden, N. K., Carr, A., Judge, A., (2013). Mortality rates at 10 years after metal-on-metal hip resurfacing compared with total hip replacement in England:

retrospective cohort analysis of hospital episode statistics. Bmj-British Medical Journal 347.

Kim, C. H., Khil, M. S., Kim, H. Y., Lee, H. U., Jahng, K. Y., (2006a). An improved hydrophilicity via electrospinning for enhanced cell attachment and proliferation. J.Biomed.Mater.Res.B Appl.Biomater. 78**,** 283-290.

Kim, D. H., Lipke, E. A., Kim, P., Cheong, R., Thompson, S., Delannoy, M., Suh, K. Y., Tung, L., Levchenko, A., (2010). Nanoscale cues regulate the structure and function of macroscopic cardiac tissue constructs. Proceedings Of The National Academy Of Sciences Of The United States Of America 107**,** 565-570.

Kim, G. M., Asran, A. S., Michler, G. H., Simon, P., Kim, J. S., (2008). Electrospun PVA/HAp nanocomposite nanofibers: biomimetics of mineralized hard tissues at a lower level of complexity. Bioinspir.Biomim. 3**,** 046003.

Kim, S. S., Park, M. S., Jeon, O., Choi, C. Y., Kim, B. S., (2006b). Poly(lactide-co-glycolide)/hydroxyapatite composite scaffolds for bone tissue engineering. Biomaterials 27**,** 1399-1409.

Kim, Y. H., Kim, J. S., Oh, S. H., Kim, J. M., (2003). Comparison of porous-coated titanium femoral stems with and without hydroxyapatite coating. J.Bone Joint Surg.Am. 85-A**,** 1682-1688.

Kohgo, T., Yamada, Y., Ito, K., Yajima, A., Yoshimi, R., Okabe, K., Baba, S., Ueda, M., (2011). Bone regeneration with self-assembling peptide nanofiber scaffolds in tissue engineering for osseointegration of dental implants. Int.J Periodontics.Restorative.Dent. 31**,** e9-16.

Kroell, A., Beaule, P., Krismer, M., Behensky, H., Stoeckl, B., Biedermann, R., (2009). Aseptic stem loosening in primary THA: migration analysis of cemented and cementless fixation. Int.Orthop. 33**,** 1501-1505.

Kurtz, S., Ong, K., Lau, E., Mowat, F., Halpern, M., (2007). Projections of primary and revision hip and knee arthroplasty in the United States from 2005 to 2030. J Bone Joint Surg.Am. 89**,** 780-785.

Kurtz, S. M., Ong, K. L., Lau, E., Bozic, K. J., Berry, D., Parvizi, J., (2010). Prosthetic joint infection risk after TKA in the Medicare population. Clin.Orthop.Relat Res. 468**,** 52-56.

Landor, I., Vavrik, P., Jahoda, D., Pokorny, D., Ballay, R., Sosna, A., (2009). Long-term experience with the combined ARBOND hydroxyapatite coating in implant osteointegration. Acta Chir Orthop.Traumatol.Cech. 76**,** 172-178.

Lee, H. J., Lim, H. J., Lee, D. Y., Jung, H., Kim, M. R., Moon, D. C., Kim, K. I., Lee, M. S., Ryu, J. H., (2010). Carabrol suppresses LPS-induced nitric oxide synthase expression by inactivation of p38 and JNK via inhibition of I-kappa B alpha degradation in RAW 264.7 cells. Biochemical and Biophysical Research Communications 391**,** 1400-1404.

Lee, K., Goodman, S. B., (2008). Current state and future of joint replacements in the hip and knee. Expert.Rev.Med.Devices 5**,** 383-393.

Leeuwenburgh, S. C., Wolke, J. G., Lommen, L., Pooters, T., Schoonman, J., Jansen, J. A., (2006). Mechanical properties of porous, electrosprayed calcium phosphate coatings. J.Biomed.Mater.Res.A 78**,** 558-569.

Lennox, D. W., Schofield, B. H., Mcdonald, D. F., Riley, L. H., (1987). A Histologic Comparison of Aseptic Loosening of Cemented, Press-Fit, and Biologic Ingrowth Prostheses. Clinical Orthopaedics and Related Research 171-191.

Lepretre, S., Chai, F., Hornez, J. C., Vermet, G., Neut, C., Descamps, M., Hildebrand, H. F., Martel, B., (2009). Prolonged local antibiotics delivery from hydroxyapatite functionalised with cyclodextrin

polymers. Biomaterials 30**,** 6086-6093.

Lew, D. P., Waldvogel, F. A., (2004). Osteomyelitis. Lancet 364**,** 369-379.

Li, M. G., Nilsson, K. G., (2001). No relationship between postoperative changes in bone density at the proximal tibia and the migration of the tibial component 2 years after total knee arthroplasty. Journal of Arthroplasty 16**,** 893-900.

Lucet, J. C., Herrmann, M., Rohner, P., Auckenthaler, R., Waldvogel, F. A., Lew, D. P., (1990). Treatment of experimental foreign body infection caused by methicillin-resistant Staphylococcus aureus. Antimicrobial Agents and Chemotherapy 34**,** 2312-2317.

Lucke, M., Schmidmaier, G., Sadoni, S., Wildemann, B., Schiller, R., Stemberger, A., Haas, N. P., Raschke, M., (2003). A new model of implant-related osteomyelitis in rats. J.Biomed.Mater.Res.B Appl.Biomater. 67**,** 593-602.

Mai, K. T., Verioti, C. A., Casey, K., Slesarenko, Y., Romeo, L., Colwell, C. W., Jr., (2010). Cementless femoral fixation in total hip arthroplasty. Am.J.Orthop.(Belle.Mead NJ) 39**,** 126-130.

Majid, K., Crowder, T., Baker, E., Baker, K., Koueiter, D., Shields, E., Herkowitz, H. N., (2011). Analysis of in vivo corrosion of 316L stainless steel posterior thoracolumbar plate systems: a retrieval study. J.Spinal Disord.Tech. 24**,** 500-505.

Massaro, C., Baker, M. A., Cosentino, F., Ramires, P. A., Klose, S., Milella, E., (2001). Surface and biological evaluation of hydroxyapatite-based coatings on titanium deposited by different techniques. Journal of Biomedical Materials Research Part A 58**,** 651-657.

Matsumura, K., Hayami, T., Hyon, S. H., Tsutsumi, S., (2009). Control of proliferation and differentiation of osteoblasts on apatite-coated poly(vinyl alcohol) hydrogel as an artificial articular cartilage

material. J.Biomed.Mater.Res.A 92**,** 1225-1232.

Mekraldi, S., Lafage-Proust, M. H., Bloomfield, S., Alexandre, C., Vico, L., (2003). Changes in vasoactive factors associated with altered vessel morphology in the tibial metaphysis during ovariectomy-induced bone loss in rats. Bone 32**,** 630-641.

Mendonca, G., Mendonca, D. B., Simoes, L. G., Araujo, A. L., Leite, E. R., Duarte, W. R., Aragao, F. J., Cooper, L. F., (2009). The effects of implant surface nanoscale features on osteoblast-specific gene expression. Biomaterials 30**,** 4053-4062.

Mermut, O., Lefebvre, J., Gray, D. G., Barrett, C. J., (2003). Structural and mechanical properties of polyelectrolyte multilayer films studied by AFM. Macromolecules 36**,** 8819-8824.

Monzon, M., Garcia-Alvarez, F., Lacleriga, A., Gracia, E., Leiva, J., Oteiza, C., Amorena, B., (2001). A simple infection model using pre-colonized implants to reproduce rat chronic Staphylococcus aureus osteomyelitis and study antibiotic treatment. J.Orthop.Res. 19**,** 820-826.

Mourino, V., Boccaccini, A. R., (2010). Bone tissue engineering therapeutics: controlled drug delivery in three-dimensional scaffolds. J.R.Soc.Interface 7**,** 209-227.

Nagarkatti, D. G., McKeon, B. P., Donahue, B. S., Fulkerson, J. P., (2001). Mechanical Evaluation of a Soft Tissue Interference Screw in Free Tendon Anterior Cruciate Ligament Graft Fixation. The American Journal of Sports Medicine 29**,** 67-71.

Nasser, S., Campbell, P. A., Kilgus, D., Kossovsky, N., Amstutz, H. C., (1990). Cementless total joint arthroplasty prostheses with titanium-alloy articular surfaces. A human retrieval analysis. Clin.Orthop.Relat Res. 171-185.

Natu, M. V., Gaspar, M. N., Ribeiro, C. A., Correia, I. J., Silva, D., de Sousa, H. C., Gil, M. H., (2011). A

poly(epsilon-caprolactone) device for sustained release of an anti-glaucoma drug. Biomed.Mater. 6**,** 025003.

Navarro, M., Michiardi, A., Castano, O., Planell, J. A., (2008). Biomaterials in orthopaedics. J.R.Soc.Interface 5**,** 1137-1158.

Ngawhirunpat, T., Opanasopit, P., Rojanarata, T., Akkaramongkolporn, P., Ruktanonchai, U., Supaphol, P., (2009). Development of meloxicam-loaded electrospun polyvinyl alcohol mats as a transdermal therapeutic agent. Pharm.Dev.Technol. 14**,** 70-79.

Ning, C., Dai, K., (2003). [Research development of hydroxyapatite-based composites used as hard tissue replacement]. Sheng Wu Yi.Xue.Gong.Cheng Xue.Za Zhi. 20**,** 550-554.

Okazaki, Y., Gotoh, E., (2005). Comparison of metal release from various metallic biomaterials in vitro. Biomaterials 26**,** 11-21.

Omar, O., Lenneras, M., Svensson, S., Suska, F., Emanuelsson, L., Hall, J., Nannmark, U., Thomsen, P., (2010). Integrin and chemokine receptor gene expression in implant-adherent cells during early osseointegration. J.Mater.Sci.Mater.Med. 21**,** 969-980.

Ong, K. L., Kurtz, S. M., Lau, E., Bozic, K. J., Berry, D. J., Parvizi, J., (2009). Prosthetic joint infection risk after total hip arthroplasty in the Medicare population. Journal of Arthroplasty 24**,** 105-109.

Park, J. B., (2012). Low dose of doxycyline promotes early differentiation of preosteoblasts by partially regulating the expression of estrogen receptors. J Surg.Res. 178**,** 737-742.

Park, J. W., (2011). Increased bone apposition on a titanium oxide surface incorporating phosphate and strontium. Clin.Oral Implants.Res. 22**,** 230-234.

Perka, C., Haas, N., (2011). Periprosthetic infection. Chirurg 82**,** 218-226.

Perla, V., Webster, T. J., (2005). Better osteoblast adhesion on nanoparticulate selenium- A promising orthopedic implant material. J.Biomed.Mater.Res.A 75**,** 356-364.

Pisuchpen, T., Chaim-Ngoen, N., Intasanta, N., Supaphol, P., Hoven, V. P., (2011). Tuning Hydrophobicity and Water Adhesion by Electrospinning and Silanization. Langmuir 27**,** 3654-3661.

Ponche, A., Bigerelle, M., Anselme, K., (2010). Relative influence of surface topography and surface chemistry on cell response to bone implant materials. Part 1: physico-chemical effects. Proc.Inst.Mech.Eng H. 224**,** 1471-1486.

Power, M. E., Olson, M. E., Domingue, P. A., Costerton, J. W., (1990). A rat model of Staphylococcus aureus chronic osteomyelitis that provides a suitable system for studying the human infection. J.Med.Microbiol. 33**,** 189-198.

Prabhakaran, M. P., Venugopal, J., Ramakrishna, S., (2009). Electrospun nanostructured scaffolds for bone tissue engineering. Acta Biomater. 5**,** 2884-2893.

Pramanik, N., Mishra, D., Banerjee, I., Maiti, T. K., Bhargava, P., Pramanik, P., (2009). Chemical synthesis, characterization, and biocompatibility study of hydroxyapatite/chitosan phosphate nanocomposite for bone tissue engineering applications. Int.J.Biomater. 2009**,** 512417.

Pulido, L., Ghanem, E., Joshi, A., Purtill, J. J., Parvizi, J., (2008). Periprosthetic joint infection: the incidence, timing, and predisposing factors. Clin.Orthop.Relat Res. 466**,** 1710-1715.

Race, A., Heffernan, C. D., Sharkey, P. F., (2010). The Addition of a Hydroxyapatite Coating Changes the Immediate Postoperative Stability of a Plasma-Sprayed Femoral Stem. Journal of Arthroplasty.

Ramaswamy, Y., Wu, C., Zreiqat, H., (2009). Orthopedic coating materials: considerations and applications. Expert.Rev.Med.Devices 6**,** 423-430.

Raquez, J. M., Barone, D. T. J., Luklinska, Z., Persenaire, O., Belayew, A., Eyckmans, J., Schrooten, J., Dubois, P., (2011). Osteoconductive and Bioresorbable Composites Based on Poly(l,l-lactide) and Pseudowollastonite: From Synthesis and Interfacial Compatibilization to In Vitro Bioactivity and In Vivo Osseointegration Studies. Biomacromolecules 12**,** 692-700.

Ren W.P, Yang SY, Fang HW, Hsu S, Wooley PH, (2003). Distinct gene expression of receptor activator of nuclear factor-kB and rank ligand in the inflammatory response to variant morphologies of UHMWPE particles. Biomaterials 24**,** 4819-4826.

Ren, W., Muzik, O., Jackson, N., Khoury, B., Shi, T., Flynn, J. C., Chakraborty, P., Markel, D. C., (2012). Differentiation of septic and aseptic loosening by PET with both 11C-PK11195 and 18F-FDG in rat models. Nucl.Med.Commun. 33**,** 747-756.

Ren, W., Zhang, R., Hawkins, M., Shi, T., Markel, D. C., (2010). Efficacy of periprosthetic erythromycin delivery for wear debris-induced inflammation and osteolysis. Inflamm.Res. 59**,** 1091-1097.

Ren, W. P., Markel, D. C., Zhang, R., Peng, X., Wu, B., Monica, H., Wooley, P. H., (2006). Association between UHMWPE particle-induced inflammatory osteoclastogenesis and expression of RANKL, VEGF, and Flt-1 in vivo. Biomaterials 27**,** 5161-5169.

Rujitanaroj, P. O., Wang, Y. C., Wang, J., Chew, S. Y., (2011). Nanofiber-mediated controlled release of siRNA complexes for long term gene-silencing applications. Biomaterials 32**,** 5915-5923.

Ryd, L., (1992). Roentgen Stereophotogrammetric Analysis of Prosthetic Fixation in the Hip and Knee Joint. Clinical Orthopaedics and Related Research 276**,** 56-65.

Sahoo, S., Ang, L. T., Goh, J. C., Toh, S. L., (2010). Growth factor delivery through electrospun nanofibers in scaffolds for tissue engineering applications. J.Biomed.Mater.Res.A 93**,** 1539-1550.

Sailaja, G. S., Sreenivasan, K., Yokogawa, Y., Kumary, T. V., Varma, H. K., (2009). Bioinspired mineralization and cell adhesion on surface functionalized poly(vinyl alcohol) films. Acta Biomater. 5**,** 1647-1655.

Sangeetha, R., Kumar, R., Doble, M., Venkatesan, R., (2010). Barnacle cement: An etchant for stainless steel 316L? Colloids Surf.B Biointerfaces. 79**,** 524-530.

Sargeant, T. D., Guler, M. O., Oppenheimer, S. M., Mata, A., Satcher, R. L., Dunand, D. C., Stupp, S. I., (2008). Hybrid bone implants: self-assembly of peptide amphiphile nanofibers within porous titanium. Biomaterials 29**,** 161-171.

Schliephake, H., Scharnweber, D., Dard, M., Robetaler, S., Sewing, A., Huttmann, C., (2003). Biological performance of biomimetic calcium phosphate coating of titanium implants in the dog mandible. J.Biomed.Mater.Res.A 64**,** 225-234.

Schmalzried, T. P., Kwong, L. M., Jasty, M., Sedlacek, R. C., Haire, T. C., OCONNOR, D. O., BRAGDON, C. R., Kabo, J. M., Malcolm, A. J., Path, M. R. C., Harris, W. H., (1992). The Mechanism of Loosening of Cemented Acetabular Components in Total Hip-Arthroplasty - Analysis of Specimens Retrieved at Autopsy. Clinical Orthopaedics and Related Research 60-78.

Schmedlen, K. H., Masters, K. S., West, J. L., (2002). Photocrosslinkable polyvinyl alcohol hydrogels that can be modified with cell adhesion peptides for use in tissue engineering. Biomaterials 23**,** 4325-4332.

Schmidmaier, G., Lucke, M., Wildemann, B., Haas, N. P., Raschke, M., (2006). Prophylaxis and treatment of implant-related infections by antibiotic-coated implants: a review. Injury 37**,** S105-S112.

Schofer, M. D., Fuchs-Winkelmann, S., Grabedunkel, C., Wack, C., Dersch, R., Rudisile, M., Wendorff, J. H., Greiner, A., Paletta, J. R., Boudriot, U., (2008). Influence of poly(L-lactic acid) nanofibers and

BMP-2-containing poly(L-lactic acid) nanofibers on growth and osteogenic differentiation of human mesenchymal stem cells. ScientificWorldJournal. 8**,** 1269-1279.

Shepperd, J. A., Apthorp, H., (2005). A contemporary snapshot of the use of hydroxyapatite coating in orthopaedic surgery. Journal of Bone & Joint Surgery - British Volume 87**,** 1046-1049.

Shin, Y. M., Hohman, M. M., Brenner, M. P., Rutledge, G. C., (2001). Experimental characterization of electrospinning: the electrically forced jet and instabilities. Polymer 42**,** 9955-9967.

Simchi, A., Tamjid, E., Pishbin, F., Boccaccini, A. R., (2011a). Recent progress in inorganic and composite coatings with bactericidal capability for orthopaedic applications. Nanomedicine: Nanotechnology, Biology and Medicine 7**,** 22-39.

Simchi, A., Tamjid, E., Pishbin, F., Boccaccini, A. R., (2011b). Recent progress in inorganic and composite coatings with bactericidal capability for orthopaedic applications. Nanomedicine. 7**,** 22-39.

Singh, R., Dahotre, N. B., (2007). Corrosion degradation and prevention by surface modification of biometallic materials. J.Mater.Sci.Mater.Med. 18**,** 725-751.

So, K., Takemoto, M., Fujibayashi, S., Neo, M., Kyomoto, M., Hayami, T., Hyon, S. H., Nakamura, T., (2007). Antidegenerative effects of partial disc replacement in an animal surgery model. Spine (Phila Pa 1976.) 32**,** 1586-1591.

Song, W., Markel, D. C., Wang, S., Shi, T., Mao, G., Ren, W., (2012). Electrospun polyvinyl alcohol-collagen-hydroxyapatite nanofibers: a biomimetic extracellular matrix for osteoblastic cells. Nanotechnology 23**,** 115101.

Song, W., Ren, W., Wan, C., Esquivel, A. O., Shi, T., Blasier, R., Markel, D. C., (2011a). A novel strontium-doped calcium polyphosphate/erythromycin/poly(vinyl alcohol) composite for bone tissue

engineering. J Biomed.Mater.Res.A 98**,** 359-371.

Song, W., Ren, W. P., Wan, C. X., Esquivel, A. O., Shi, T., Blasier, R., Markel, D. C., (2011b). A novel strontium-doped calcium polyphosphate/erythromycin/poly(vinyl alcohol) composite for bone tissue engineering. Journal of Biomedical Materials Research Part A 98A**,** 359-371.

Song, Y., Zhang, S., Li, J., Zhao, C., Zhang, X., (2010a). Electrodeposition of Ca-P coatings on biodegradable Mg alloy: in vitro biomineralization behavior. Acta Biomater. 6**,** 1736-1742.

Song, Y. l., Li, C. x., Li, D. H., Zhang, H. p., (2010b). Sustained release of insulin-like growth factor-1 from poly(lactide-co-glycolide) microspheres improves osseointegration of dental implants in type 2 diabetic rats. European journal of pharmacology 640**,** 226-232.

Springer, B. D., Connelly, S. E., Odum, S. M., Fehring, T. K., Griffin, W. L., Mason, J. B., Masonis, J. L., (2009). Cementless femoral components in young patients: review and meta-analysis of total hip arthroplasty and hip resurfacing. J.Arthroplasty 24**,** 2-8.

Stanishevsky, A., Chowdhury, S., Chinoda, P., Thomas, V., (2008). Hydroxyapatite nanoparticle loaded collagen fiber composites: Microarchitecture and nanoindentation study. Journal of Biomedical Materials Research Part A 86A**,** 873-882.

Steens, W., Schneeberger, A. G., Skripitz, R., Fennema, P., Goetze, C., (2010). Bone remodeling in proximal HA-coated versus uncoated cementless SL-Plus((R)) femoral components: a 5-year follow-up study. Arch.Orthop.Trauma Surg. 130**,** 921-926.

Su, Y., Su, Q. Q., Liu, W., Lim, M., Venugopal, J. R., Mo, X. M., Ramakrishna, S., Al-Deyab, S. S., El-Newehy, M., (2012a). Controlled release of bone morphogenetic protein 2 and dexamethasone loaded in core-shell PLLACL-collagen fibers for use in bone tissue engineering. Acta Biomaterialia 8**,** 763-771.

Su, Y., Su, Q., Liu, W., Lim, M., Venugopal, J. R., Mo, X., Ramakrishna, S., Al-Deyab, S. S., El-Newehy, M., (2012b). Controlled release of bone morphogenetic protein 2 and dexamethasone loaded in coreΓÇôshell PLLACLΓÇôcollagen fibers for use in bone tissue engineering. Acta Biomaterialia 8**,** 763-771.

Sundararaghavan, H. G., Metter, R. B., Burdick, J. A., (2010). Electrospun fibrous scaffolds with multiscale and photopatterned porosity. Macromol Biosci. 10**,** 265-270.

Sundfeldt, M., Carlsson, L. V., Johansson, C. B., Thomsen, P., Gretzer, C., (2006). Aseptic loosening, not only a question of wear: a review of different theories. Acta Orthop 77**,** 177-197.

Szentivanyi, A., Chakradeo, T., Zernetsch, H., Glasmacher, B., (2011). Electrospun cellular microenvironments: Understanding controlled release and scaffold structure. Advanced Drug Delivery Reviews 63**,** 209-220.

Taira, M., Lautenschlager, E. P., (1992). In vitro corrosion fatigue of 316L cold worked stainless steel. J.Biomed.Mater.Res. 26**,** 1131-1139.

Tan, K. S., Qian, L., Rosado, R., Flood, P. M., Cooper, L. F., (2006). The role of titanium surface topography on J774A.1 macrophage inflammatory cytokines and nitric oxide production. Biomaterials 27**,** 5170-5177.

Tang, Y., Du, Y., Li, Y., Wang, X., Hu, X., (2009). A thermosensitive chitosan/poly(vinyl alcohol) hydrogel containing hydroxyapatite for protein delivery. J.Biomed.Mater.Res.A 91**,** 953-963.

Tanna, S., Taylor, M. J., Sahota, T. S., Sawicka, K., (2006). Glucose-responsive UV polymerised dextran-concanavalin A acrylic derivatised mixtures for closed-loop insulin delivery. Biomaterials 27**,** 1586-1597.

Taubenberger, A. V., Woodruff, M. A., Bai, H. F., Muller, D. J., Hutmacher, D. W., (2010). The effect of unlocking RGD-motifs in collagen I on pre-osteoblast adhesion and differentiation. Biomaterials 31**,** 2827-2835.

Tomisa, A. P., Launey, M. E., Lee, J. S., Mankani, M. H., Wegst, U. G., Saiz, E., (2011). Nanotechnology approaches to improve dental implants. Int.J.Oral Maxillofac.Implants. 26 Suppl**,** 25-44.

Torres-Giner, S., Gimeno-Alcaniz, J. V., Ocio, M. J., Lagaron, J. M., (2009). Comparative performance of electrospun collagen nanofibers cross-linked by means of different methods. ACS Applied Materials & Interfaces 1**,** 218-223.

Wahl, D. A., Czernuszka, J. T., (2006a). Collagen-hydroxyapatite composites for hard tissue repair. Eur.Cell Mater. 11**,** 43-56.

Wahl, D. A., Czernuszka, J. T., (2006b). Collagen-hydroxyapatite composites for hard tissue repair. Eur.Cell Mater. 11**,** 43-56.

Wahl, D. A., Sachlos, E., Liu, C., Czernuszka, J. T., (2007). Controlling the processing of collagen-hydroxyapatite scaffolds for bone tissue engineering. J.Mater.Sci.Mater.Med. 18**,** 201-209.

Waldvogel, F. A., Medoff, G., Swartz, M. N., (1970). Osteomyelitis: a review of clinical features, therapeutic considerations and unusual aspects. 3. Osteomyelitis associated with vascular insufficiency. N.Engl.J.Med. 282**,** 316-322.

Wang, X., Gittens, R. A., Song, R., Tannenbaum, R., Olivares-Navarrete, R., Schwartz, Z., Chen, H., Boyan, B. D., (2011). Effects of structural properties of electrospun TiO(2) nanofiber meshes on their osteogenic potential. Acta Biomater.

Wang, X. K., Gittens, R. A., Song, R., Tannenbaum, R., Olivares-Navarrete, R., Schwartz, Z., Chen, H. F.,

Boyan, B. D., (2012). Effects of structural properties of electrospun TiO2 nanofiber meshes on their osteogenic potential. Acta Biomaterialia 8**,** 878-885.

Ward, K. H., Olson, M. E., Lam, K., Costerton, J. W., (1992). Mechanism of persistent infection associated with peritoneal implants. Journal of Medical Microbiology 36**,** 406-413.

Wassell, D. T. H., Hall, R. C., Embery, G., (1995). Adsorption of Bovine Serum-Albumin Onto Hydroxyapatite. Biomaterials 16**,** 697-702.

Wei, G. B., Ma, P. X., (2004). Structure and properties of nano-hydroxyapatite/polymer composite scaffolds for bone tissue engineering. Biomaterials 25**,** 4749-4757.

White, C. A., Carsen, S., Rasuli, K., Feibel, R. J., Kim, P. R., Beaule, P. E., (2012a). High Incidence of Migration with Poor Initial Fixation of the Accolade (R) Stem. Clinical Orthopaedics and Related Research 470**,** 410-417.

White, C. A., Carsen, S., Rasuli, K., Feibel, R. J., Kim, P. R., Beaule, P. E., (2012b). High Incidence of Migration with Poor Initial Fixation of the Accolade((R)) Stem. Clin.Orthop Relat Res 470**,** 410-417.

Wu, L. L., Yuan, X. Y., Sheng, J., (2005). Immobilization of cellulase in nanofibrous PVA membranes by electrospinning. Journal of Membrane Science 250**,** 167-173.

Xu, H. H. K., Weir, M. D., Burguera, E. F., Fraser, A. M., (2006). Injectable and macroporous calcium phosphate cement scaffold. Biomaterials 27**,** 4279-4287.

Xu, L. C., Siedlecki, C. A., (2012). Submicron-textured biomaterial surface reduces staphylococcal bacterial adhesion and biofilm formation. Acta Biomater. 8**,** 72-81.

Xu, W., Ganz, C., Weber, U., Adam, M., Holzhuter, G., Wolter, D., Frerich, B., Vollmar, B., Gerber, T., (2011). Evaluation of injectable silica-embedded nanohydroxyapatite bone substitute in a rat tibia defect

model. Int.J.Nanomedicine. 6**,** 1543-1552.

Yamada, H., Yoshihara, Y., Henmi, O., Morita, M., Shiromoto, Y., Kawano, T., Kanaji, A., Ando, K., Nakagawa, M., Kosaki, N., Fukaya, E., (2009). Cementless total hip replacement: past, present, and future. J.Orthop Sci. 14**,** 228-241.

Yang, S. Y., Yu, H., Gong, W., Wu, B., Mayton, L., Costello, R., Wooley, P. H., (2007). Murine model of prosthesis failure for the long-term study of aseptic loosening. J.Orthop.Res. 25**,** 603-611.

Yao, L., Haas, T. W., Guiseppi-Elie, A., Bowlin, G. L., Simpson, D. G., Wnek, G. E., (2003). Electrospinning and stabilization of fully hydrolyzed poly(vinyl alcohol) fibers. Chemistry of Materials 15**,** 1860-1864.

Yoon, K. S., Kim, H. J., Lee, J. H., Kang, S. B., Seong, N. H., Koo, K. H., (2007). A randomized clinical trial of cementless femoral stems with and without hydroxyapatite/tricalcium-phosphate coating: an 8- to 12-year follow-up study. Journal of Arthroplasty 22**,** 504-508.

Yoshimoto, H., Shin, Y. M., Terai, H., Vacanti, J. P., (2003). A biodegradable nanofiber scaffold by electrospinning and its potential for bone tissue engineering. Biomaterials 24**,** 2077-2082.

Zhang, C., Li, Z. A., Cheng, X. R., Xiao, Q., Li, H. B., (2010). Hydroxyapatite crystals biologically inspired on titanium by using an organic template based on the copolymer of acrylic acid and itaconic acid. J.Biomed.Mater.Res.A 92**,** 63-69.

Zhang, C., Tang, T. T., Ren, W. P., Zhang, X. L., Dai, K. R., (2007). Inhibiting wear particles-induced osteolysis with doxycycline. Acta Pharmacol.Sin. 28**,** 1603-1610.

Zhang, R., Xu, D., Landeryou, T., Toth, C., Dimaano, N., Berry, J., Evans, J., Hawkins, M., (2004). Ectopic bone formation using osteogenic protein-1 carried by a solution precipitated hydroxyapatite. J.Biomed.Mater.Res.A 71**,** 412-418.

Zhou, Y. S., Yang, D. Z., Chen, X. M., Xu, Q., Lu, F. M., Nie, J., (2008). Electrospun water-soluble carboxyethyl chitosan/poly(vinyl alcohol) nanofibrous membrane as potential wound dressing for skin regeneration. Biomacromolecules 9**,** 349-354.

ABSTRACT

DEVELOPMENT AND APPLICATION OF BIOMIMETIC ELECTROSPUN NANOFIBERS IN TOTAL JOINT REPLACEMENT

by

WEI SONG

May 2014

Advisor: Dr. Weiping Ren

Major: Biomedical Engineering

Degree: Doctor of Philosophy

Failure of osseointegration (direct anchorage of an implant by bone formation at the bone-implant surface) and implant infection (such as that caused by *Staphylococcus aureus, S. aureus*) are the two main causes of implant failure and loosening. There is a critical need for orthopedic implants that promote rapid osseointegration and prevent bacterial colonization, particularly when placed in bone compromised by disease or physiology of the patients. A better understanding of the key factors that influence cell fate decisions at the bone-implant interface is required. Our study is to develop a class of “bone-like” nanofibers (NFs) that promote osseointegration while preventing bacterial colonization and subsequent infections. This research goal is supported by our preliminary data on the preparation of coaxial electrospun NFs composed of polycaprolactone (PCL) and polyvinyl alcohol (PVA) polymers arranged in a core-sheath shape. The PCL/PVA NFs are biocompatible and biodegradable with appropriate fiber diameter, pore size and mechanical strength, leading to enhanced cell adhesion, proliferation and differentiation of osteoblast precursor cells. The objective is to

develop functionalized “bone-like” PCL/PVA NFs matrix embedded with antibiotics (doxycycline (Doxy), bactericidal and anti-osteoclastic) on prosthesis surface. Through a rat tibia implantation model, the Doxy incorporated coaxial NFs has demonstrated excellent in promoting osseointegration and bacteria inhibitory efficacy. NFs coatings significantly enhanced the bonding between implant and bone remodeling within 8 weeks. The SA-induced osteomyelitis was prevented by the sustained release of Doxy from NFs. The capability of embedding numerous bio-components including proteins, growth factors, drugs, etc. enables NFs an effective solution to overcome the current challenged issue in Total joint replacement. In summary, we proposed PCL/PVA electrospun nanofibers as promising biomaterials that can be applied on joint replacement prosthesis to improve osseointegration and prevent osteomyelitis.

AUTOBIOGRAPHICAL STATEMENT

Wei Song
Department of Biomedical engineering
Wayne State University, College of Engineering,
Detroit, MI 48201
TEL: 313-421-1648
E-mail: ea4029@wayne.edu

EDUCATION

Ph.D Candidate of Biomedical Engineering, July 2014 (expected)
● **Wayne State University**, Department of Biomedical engineering, Detroit, MI 48201
Master of biomedical engineering, July 2009-
● **Sichuan University**, College of Polymer Science and Engineering, Chengdu, P.R.China.
Bachelor of polymer science and engineering, July 2006
● **Sichuan University**, College of Polymer Science and Engineering, Chengdu, P.R.China.

Research Experience

Thomas C. Rumble University Graduate Fellowship 2012-2013
Teaching and researching assistant July 2009-2012
Wayne State University, Department of Biomedical Engineering
● Technical skills: Bio-ceramics and bio-polymer materials synthesize, materials modification and characterization technique, cell culture, flow cytometry and quantitative PCR.
● Train and direct new graduate students and undergraduate students in experiments

Publications

● **Song. W**, Chen.Y.W, Shi.G.Q, Zhang.X.H, Yu.X.X, Wan.C.X. "The research on the preparation and character of Chitosan with different Degree of Deacetylation". ***Journal of Functional Materials,*** Vol.38, No.10: 1705-1708.
● **Song. W,** Tian. M, Tian. Y.F Yu.X.X, Wan.C.X. "The study on the degradation and mineralization mechanism of ion-doped Calcium poly-phosphate *in vitro*". ***Journal of Biomedical Material Research Part B: Applied Biomaterials***, 2009, Vol. 89B: 430-438.
● **Song. W**, Ren WP, Wan, CX, Esquivel, AO, Shi, T, Blasier R and Markel DC: A novel strontium-doped calcium polyphosphate/erythromycin/poly (vinyl alcohol) composite for bone tissue engineering ***J. Bio. Mat. Res. Part A*****.** 98(3):359-371, 2011
● **W Song**, Q Wang, C Wan, T Shi, DC Markel, R Blaiser and Ren WP: A novel alkali metals/ strontium co-substituted calcium polyphosphate scaffolds in bone tissue engineering. ***J. Bio. Mat. Res. Part B*****.** 98B(2):255-262, 2011
● **W Song**, Ren WP, T Shi, R Blaiser and DC Markel: Cyclodextrin-erythromycin complexes as a drug delivery device for orthopedic application. ***International J Nanomedicine,*** 6:3173-3186, 2011
● **W Song**, DC Markel, T Shi, and Ren WP: Poly (vinyl alcohol)/collagen/hydroxyapatite hydrogel: Properties and in vitro cellular response. ***J Biomed Mater Res Part A***: 100A: 3071–3079, 2012
● **W Song**, DC Markel, S Wang, R Blasier, T Shi, GZ Mao, and Ren WP: Electrospun polyvinyl alcohol-collagen-hydroxyapatite nanofibers: biomimetic extracellular matrix for osteoblastic cells. ***Nanotechnology***, 23, 115101, 2012
● **W Song**, XW Yu, DC Markel, T Shi and WP Ren: Coaxial PCL/PVA electrospun nanofibers: osseointegration enhancer and controlled drug release device. ***Biofabrication***, 5 (3), 035006, 2013
● Weiping P Ren, **Wei Song**, et. al: Effect of erythromycin-doped calcium polyphosphate scaffold composite in a mouse pouch infection model. ***J Biomed Mater Res Part B*** (early view)